DOKUZ EYLÜL UNIVERSITY

GRADUATE SCHOOL OF NATURAL AND APPLIED SCIENCES

COMPARING TWO DIFFERENT SLIP ENERGY DRIVES USED IN WECS BASED ON FUZZY LOGIC CONTROLLER

by

Abdül BALIKCI

January, 2008

İZMİR

COMPARING TWO DIFFERENT SLIP ENERGY DRIVES USED IN WECS BASED ON FUZZY LOGIC CONTROLLER

A Thesis Submitted to the
Graduate School of Natural and Applied Sciences of Dokuz Eylül University
In Partial Fulfillment of the Requirements for the Degree of Master of Science
in Electrical-Electronically Engineering, Applied Electronically Program

by

Abdül BALIKCI

January, 2008

İZMİR

M.Sc THESIS EXAMINATION RESULT FORM

We have read the thesis entitled **COMPARING TWO DIFFERENT SLIP ENERGY DRIVES USED IN WECS BASED ON FUZZY LOGIC CONTROLLER** completed by **ABDÜL BALIKÇI** under supervision of **Prof. Dr. EYÜP AKPINAR** and we certify that in our opinion it is fully adequate, in scope and in quality, as a thesis for the degree of Master of Science.

Prof. Dr. Eyüp AKPINAR

Supervisor

(Jury Member)

(Jury Member)

Prof. Dr. Cahit HELVACI
Director
Graduate School of Natural and Applied Sciences

ACKNOWLEDGEMENTS

I express my deepest gratitude to my advisor Prof. Dr. Eyüp AKPINAR for his guidance and support in every stage of my research. The technique background research experience and the research experience I have gained under his care will be valuable asset to me in the future.

This thesis was carried out as a part of project, 'Türkiye Elektrik Sisteminde Güç Kalitesine Etki Eden Değişkenleri ve Güç Akışını İzleme, Problemlerin Tespiti, Değerlendirilmesi ve Karşı Önlemlerin Hayata Geçirilmesi Projesi' sponsored by Turkish Scientific and Research Council (TÜBİTAK) under contract no. 105G129 (106G012). I would like to thank them for their financial support.

I also would like to thank my parents for their understanding and never ending support throughout my life.

Abdül BALIKCI

COMPARING TWO DIFFERENT SLIP ENERGY DRIVES USED IN WECS BASED ON FUZZY LOGIC CONTROLLER

ABSTRACT

This thesis analysis and compare two types of slip energy systems in aspect of speed control under fuzzy logic PI controller for power quality issues. Both systems have been used in wind energy conversion systems. Harmonic currents injected to the power system are investigated as well as the other measures taken into consideration.

Simulations are carried out in MATLAB / Simulink and application software is written in TMS320F2812 eZdsp by using C language. Their advantage and disadvantage and working principles is examined.

Keywords : Fuzzy logic , Step Up Chopper , Boost Converter, DSP 2812

BULANIK MANTIK DENETİM TABANLI İKİ FARKLI KAYMA ENERJİSİ DENETİMİNİN RUZGAR TÜRBİNLERİ İÇİN KARŞILAŞTIRILMASI

ÖZ

Bu tezde, bulanık mantık PI kontrolör kullanılarak, iki farklı kayma enerjisi sistemi hız kontrolü yapılarak güç kalitesi açısından analiz edildi. Bu iki sistemde rüzgar enerjisi dönüşüm sistemlerinde kullanılmaktadır. Bu iki sistem tarafından güç sistemine verilen harmonik akımları incelendi ayrıca diğer ölçüm sonuçları dikkate alındı

Simülasyon kısmı MATLAB/simulink ortamında yapılıp uygulama yazılımı C ortamında yazılıp TMS320F2812 DSP kitine yüklenip laboratuar çalışması yapıldı.avantaj dezavantaj ve çalışma prensipleri incelendi.

Anahtar Sözcükler : Bulanık Mantık , Gerilim Arttırcı DC konvertör , DSP 2812

CONTENTS

CHAPTER ONE

INTRODUCTION

Slip energy recovery induction motor is well known for its low cost, simple control circuitry and high efficiency even at low speed at induction machine (IM) drive. It should be noted that the limited speed range is not an inherent defect of slip energy recovery drives; the KVA ratings and hence cost of the rectifier/inverter combination is considerably reduced however by limiting the speed range. Full speed control from the maximum full load speed down to a few Hz is possible provided the required rectifier/inverter rating.

Figure 1.1 shows a schematic of a slip energy recovery drive. A wound rotor IM is needed. The three phase rotor voltages are rectified with a diode bridge rectifier and fed into a dc link inductor to smooth out the current. This dc link current is then inverted and fed back to the mains using an interposing transformer. The transformer turns ratio depends on the required speed range and the motor stator to rotor turns ratio. If the average value of the inverter input voltage, U_{d2}, is zero, then the maximum motor speed is obtained. Increasing U_{d2} causes a consequent reduction in the motor speed. Thus speed control is achieved. In recent applications, the recovery transformer is replaced by the chopper circuits located into the dc link between rectifier and inverter.

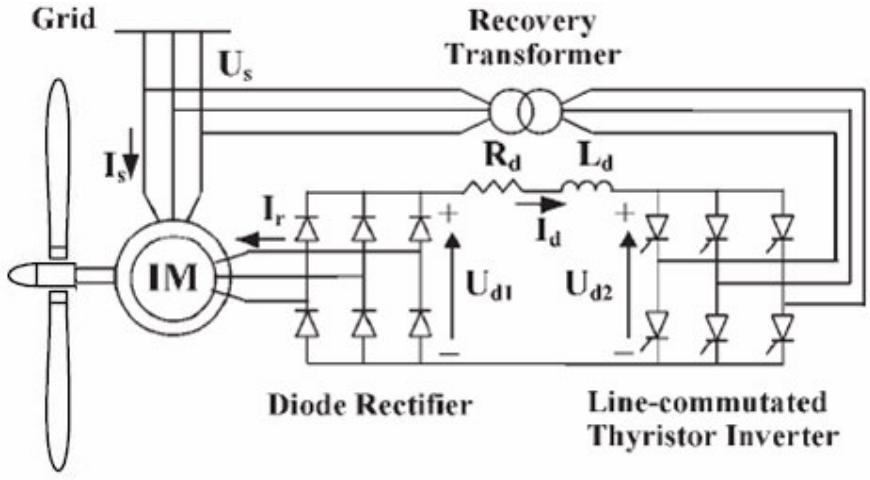

Figure 1.1 Slip Energy Recovery Induction Motor (IM) Drive

Wind energy conversion is gained tremendous attention and developed rapidly in recent years. It has been demonstrated to be both technically and economically viable. It is expected that current developments in gearless, variable speed generators with power electronics grid interface will lead to a new generation of quiet, efficient, economical wind turbines. The modular, multi-pole, permanent magnet, generator has been designed to have moderate dimensions, leading to a wind turbine outline of pleasing appearance. For best aerodynamic efficiency, the shaft speed should be varied in proportion to wind speed. Renewable sources often produce power and voltage varying with natural conditions and must be connected into the utility to be efficiently exploited. The power electronic converters are usually required for the utility interface. Recent developments made the trade-off benefits exceed the cost premium of machine in the power ranges up to several hundred kW. Considering these trends, one of the best topologies for wind power conversion system is full size AC-DC-AC converter.

It is not possible to control the generator torque with the diode bridge rectifier. Then, the boost chopper circuit is added to improve the variable-speed range. The boost converter can control the DC link current regardless of the induced voltage value. In low wind speed range in which the diode bridge rectifier can not control the generator torque, the boost converter scheme can control the generator torque by controlling the DC link current.

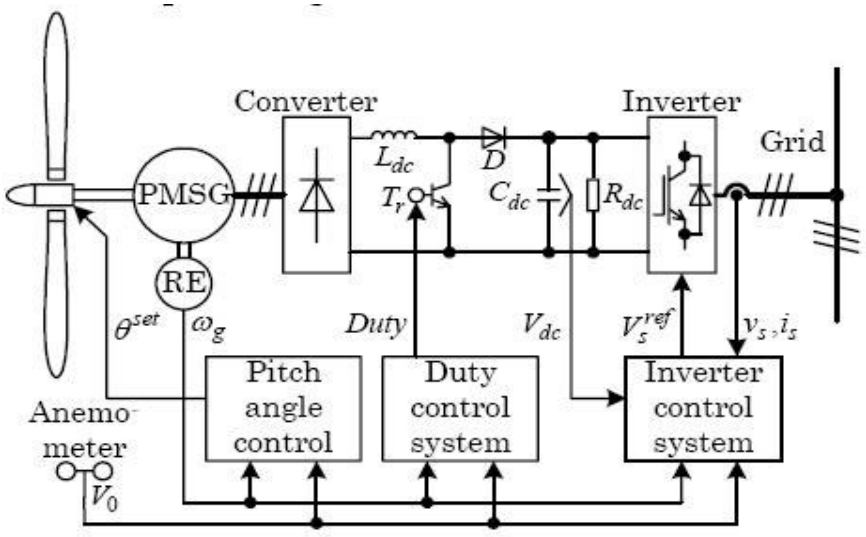

Figure 1.2 Permanent magnet synchronous generator (PMSG) with boost chopper

Generally, the slip energy recovery system has a wound induction machine, diode rectifier, inverter and a transformer. There is an inductor between diode rectifier and inverter to filter current ripples. In this thesis, inductor and line commutated inverter or PWM inverter are removed. Two different type of slip energy system is analyzed and compared in thesis. One of them has boost converter with a single resistor and the other contains three phase resistor and chopper at the rotor terminals.

Content of the thesis can be summarized briefly as follows;

Chapter two contains the fuzzy logic used in the control system. Advantage and disadvantage of fuzzy logic controller is explained and compared to digital PI. General structure of fuzzy logic controller is given and this structure is examined.

Chapter three describes the step up chopper circuit. Firstly, the general structure of chopper is explained. The continuous and discontinuous current modes of operations are considered. The effect of parasitic resistance is examined, formulation of parasitic resistance effect is given and effect of parasitic resistance explained in graphically.

Chapter four dedicated for slip energy system. Two different systems are examined in this thesis, one of them is boost converter with a single resistor and the other is three chopped resistor system. In this chapter, both systems are examined for some parameter, active power , reactive power, input voltage, input current and harmonic effect of this systems.

Chapter five consists of harmonic content of drive circuits. In this chapter, these systems are examined under three different switching frequency and three different speed combination. All result is compared in experimental work and also MATLAB/simulink simulation.

Chapter six concerned with conclusions.

CHAPTER TWO

FUZZY LOGIC CONTROL

Fuzzy Logic was initiated in 1965 by Lotfi A. Zadeh, professor for computer science at the University of California in Berkeley. Since the time , the subject has been the focus of many independent research investigations by mathematicians , scientists and engineers.

Fuzzy logic control (FLC) is used linguistic approach in system control. Logic is close to human brain thinking because all the control rules and variables are expressed in linguistic terms. It is advantage for control some system which mathematical model is not precise.. It can provide the ability to control complex systems without needing accurate knowledge on those systems. But there is need to experience user to design control rules and variables correctly. FLC seems to offer an effective solution in the control of non-linear and time varying systems.

The quality of the fuzzy approximation depends on experience of the user who prepare the rules . Fuzzy system is a approximate function which approximate to every system which can be linear or non linear system . So fuzzy rules and fuzzy set must be chosen correctly

2.1 Background

In decade after Dr. Zadeh's seminal paper on fuzzy sets , many theoretical developments in fuzzy logic took place in U.S. , Europe and Japan . from mid-1970 to present Japanese researcher have been primary force in advancing the practical implementation of the theory .they have done an excellent hob of commercializing this technology and now there are patents over 2000 on fuzzy.

Fuzzy logic was first proposed by Lotfi A. Zadeh of the University of California at Berkeley in a 1965 paper. He elaborated on his ideas in a 1973 paper that introduced the concept of "linguistic variables", which in this article equates to

variable defined as a fuzzy set. Other research followed, with the first industrial application, a cement kiln built in Denmark, coming on line in 1975.

Fuzzy systems were largely ignored in the US because they were associated with artificial intelligence, a field that periodically oversells itself and which did so in a big way in the mid-1980s, resulting in a lack of credibility in the commercial domain.

The Japanese did not have this prejudice. Interest in fuzzy systems was sparked by Seiji Yasunobu and Soji Miyamoto of Hitachi, who in 1985 provided simulations that demonstrated the superiority of fuzzy control systems for the Sendai railway. Their ideas were adopted, and fuzzy systems were used to control accelerating, braking, and stopping when the line opened in 1987.

Another event in 1987 helped promote interest in fuzzy systems. During a international meeting of fuzzy researchers in Tokyo that year, Takeshi Yamakawa demonstrated the use of fuzzy control, through a set of simple dedicated fuzzy logic chips, in an "inverted pendulum" experiment. This is a classic control problem, in which a vehicle tries to keep a pole mounted on its top by a hinge upright by moving back and forth.

Observers were impressed with this demonstration, as well as later experiments by Yamakawa in which he mounted a wine glass containing water or even a live mouse to the top of the pendulum. The system maintained stability in both cases. Yamakawa eventually went on to organize his own fuzzy-systems research lab to help exploit his patents in the field.

Following such demonstrations, the Japanese became infatuated with fuzzy systems, developing them for both industrial and consumer applications. In 1988 they established the Laboratory for International Fuzzy Engineering (LIFE), a cooperative arrangement between 48 companies to pursue fuzzy research. Japanese

companies developed a wide range of products using fuzzy logic, ranging from washing machines to autofocus cameras and industrial air conditioners.

Some work was also performed on fuzzy logic systems in the US and Europe, and a number of products were developed using fuzzy logic controllers. However, little has been said about the technology in recent years, which implies that it has either become such an ordinary tool that it is no longer worth much comment, or it turned out to be an industrial fad that has now generally died out.

2.2 Advantage Of Fuzzy Logic

Here is a list of general advantages about fuzzy logic.

•Fuzzy logic is conceptually easy to understand. The mathematical concepts behind fuzzy reasoning are very simple. What makes fuzzy nice is the “naturalness” of its approach and not its far-reaching complexity.

•Fuzzy logic is flexible. With any given system, it’s easy to massage it or layer more functionality on top of it without starting again from scratch.

•Fuzzy logic is tolerant of imprecise data. Everything is imprecise if you look closely enough, but more than that, most things are imprecise even on careful inspection. Fuzzy reasoning builds this understanding into the process rather than tacking it onto the end.

•Fuzzy logic can model nonlinear functions of arbitrary complexity. You can create a fuzzy system to match any set of input-output data. This process is made particularly easy by adaptive techniques like ANFIS (Adaptive Neuro-Fuzzy Inference Systems) which are available in the Fuzzy Logic Toolbox.

•Fuzzy logic can be built on top of the experience of experts. In direct contrast to neural networks, which take training data and generate opaque,

impenetrable models, fuzzy logic lets you stand on the shoulders of people who already understand your system.

•Fuzzy logic can be blended with conventional control techniques. Fuzzy systems don't necessarily replace conventional control methods. In many cases fuzzy systems augment them and simplify their implementation.

•Fuzzy logic is based on natural language. The basis for fuzzy logic is the basis for human communication. This observation underpins many of the other statements about fuzzy logic.

2.3 Structure of Fuzzy System

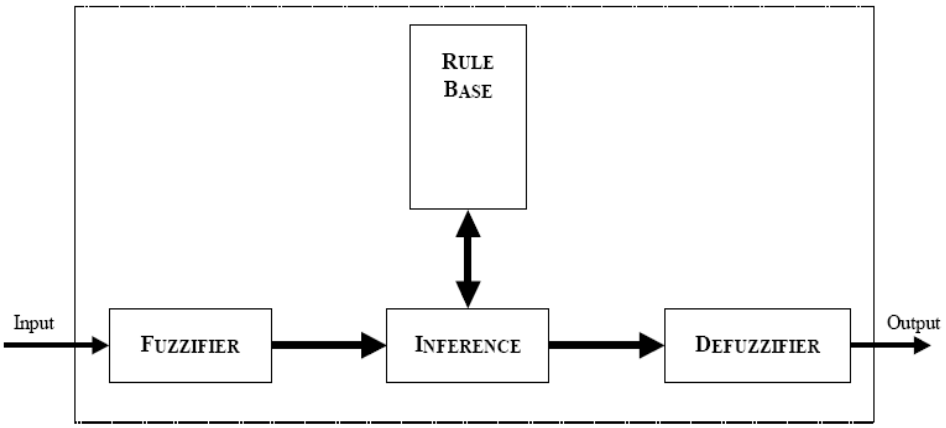

Figure 2.1 General structure of Fuzzy logic controller

Fuzzy systems is occurred four main operation which are called as fuzzifier, inference, rule base, defuzzifier.

2.3.1 Fuzzifier

Fuzzification is a process of making a crisp quantity fuzzy. Fuzzification converts mathematical parameters to linguistic parameter. At the fuzzification, membership function is used on the contrary classical set theory. In classical set theory. In classical set theory output change between 0 and 1 but there is no interval value between [0,1] .

$$\mu_s = \begin{cases} 0 \; if \; x \notin S \\ 1 \; if \; x \in S \end{cases} \quad (2\text{-}1)$$

In classic for different input (x) value goes either 0 or 1.

$$\mu_{A(x)} \in [0,1] \quad (2\text{-}2)$$

In fuzzy set output can be change interval 0 and 1 for any input values like formula 2-2.

In classical sets the transition for an element in the universe between membership and non membership in a given set is abrupt and well-defined which is said to crisp. For an element in a universe that contains fuzzy sets, this transition can be gradual. This transition among various degrees of membership can be thought of as conforming to the fact that the boundaries of the fuzzy sets are vague and ambiguous. Hence, membership of an element from the universe in this set is measured by a function that attempts to describe vagueness and ambiguity. Fuzzy set containing elements that have varying degrees of membership in a set. In fuzzy set an element can be member of other membership function on the contrary classical set. In classical set an element must be complete membership. (Ross ,1995)

A notation convention for fuzzy sets when the universe of discourse X is discrete, is as follows for a fuzzy set A

$$A = \left\{ \frac{\mu_A(x1)}{x1} + \frac{\mu_A(x2)}{x2} + \ldots \right\} = \left\{ \sum_i \frac{\mu_A(x_i)}{x_i} \right\} \quad (2\text{-}3)$$

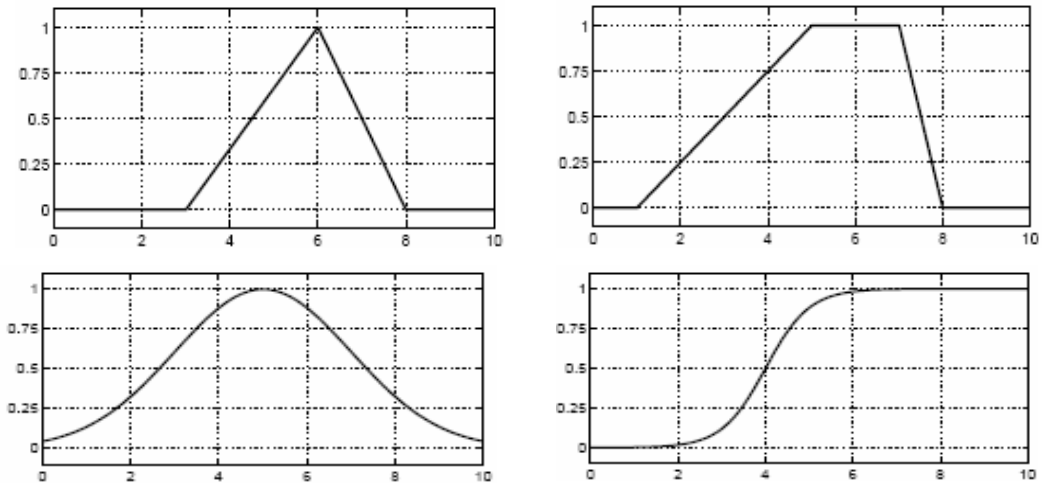

Figure 2.2 Commonly used membership function

These membership functions are used for generally in fuzzy logic control application , triangle and trapezoidal most common between them. Because both of them are applied in microcontroller easier than others.

If we define fuzzy set as A,B on the universe X, some operation can be made in this set such as union, intersection, complement.

$$\mu_{A\cup B} = \max\{ \mu_A(x) \cup \mu_B(x) \} \qquad \text{union operation} \qquad (2\text{-}4)$$

$$\mu_{A\cap B} = \min\{ \mu_A(x) \cap \mu_B(x) \} \qquad \text{intersection operation} \qquad (2\text{-}5)$$

$$\mu_{A'} = 1 - \mu_A(x) \qquad \text{complement operation} \qquad (2\text{-}6)$$

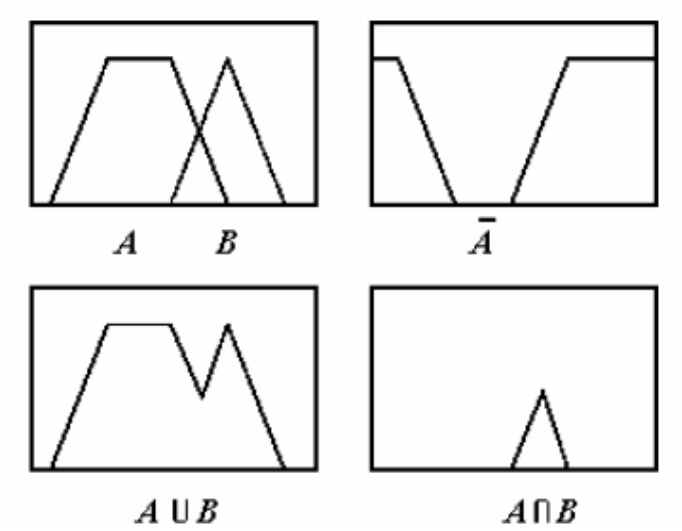

Figure 2.3 Fuzzy set operation result

2.3.2 Inference and Rule Base

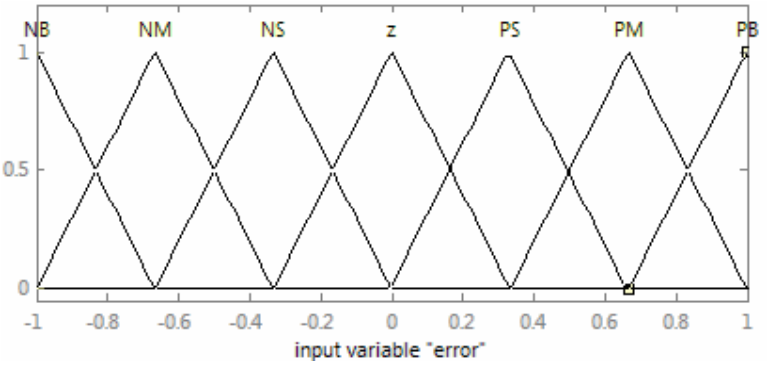

Figure 2.4 Error and change of error function in linguistic form

At the experimental work there are 7 different membership function for error and change of error inputs So there are 49 rules for choosing 7 different output. Due to apply in the microcontroller.

This membership function is occurred in linguistic term. Error function can be determine as negative big (NB), negative medium (NM), negative small (NS), zero (Z), positive small (PS), positive medium (PM), positive big (PB) and also change of error function is the same with error function.

Fuzzy controller use its experience and write fuzzy rules. Decision is based on fuzzy rules which combine some manner and determine which fuzzy set will be activated. Result obtained after some method, for example max-min method most general method for obtaining decision.

Rules are written in “if - then” format with linguistic variable, for example for one input fuzzy logic it can be written like below

IF (error is positivebig) THEN (the output is positivebig)

That means if the measured signal is much far from desired signal (error is high value) fuzzy will increase the output highly to reach desired signal.

IF (error is PB and change of error is PS) THEN (the output is PB)

Above there is two inputs fuzzy system , at this time fuzzy system deal with error(e) and change of error(ce) signal same time.

$$\mu(y)= \max\{ \min \{ \mu_e(xi) , \mu_{ce}(xi) \} \} \qquad (2\text{-}7)$$

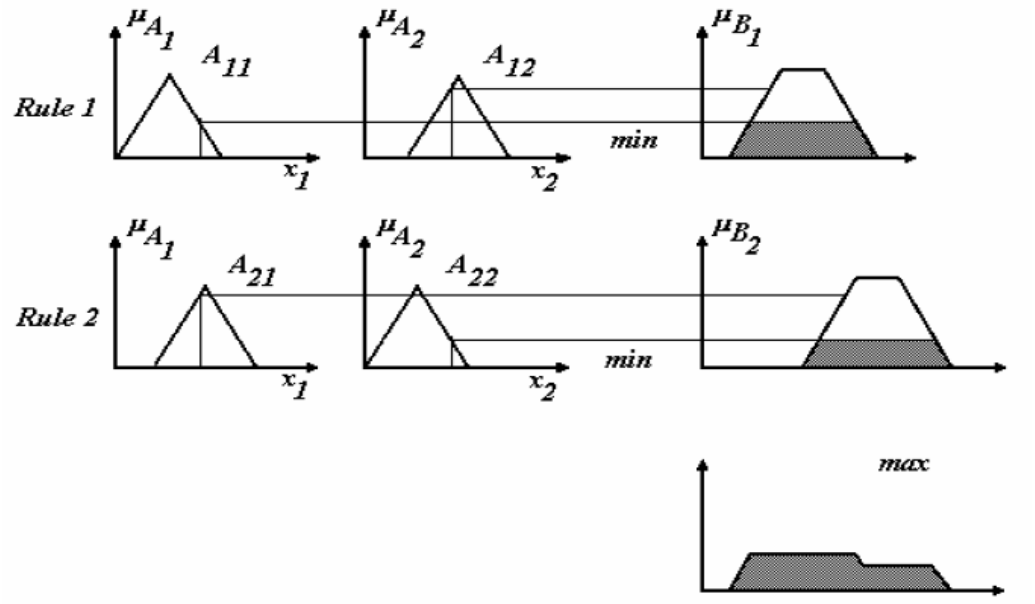

Figure 2.5 Graphical representation of max-min method

At the figure 2.5 rule 1 trigged two different triangular fuzzy set and resultant of rule 1 is $\mu_{b1.}$ it is minimum of this two fuzzy set μ_{A1} ,μ_{A2} respectively. At rule 2 same thing is valid, too. Resultant waveform can be obtained by union(max) of rule1 and rule2 which are μ_{B1} ,μ_{B2} respectively.

2.3.3 Defuzzifier

Defuzzification is the conversion of a fuzzy quantity to a precise quantity. The output of a fuzzy process can be the logical union of two or more fuzzy membership functions defined on the universe of discourse of the output variable. (Ross ,1995) At the figure 2.6 there is output of fuzzy sets which envelope of two triangular shape which firstly applied min operator then applied max operator. So output is not a known shape like triangular or any shape, there is need to operator defuzzify it.

At least seven methods in the literature, among the many that have been proposed by investigators in recent years Four of these methods is illustrated here briefly.

Max-Membership Principle: this method also known as height method, this scheme is limited to peaked output functions. Algebraic function of this method is

$$\mu_c(z^*) \geq \mu_c(z) \qquad \text{for all } z \in Z \qquad (2\text{-}8)$$

Centroid Method: this procedure is most prevalent an physically appealing of all the defuzzification methods . It is also called as center of gravity methods.

$$Z^* = \frac{\int \mu c(z).z dz}{\int \mu c(z).dz} \qquad (2\text{-}9)$$

Weighted Average Method: This method is only valid for symmetrical output membership function. It is given by the algebraic expression

$$Z^* = \frac{\sum \mu c(z).z}{\sum \mu c(z)} \qquad (2\text{-}10)$$

This weighted average method is formed by weighted each membership function in the output by its respective maximum membership value.

Mean-Max Membership: this method is closely related to the fist method, except that the locations of the maximum membership can be non-unique. This method is given by expression below. (Ross, 1995)

$$Z^* = \frac{a+b}{2} \qquad (2\text{-}11)$$

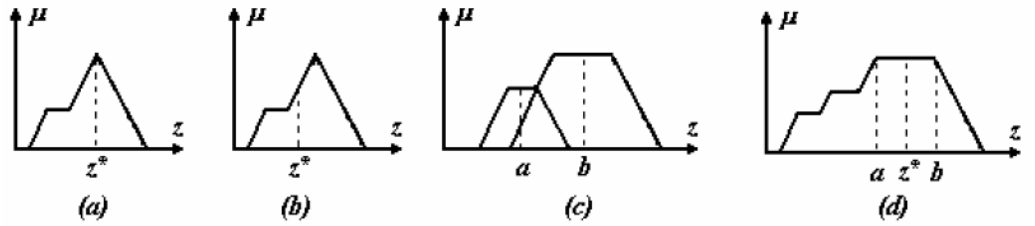

Figure 2.6 graphical representation of methods- a)Max-Membership b) Centroid c) Weighted Average d)Mean-Max

2.4 Design And Implementation

2.4.1 Design of Fuzzy Controller

All system are design and simulated on computer program which is MATLAB/Simulink. Firstly fuzzy interface is created by using MATLAB FIS editor. Type of fuzzy logic is chosen as sugeno type. Because sugeno type fuzzy easy for defuzzification operation in DSP. There are two input whose are error and change of error inputs and also there is an output.

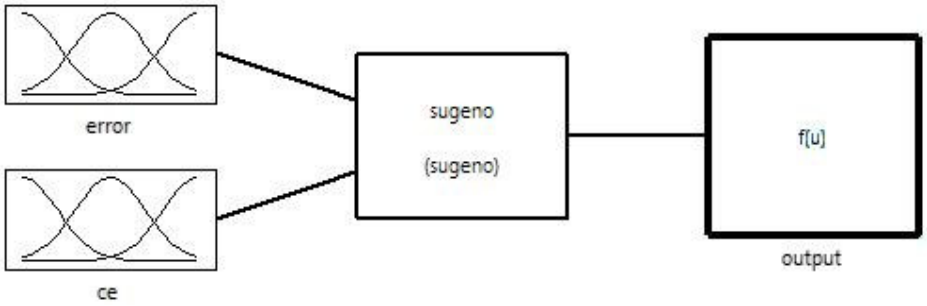

Figure 2.7 Fuzzy logic in general form

Error and change of error inputs are chosen triangular form, it is easy to apply in DSP, Because every input take an triangle and DSP must be solve value which is crossed by error signal. Fuzzy set of the error input can be seen figure2.8, shape of fuzzy set is important here triangle is narrow when error is too small, on the contrary when the error is big triangle is bigger. It will be taken speed of the induction machine and it is compared with reference signal and error signal is produced. Aim of this fuzzy set shape when rotor speed much smaller than reference, fuzzy output will be more higher and also when rotor speed much higher than reference speed, fuzzy output will be more higher ,too. When rotor speed reach reference speed change of output will be smaller but at this time fuzzy output will more sensitive than first situation.

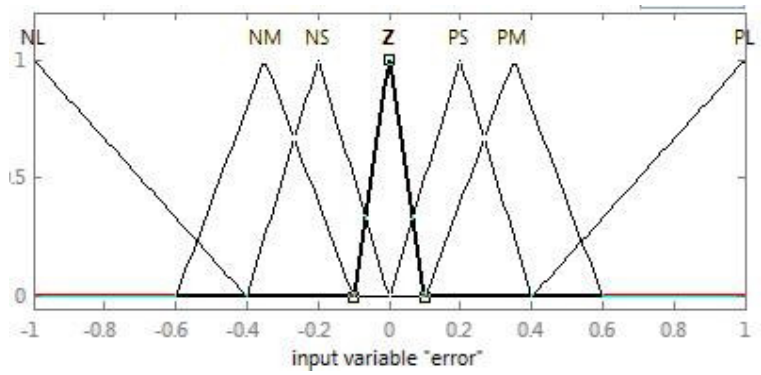

Figure 2.8 Fuzzy Set of Simulation and Experimental work for error(e) and change of error(ce)

At the figure 2.9 surface of my fuzzy logic is can be seen. When error and change of error near to value 1, output of my fuzzy produce 1. I used fuzzy logic as pi controller

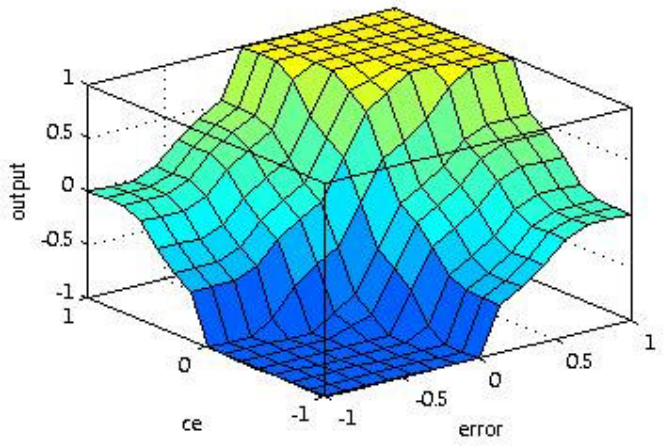

Figure 2.9 Surface of fuzzy logic

ce / e	NL	NM	NS	Z	PS	PM	PL
PL	NL	NL	NL	NL	NM	NS	Z
PM	NL	NL	NL	NM	NS	Z	PS
PS	NL	NL	NM	NS	Z	PS	PM
Z	NL	NM	NS	Z	PS	PM	PL
NS	NM	NS	Z	PS	PM	PL	PL
NM	NS	Z	PS	PM	PL	PL	PL
NL	Z	PS	PM	PL	PL	PL	PL

Figure 2.10 Rule table for fuzzy

ce / e	NL	NM	NS	Z	PS	PM	PL
PL	-1,00	-1,00	-1,00	-1,00	-0,6	-0,3	0
PM	-1,00	-1,00	-1,00	-0,6	-0,3	0	0,3
PS	-1,00	-1,00	-0,6	-0,3	0	0,3	0,6
Z	-1,00	-0,6	-0,3	0	0,3	0,6	1.0
NS	-0,6	-0,3	0	0,3	0,6	1.0	1.0
NM	-0,3	0	0,3	0,6	1.0	1.0	1.0
NL	0	0,3	0,6	1.0	1.0	1.0	1.0

Figure 2.11 Rule table for fuzzy as output value

Fuzzy logic is used as pi controller. So it used incremental form at output of the fuzzy. At the figure 2.12 control shape can be seen , controller measure speed and subtract it from reference speed ,result is error of the signal and also at the controller error signal is delayed one sample and subtract error signal which gives change of error signal. These two inputs enter the fuzzy controller and after the fuzzy gives result output is delayed one sample and add output, this called as fuzzy pi control.

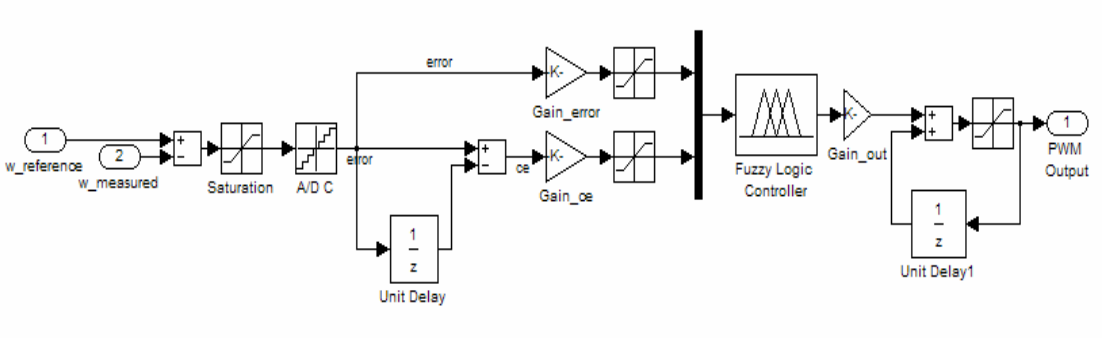

Figure 2.12 Fuzzy logic PI controller schematic

CHAPTER THREE

STEP UP CHOPPER

3.1 Step Up Chopper

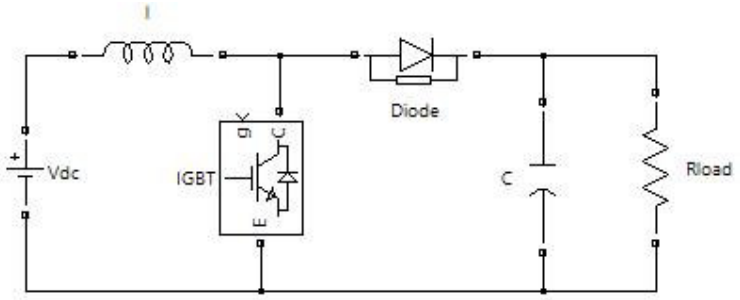

Figure 3.1 Schematic of boost converter

Step up chopper is known as boost converter, step up converter. Step up chopper is a power converter with an average output dc voltage greater than its average input dc voltage. At least one energy storage element is present in step up chopper circuit. This circuit is kind of fly-back circuit, because energy is transferred to load only power electronic switch is off position. Step up chopper has two semiconductor element, main switch is used as igbt, mosfet and transistor, second switch is diode.

For high efficiency, the SMPS switch must turn on and off quickly and have low losses. The advent of a commercial semiconductor switch in the 1950's represented a major milestone that made SMPSs such as the boost converter possible. Semiconductor switches turned on and off more quickly and lasted longer than other switches. The major DC to DC converters were developed in the early-1960s when semiconductor switches had become available. industry's need for small, lightweight, and efficient power converters led the converter's rapid development include step up converter.

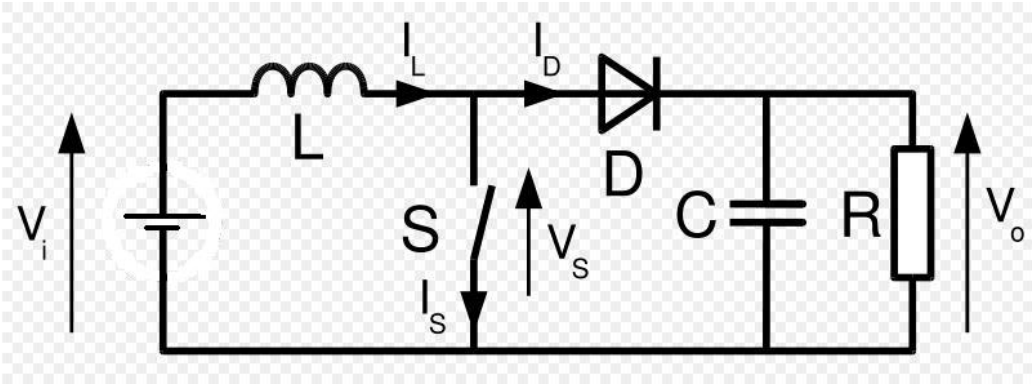

Figure 3.2 General structure of boost converter

Boost converter has two different working states which are S switch is on and S switch is off state. S switch is chosen as igbt in my experimental and simulation work.

When igbt is on state DC source short circuited by inductance diode is reverse biased So it is not conduct. At this time inductance current increase and energy is stored in inductance. At the figure 3.3 igbt on-state situation can be seen.

When igbt is off state DC source is connected serial with inductance and this time diode is forward biased So capacitor is charged and load is fed by stored energy of inductance and also DC source . At the figure 3.3 igbt off-state situation can be seen.

S switch (igbt) can be driven some different way for example pulse width modulation(PWM) or different frequency signal like hysteresis controlled signal. In my work I used PWM signal which frequency is 500, 2000, 5000 Hz. These all frequency is tried in order to realize difference of them.

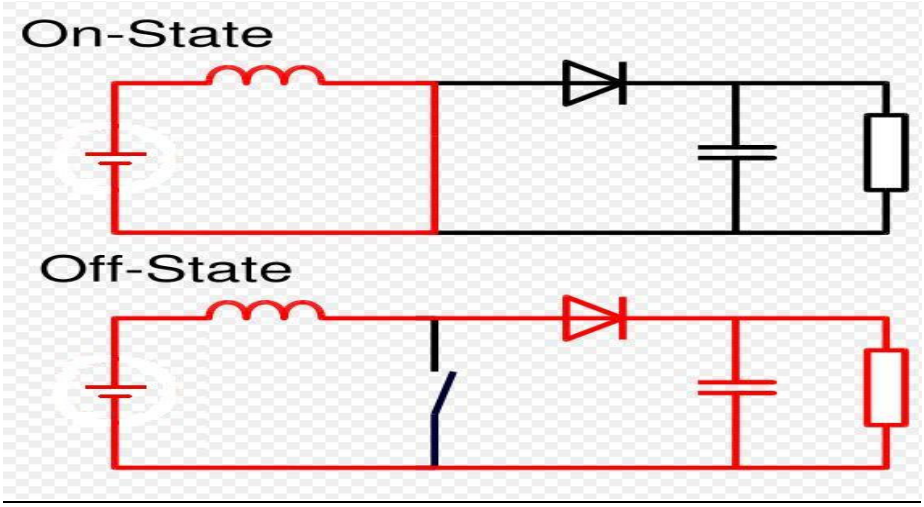

Figure 3.3 Two working mode of boost converter

Step up chopper has two different working mode

3.1.1 Continuous current mode

At this mode inductance current does not fall to zero. Typical waveform can be seen in figure 3.4. At switch is turn on inductance current increase to Imax and high capacitance stabilize the output voltage When switch is turn off inductance current is decrease because it feed capacitor and resistance over diode.

This mode can appear when switching frequency is low or inductance is really high.

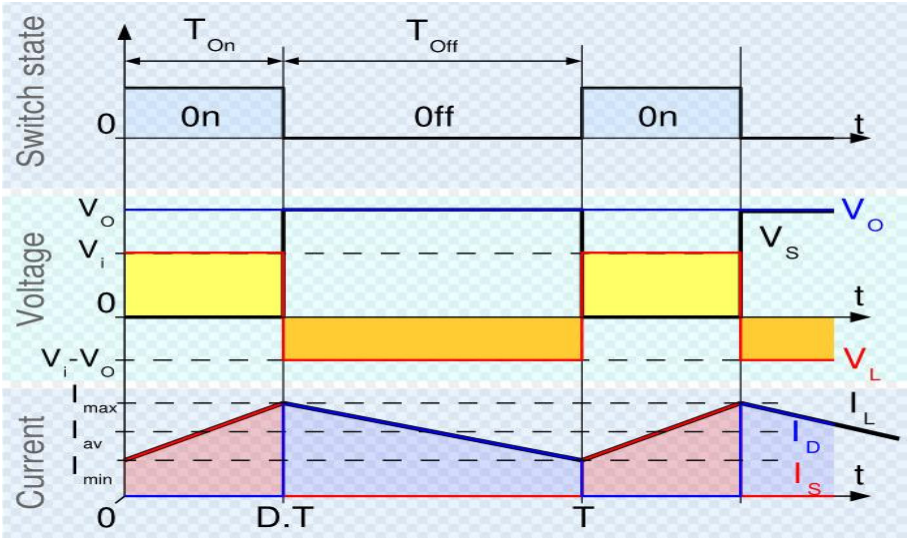

Figure 3.4 graph for continuous current mode

When igbt is on position, input voltage appear on inductance. Current of inductance change versus time like formula (3-1).

$$V_i = L\frac{dI_L(t)}{dt} \tag{3-1}$$

$$\frac{\Delta I_L}{\Delta t} = \frac{V_i}{L} \tag{3-2}$$

At igbt on situation current can be found as formula (3-3), its end maximum point of the current it is D.T point in figure 3.4

$$\Delta I_L(on) = \int_0^{DT} \frac{V_i(t)}{L} dt \tag{3-3}$$

Result of integration is seen formula (3-4). D is a duty cycle of PWM signal and T is a period of the PWM signal. D is changing from 0 to 1. 1 shows igbt totally on position and 0 shows igbt never turn on.

$$\Delta I_L(on) = \frac{V_i DT}{L} \tag{3-4}$$

When igbt is turn off, inductance current flows through load over diode. If diode forward voltage drop is neglected and capacitance value is high enough to stabilize output voltage, formulation can be write like formula (3-5).

$$V_i - V_0 = L\frac{dI_L(t)}{dt} \tag{3-5}$$

$$\frac{\Delta I_L}{\Delta t} = \frac{V_i - V_o}{L} \tag{3-6}$$

Variation of inductance current at igbt off situation is seen (3-7)

$$\Delta I_L(off) = \int_0^{(1-D)T} \frac{V_i(t) - V_o(t)}{L} dt \tag{3-7}$$

Result of integration is seen (3-8)

$$\Delta I_L(off) = \frac{(V_i - V_o)(1-D)T}{L} \qquad (3\text{-}8)$$

In constant switching frequency inductor current must be equal to beginning and end commutation cycle as seen formula (3-9)

$$\Delta I_L(on) = -\Delta I_L(off) \qquad (3\text{-}9)$$

If we substitute the equivalent of inductance current which is shown for on and off position of igbt at formula (3-9) ,formula (3-10) can be obtained.

$$\frac{V_i DT}{L} = \frac{(V_i - V_o)(1-D)T}{L} \qquad (3\text{-}10)$$

If we simplify this formula we can obtain as result formula (3-11).

$$\frac{V_o}{V_i} = \frac{1}{(1-D)} \qquad (3\text{-}11)$$

Result of this formula (3-11), every time output signal of the converter is higher than input signal and when duty cycle is reach to 1 output voltage is reach to infinite value, too.

3.1.2 Discontinuous current mode

In some case, Energy requirement of load is small enough to be transferred in short time like one period. At this case inductance current goes zero that means inductance completely discharge its energy in a period. At the figure 3.5 it can be seen in a period inductance current I_L goes to zero before igbt is turned on again.

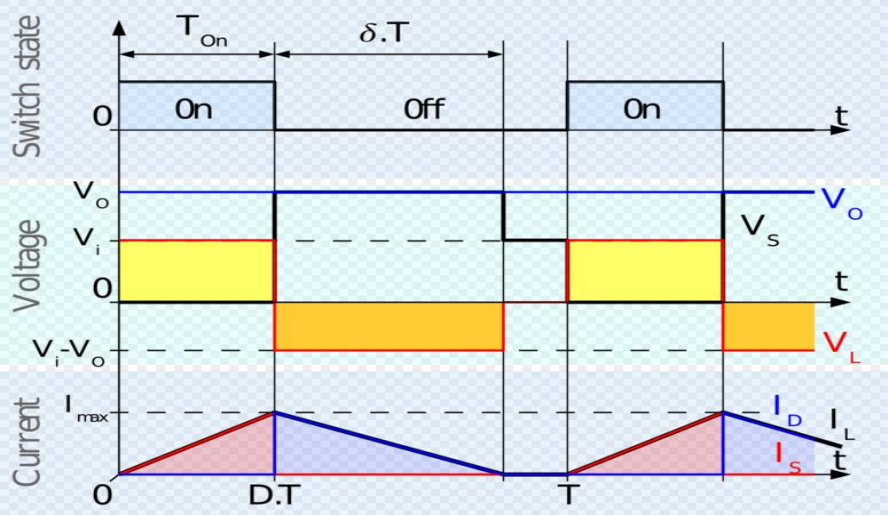

Figure 3.5 Graph for discontinuous current mode

Inductor current is 0 at the initial situation, so it reach maximum point during t=DT like formula (3-12)

$$I_L(\max) = \int_0^{DT} \frac{V_i(t)}{L} dt \qquad (3\text{-}12)$$

$$I_L(\max) = \Delta I_L(on) = \frac{V_i DT}{L} \qquad (3\text{-}13)$$

Minimum point of inductance current (I_L(min)) is zero, so at the δT time later current goes to zero, so we can write formula (3-14)

$$\Delta I_L(off) = \int_0^{\delta T} \frac{V_i(t) - V_o(t)}{L} dt \qquad (3\text{-}14)$$

$$\Delta I_L(off) = \frac{(V_i - V_o)\delta T}{L} \qquad (3\text{-}15)$$

At the same manner in continuous current mode (3-16) can be written

$$\Delta I_L(on) = -\Delta I_L(off) \qquad (3\text{-}16)$$

When we substitute them formula (3-17) is obtained

$$\frac{V_i DT}{L} = \frac{(V_i - V_o)\delta T}{L} \qquad (3\text{-}17)$$

If formula (3-17) is simplified and taken δ, formula (3-18) is obtained

$$\delta = \frac{V_i D}{V_o - V_i} \qquad (3\text{-}18)$$

Output current is equal to diode current in the boost converter, diode current can be seen in the figure 3.5. If it is assumed this current is linearly decreasing like figure 3.5 , output current can be written the like formula (3-19)

$$I_o = I_d = \frac{I_L(\max)\delta}{2} \qquad (3\text{-}19)$$

If $I_L(max)$ and δ are substituted into the formula (3-19), (3-21) is obtained

$$I_o = \frac{ViDT}{2L}\frac{V_i D}{V_o - V_i} \qquad (3\text{-}20)$$

$$I_o = \frac{Vi^2 D^2 T}{2L(V_o - V_i)} \qquad (3\text{-}21)$$

If formula (3-21) is arranged, input-output voltage equation can be found like (3-22)

$$\frac{V_o}{V_i} = 1 + \frac{V_i D^2 T}{2LI_o} \qquad (3\text{-}22)$$

At the above resultant input-output voltage equation is found. It can be seen discontinuous mode has more complex voltage expression than continuous mode. At continuous mode output voltage depends on only duty cycle (D) but at discontinuous

mode output voltage depends on input voltage, output current, duty cycle, period of the PWM signal and inductance value.

3.1.3 Effect of Inductance Resistance

At the above analysis there is not active power dissipated element like resistor which can be inductance resistance or wire resistance. So all analysis made as power is transmitted completely. But this parasitic resistance is exist in the boost converter circuit. I try to explain effect of inductance resistance on duty cycle at the boost converter. At this analysis, it is assumed inductance has resistance(R_L) which serial with inductance.

$$V_L = L\frac{dI_L(t)}{dt} + R_L I_L \qquad (3\text{-}23)$$

If we continuous current mode when igbt is off state, diode is forward biased and at this time average voltage is

$$V_i = (1-D)V_o \qquad (3\text{-}24)$$

Output current is equal to inductor current during igbt off state, So average inductor current is

$$I_L = \frac{I_o}{1-D} \qquad (3\text{-}25)$$

If we assume load capacitor really high and its result load voltage is constant that means ripple on the output voltage is really negligible, it can be assumed that the load (R) is purely resistive, so formula can be obtain like formula (3-26),

$$I_L = \frac{V_o}{(1-D)R} \qquad (3\text{-}26)$$

If I_L put in the previous equation, formula (3-27) is obtained,

$$V_i = R_L \frac{V_o}{(1-D)R} + (1-D)V_o \qquad (3\text{-}27)$$

It can be written as formula (3-28)

$$\frac{V_o}{V_i} = \frac{1}{\frac{R_L}{(1-D)R} + 1 - D} \qquad (3\text{-}28)$$

At the formula (3-28), if inductance resistance is selected as zero, boost converter normal formula is obtained. Due to the equation above while the inductance resistance increases, the voltage gain of converter decreases and also inductance resistance is effected by duty cycle. The figure 3.6 gives the variation of voltage with respect to parasitic resistance.

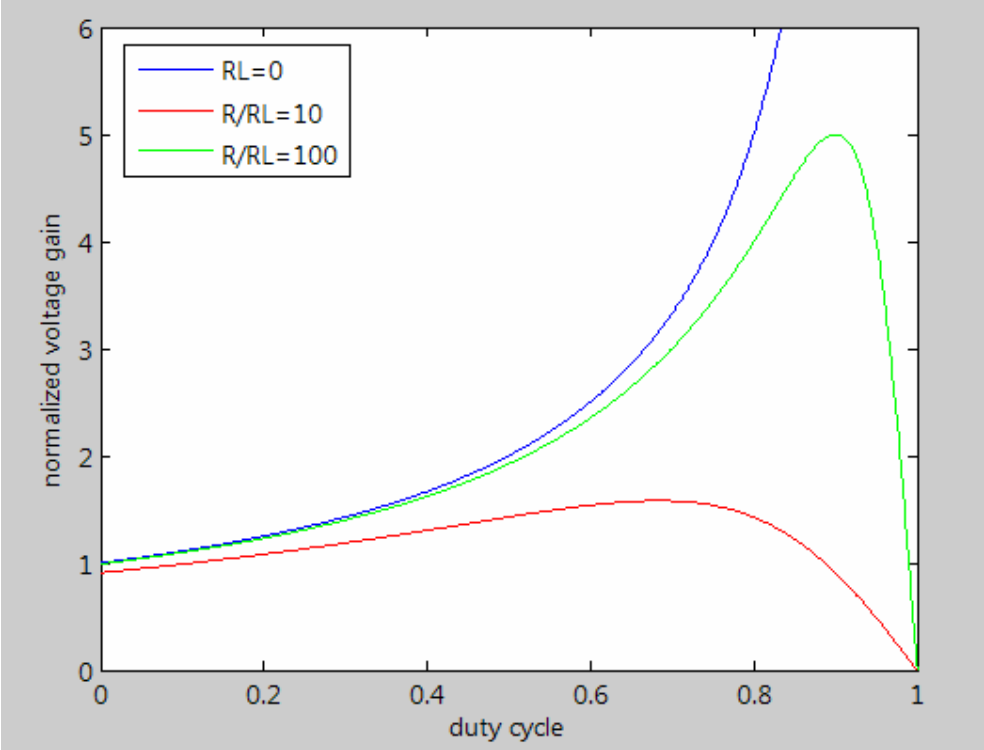

Figure 3.6 Effect of parasitic resistance in boost converter

It can be seen in the figure 3.6, if there is no parasitic resistance in the circuit output voltage gain goes to infinite when duty cycle exceed %80. But in the real work there is a inductance resistance in the circuit. At this time, it can be seen formula (3-28), output voltage gain related with duty cycle and output resistance and also resistance of inductance. At the figure 3.6 ratio on output resistance and inductance resistance (R/R_L) =100 maximum gain is obtained at duty cycle is equal to %90 , at this time maximum gain is 5,0. if (R/R_L) =10 at this time maximum gain is obtained at duty cycle is equal to %70, at this time maximum gain is 1,58. Matlab source code of this graph can be found at appendix.

CHAPTER FOUR

APPLICATION OF FUZZY LOGIC ON SPEED CONTROL OF WOUND ROTOR

4.1 Boost Chopper with Single Resistor

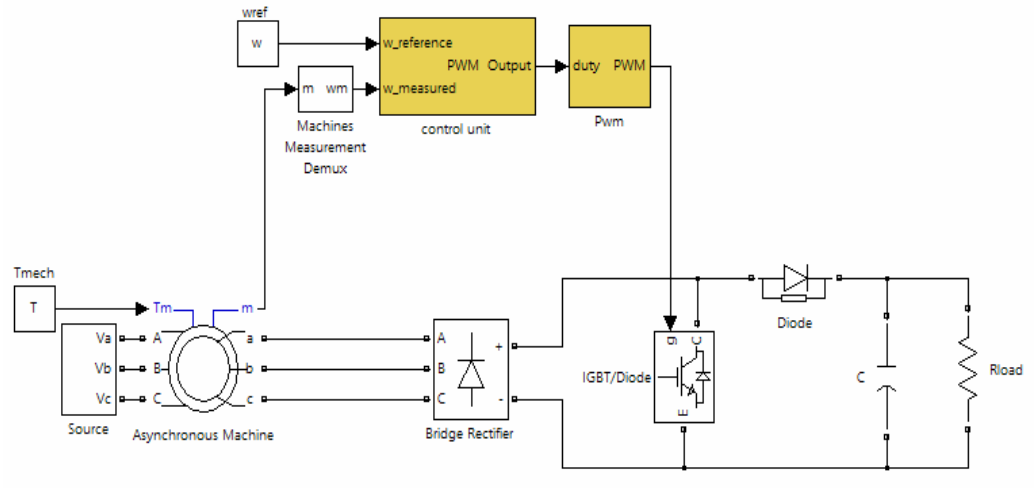

Figure 4.1 Schematic of the system

At simulation, induction machine parameters given in Appendix A are measured and used. The capacitor value is chosen as 1175 μF and load resistance is chosen 96 Ω. At the simulation, fuzzy logic controller is used, its all parameters and model same with experimental work.

In application, the shaft of the DC generator is coupled to wound rotor induction machine and 3.3 Nm load is applied. Torque is set to the wound rotor induction machine by the sperately excited DC generator at speed 1100 rpm.

4.1.1 Experiment and Simulation work at the frequency of 2 KHz.:

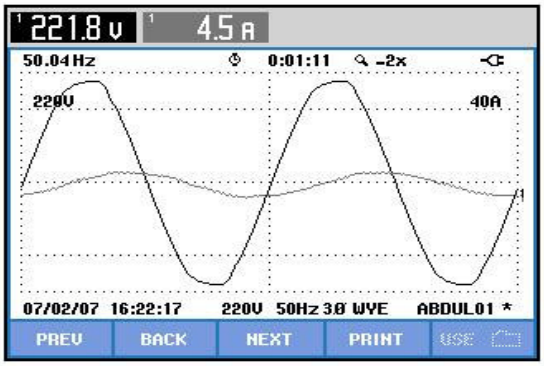

Figure 4.2 Input voltage and input current in application

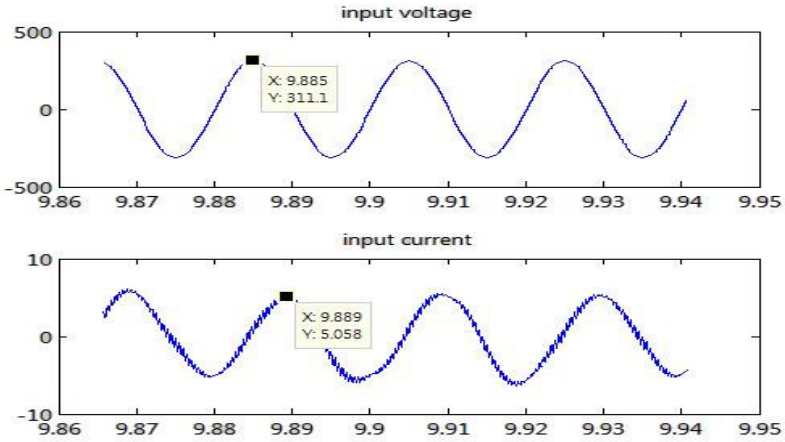

Figure 4.3 Source voltage and Source current waveform of phase A
(Matlab/Simulink simulation result) .

In figure 4.2 shows the variation of voltage and current in experiment and figure 4.3 shows simulation result.

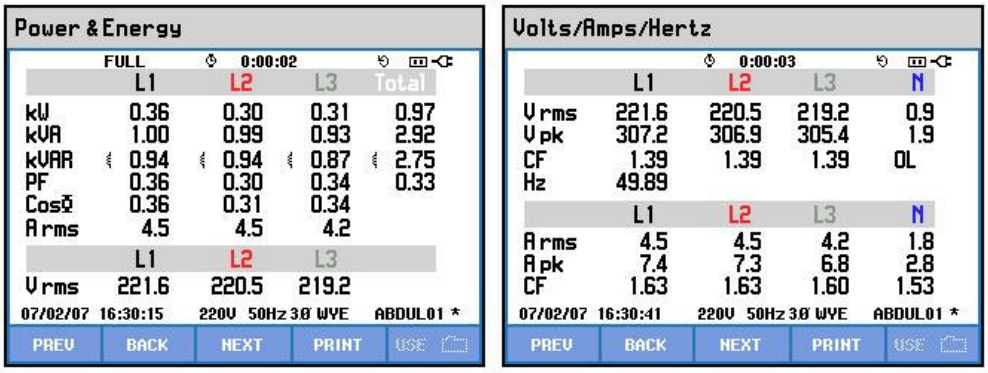

Figure 4.4 Input active ,reactive power and input voltage and current table in application

If the figure 4.4 is compared with table 4.1, it can be seen that the results of Matlab model and experimental output are very near to each other. The duty cycle is %54 for 2Khz driving frequency.

Table 4.1 Results of simulation

P (W)	Q (VAR)	S (VA)	Cos∅	Vinput(rms)	Iinput(rms)
800	2500	2625	0,3	220	3,92

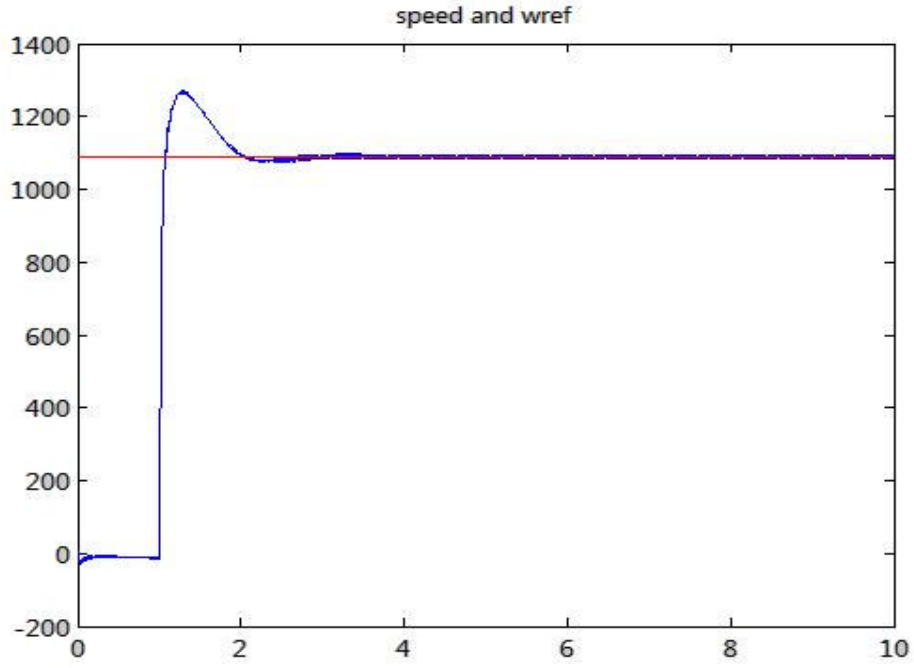

Figure 4.5 Reference signal and actual motor speed in Matlab/simulink simlation

When the motor speed goes to 1090 rpm, the gate signal is applied in simulation.

Result of Matlab simulation and output of experimental work can be seen from figure 4.6 to 4.9. These graph shows that simulation results and experimental results are consistent. In figure 4.8 and 4.9 shows DC step up chopper works only continuous current mode. In this thesis other gate pwm frequency is examined and at discontinuous current mode can be seen there.

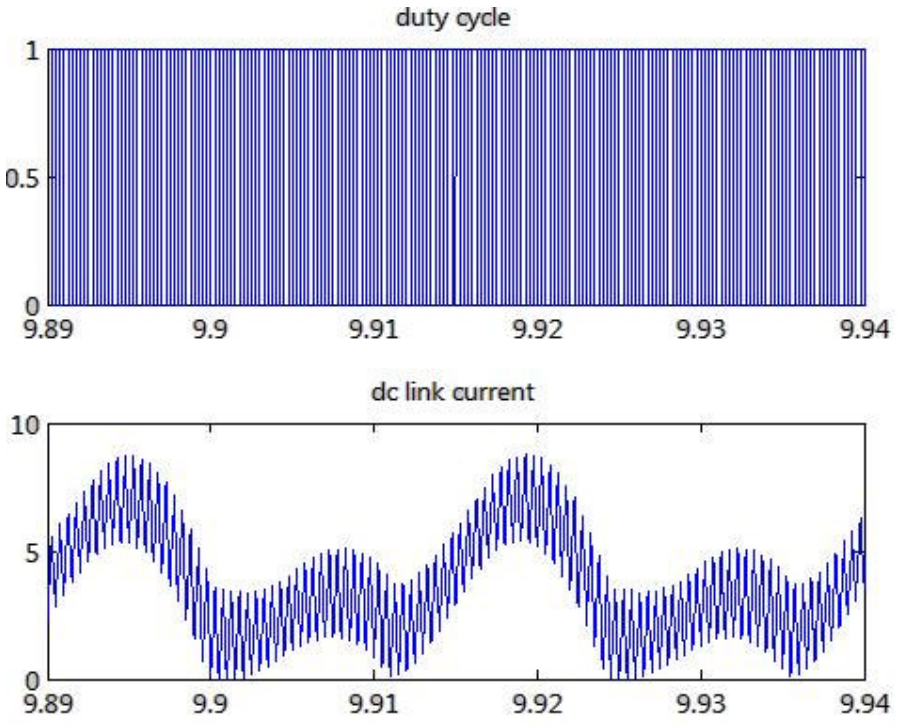

Figure 4.6 Duty cycle and DC link current in MATLAB/Simulink simulation

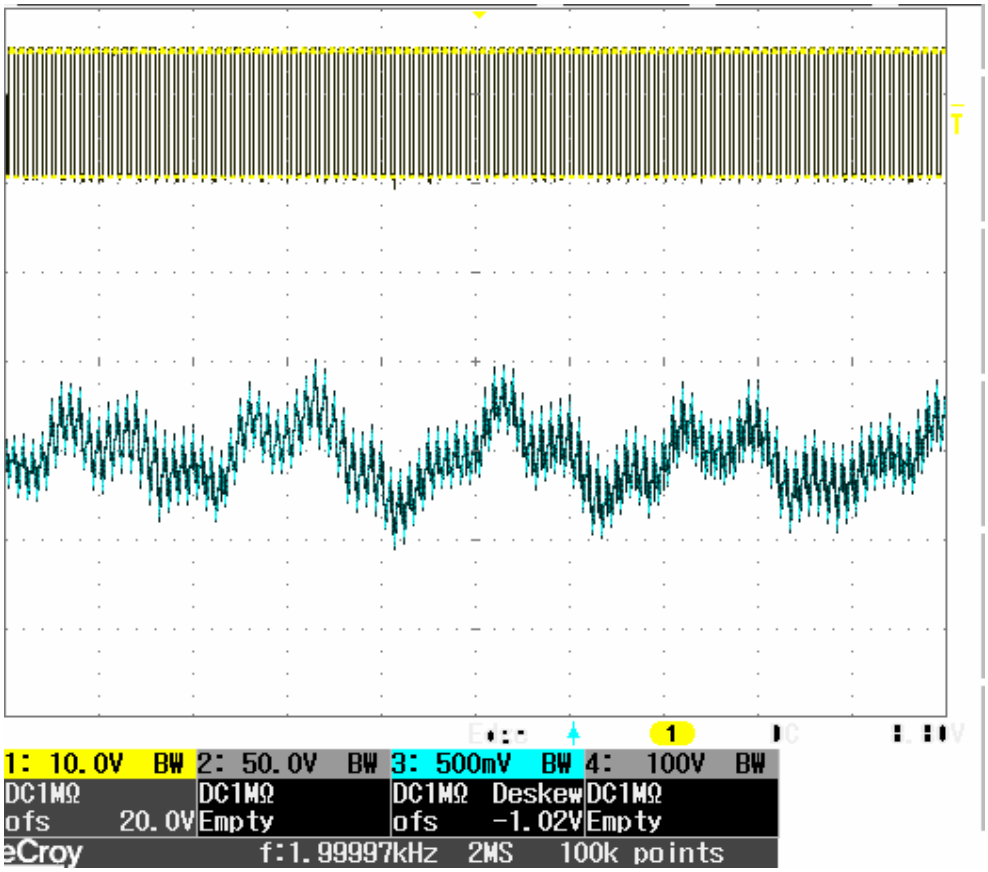

Figure 4.7 Duty cycle and DC link current in application

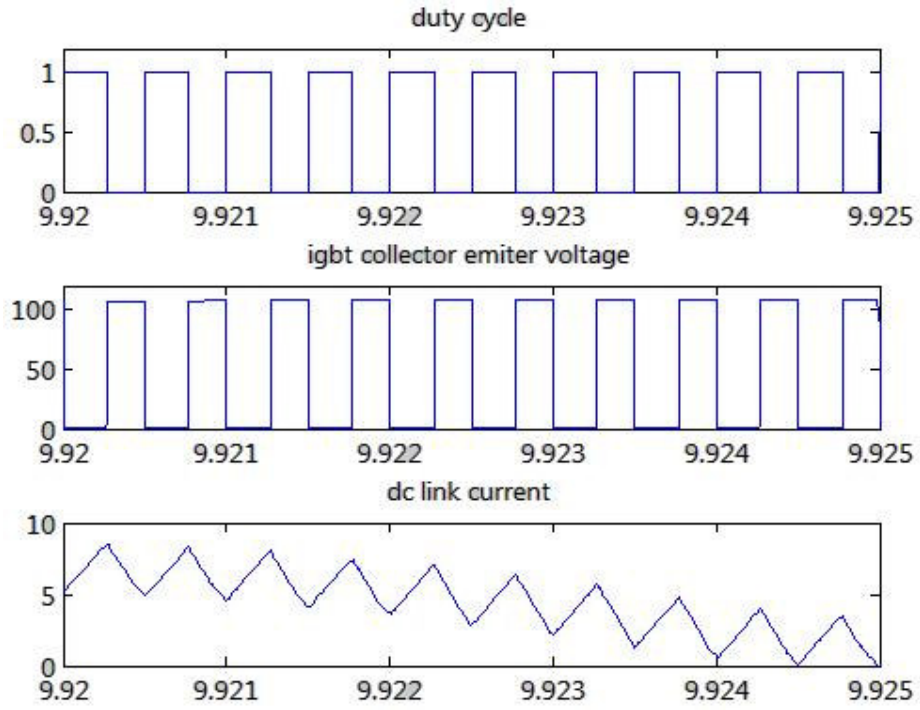

Figure 4.8 Duty cycle and DC link current in MATLAB/Simulink simulation

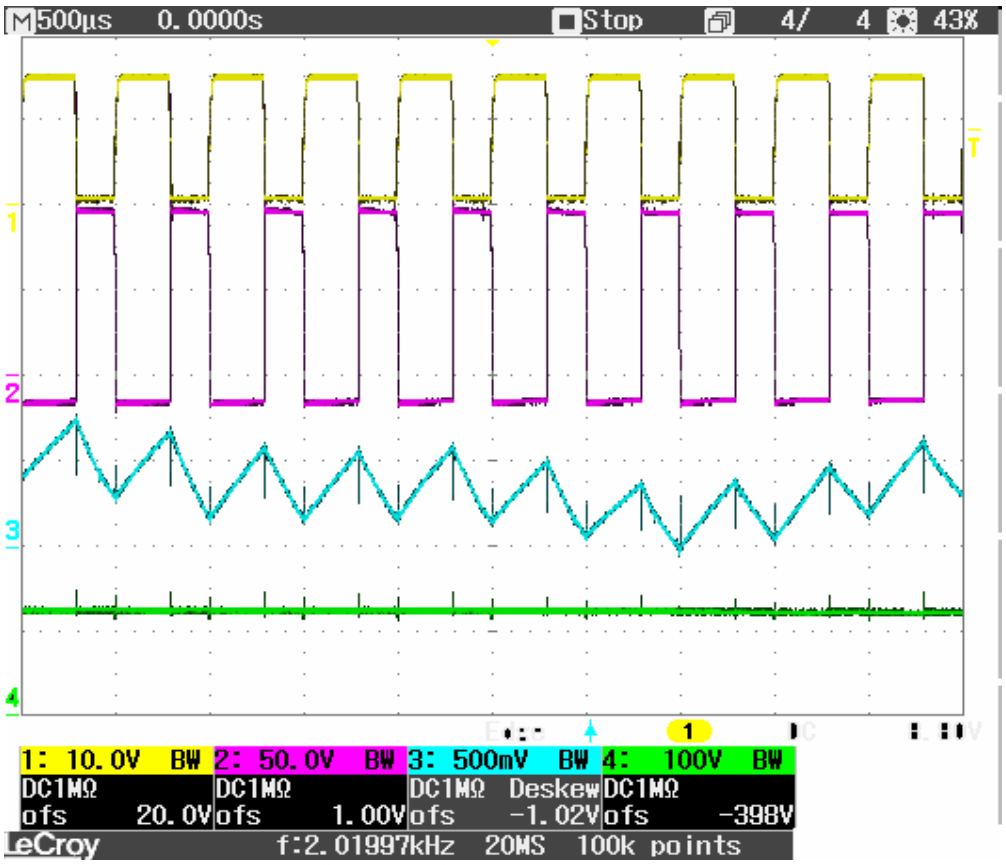

Figure 4.9 Duty cycle and DC link current in application

4.1.2 Experiment and Simulation work at the frequency of 5 KHz.:

Three phase voltage and current waveform are taken from source side which can be seen figure 4.10 and phase A voltage and current is seen same graph and also rotor current voltage and current is seen figure 4.11 ,too

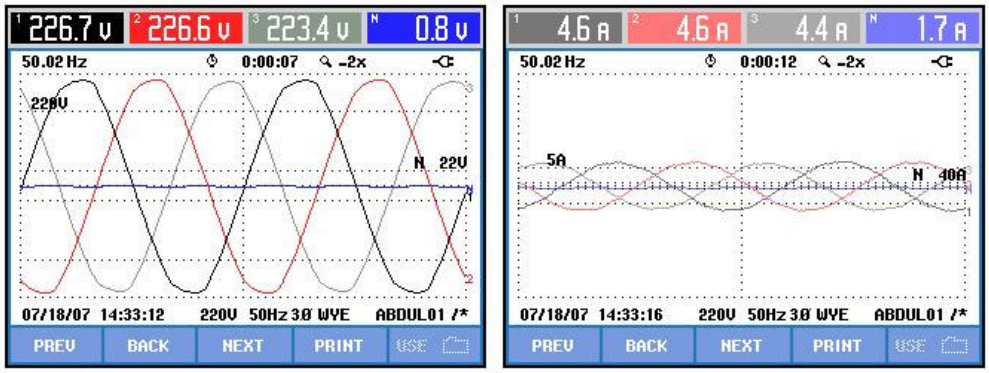

Figure 4.10 Source voltage and source current waveform at experiment

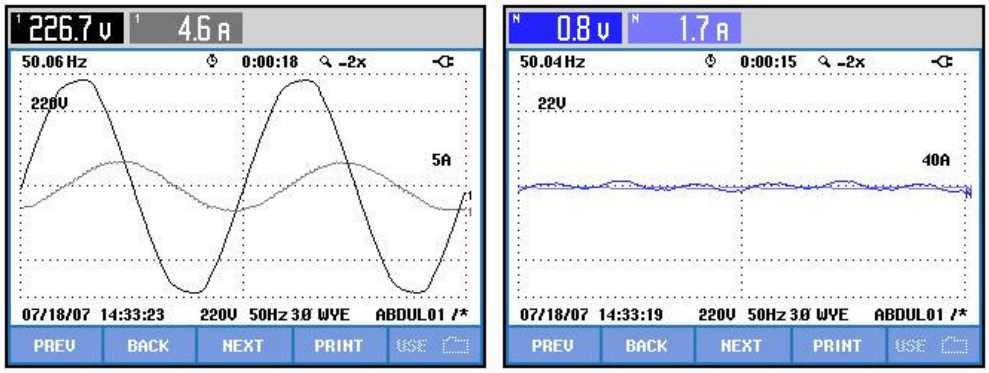

Figure 4.11 Source voltage and Source current waveform in phase A at same graph and neutral voltage and current

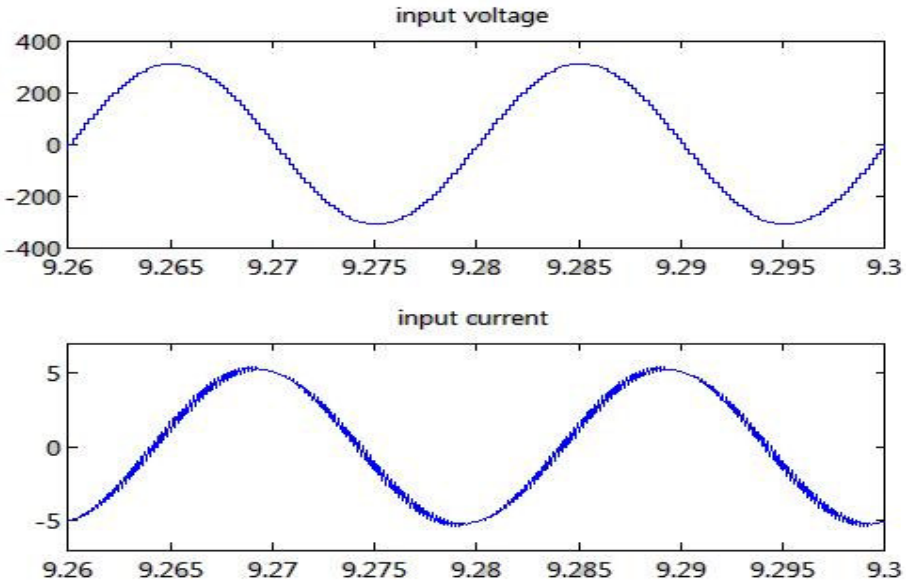

Figure 4.12 Source voltage and Source current waveform of phase A
(Matlab/Simulink simulation result) .

Figure 4.11 and figure 4.12 show the experimental and simulation results which are consistent.

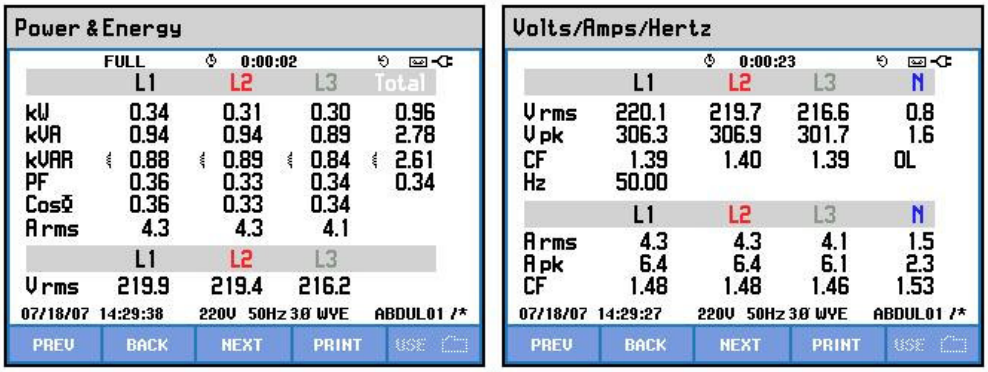

Figure 4.13 Active ,reactive power and input voltage and input current for experimental work

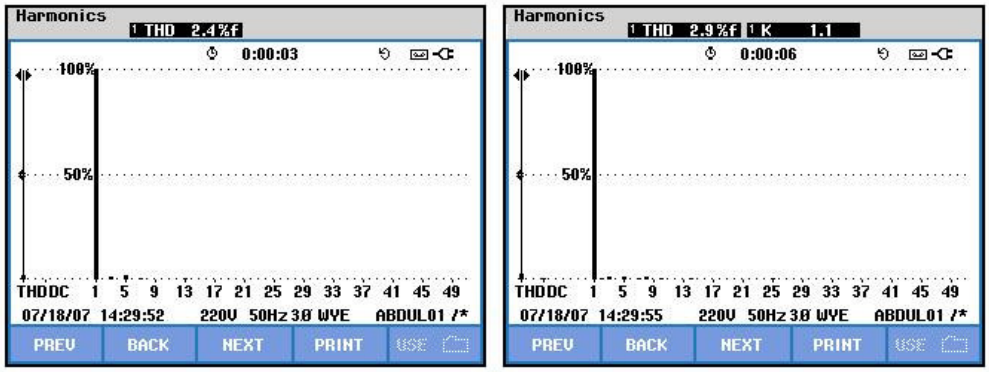

Figure 4.14 Voltage and current harmonics in source

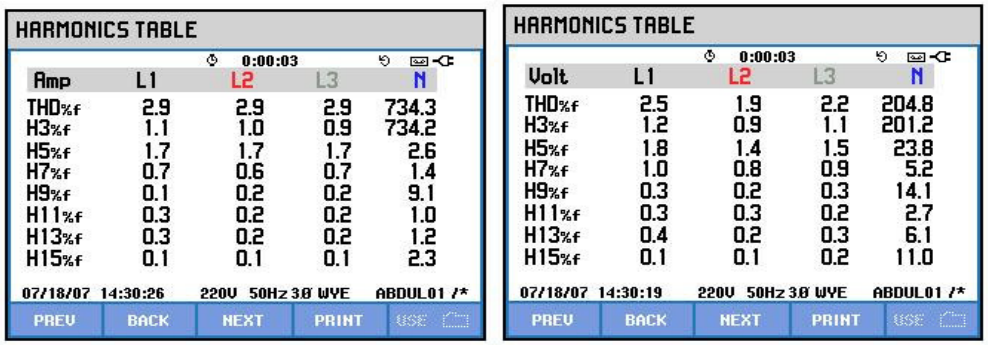

Figure 4.15 Voltage and current harmonics as table

At figure 4.14 and figure 4.15, effect of harmonic content in source voltage and current waveform is seen as table and graph, respectively. It can be seen in these table, current and voltage harmonics are not effective. Is spite of most effective harmonic is fifth harmonic , total harmonic distortion of voltage is %2.4 an current is % 2.9, that means harmonic effect is too low.

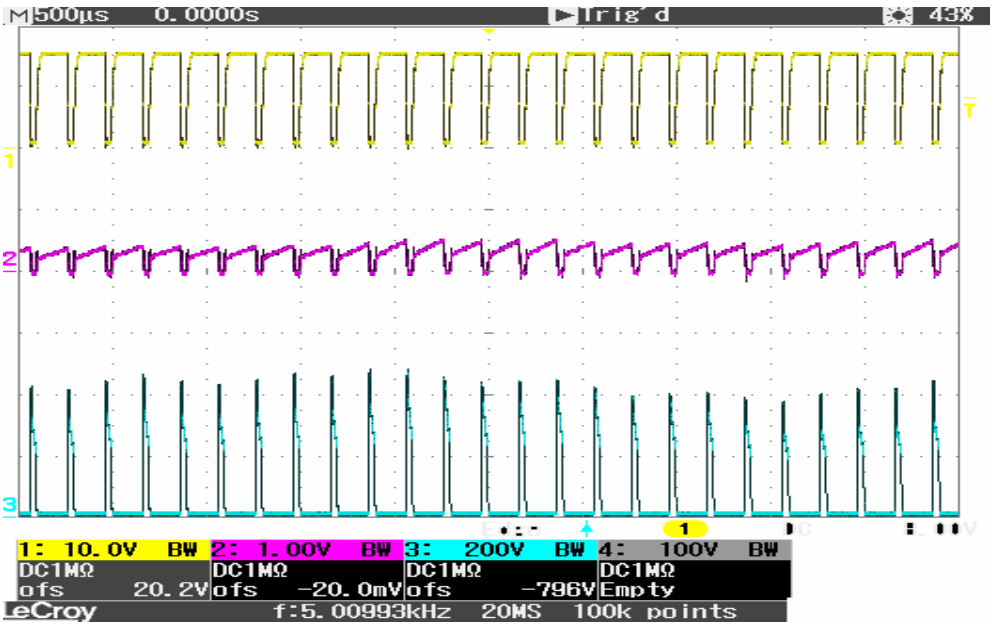

Figure 4.16 Duty cycle, IGBT current Ic , IGBT voltage Vce

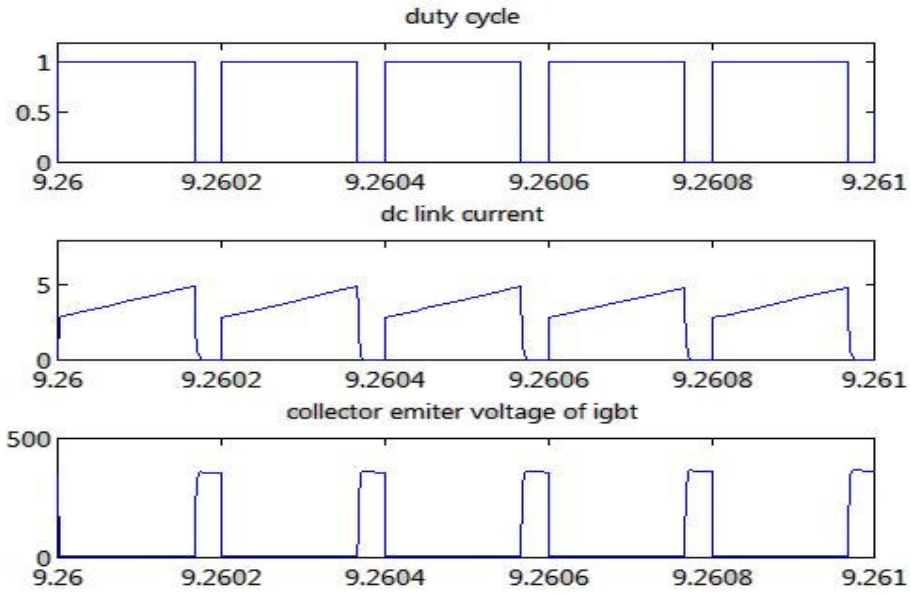

Figure 4.17 Duty cycle, IGBT current Ic , IGBT voltage Vce in matlab simulation

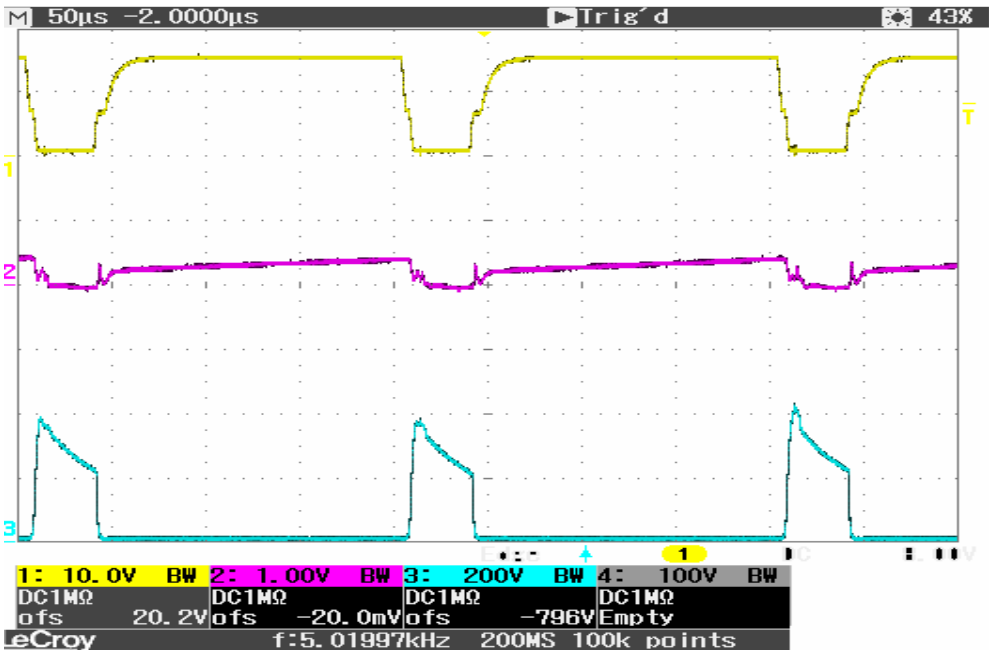

Figure 4.18 Duty cycle, IGBT current Ic , IGBT voltage Vce

In figure 4.16 experimental result can be seen , at this figure duty cycle is seen as %84 on igbt, maximum point of current is seen as 5 amper and voltage of on emitter collector of igbt is near to 300 volt. In figure 4.17 simulation result can be seen at the simulation duty cycle is seen as % 83 , it can be seen peak point of voltage and current is similar to the experimental result, only differences at these figures minimum point of collector emitter voltage is different in simulation and experimental result.

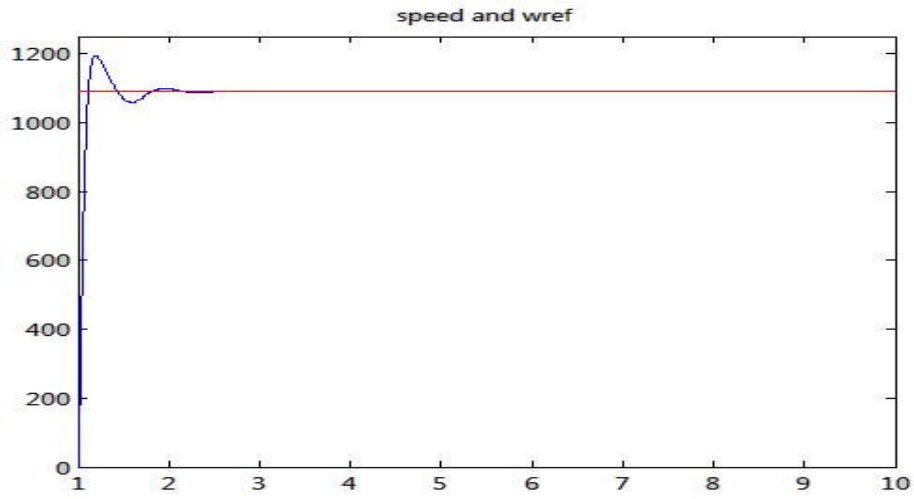

Figure 4.19 Reference speed and actual speed of induction motor in MATLAB/simulink simulation result

4.1.3 Experimental and simulation work for 0.5 Khz switching frequency

3.3 Nm. Torque is applied to the induction machine in simulation and experimental analysis. This torque is applied by seperately excited dc machine.

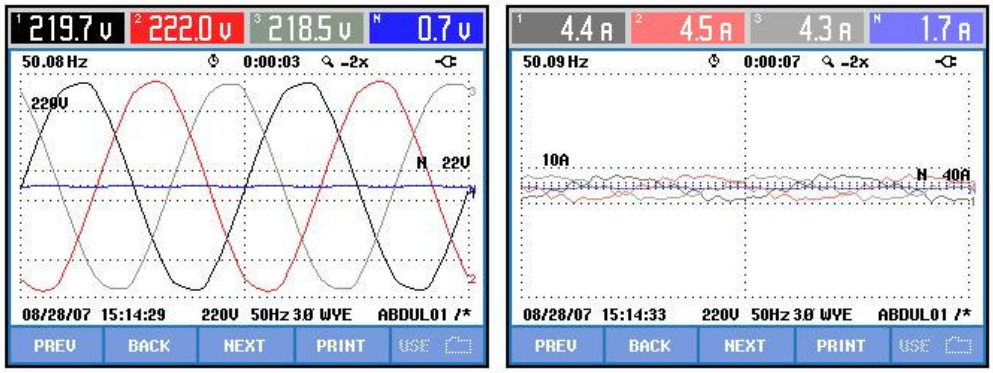

Figure 4.20 Input voltage and current signal for three phase

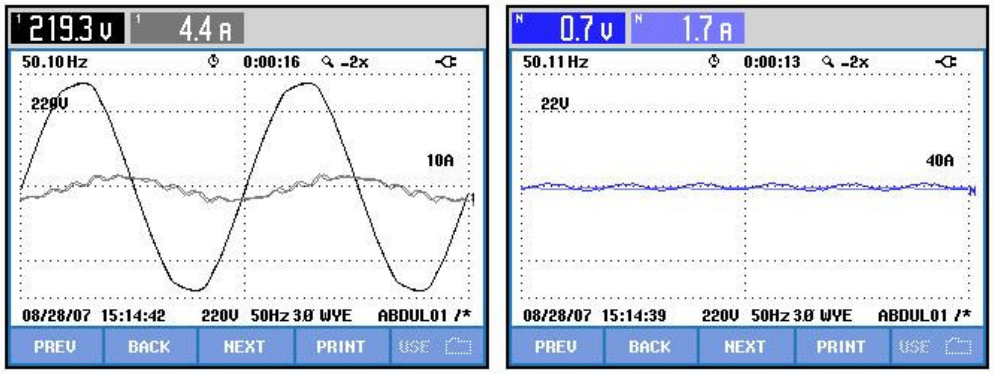

Figure 4.21 Input voltage ,current signal and neutral voltage , current signal

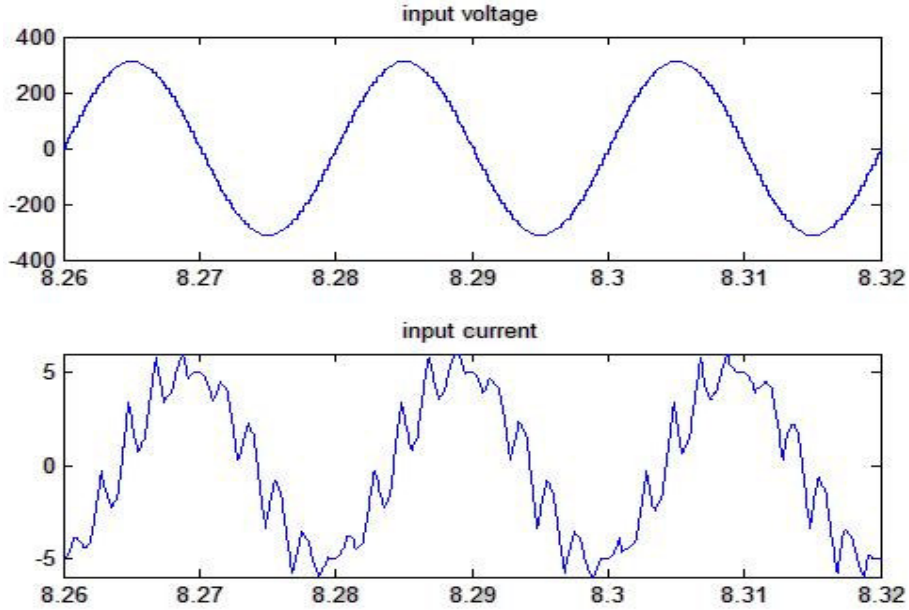

Figure 4.22 Input voltage and current signal in matlab simulation result

Experimental result of input voltage and input current waveform is seen in figure 4.21 and MATLAB/Simulink simulation result is seen in figure 2.22. It can be seen in these results that the voltage and current waveform are similar in both experimental and theoretical work. Harmonics of input current is effective in both simulation and experimental result. In figure 2.21 there is some disturbance in input voltage because of IGBT switching frequency is low which is 500 Hz.

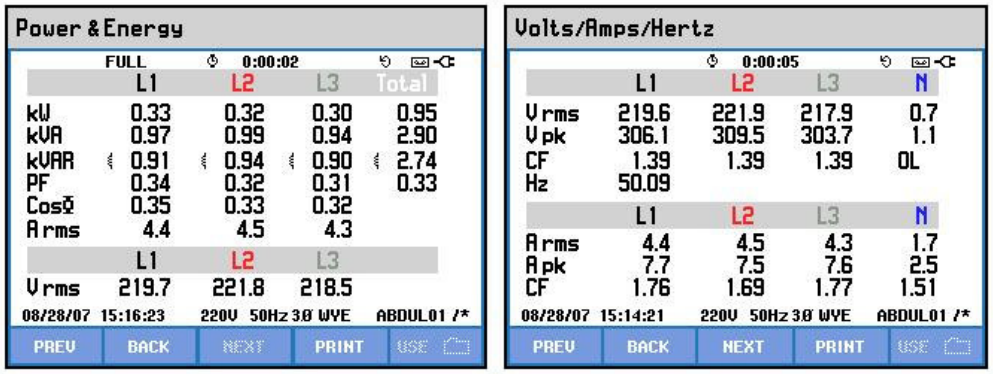

Figure 4.23 Active ,reactive power and input voltage , current value

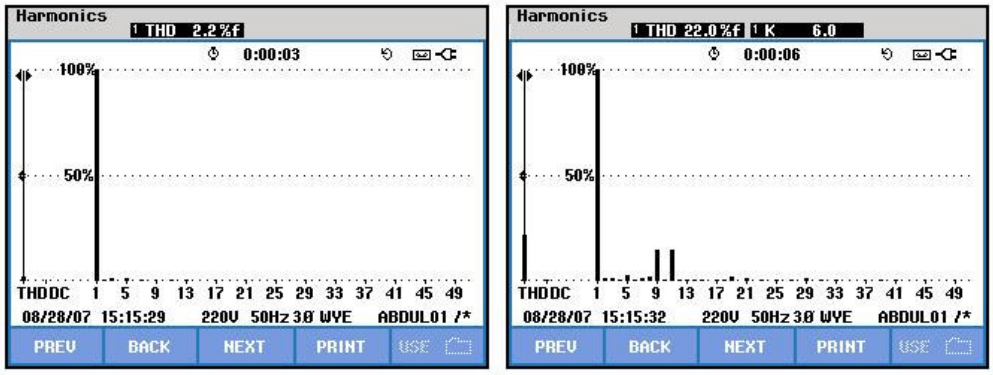

Figure 4.24 Input voltage and current harmonics

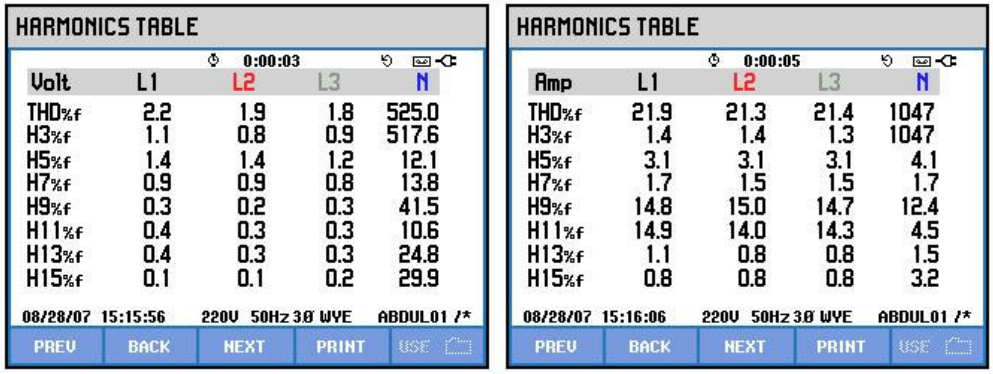

Figure 4.25 Voltage and current harmonics as table

In figure 4.24 , voltage and current harmonic of the system is seen as graphically and in figure 4.25 this harmonic content is shown as numerically. In figure 4.24 voltage total harmonic distortion is seen as %2.3 it can be said voltage harmonic is not effective. But current total harmonic distortion is %24 , that means harmonic content is effective and current signal is really distorted. In current harmonis graph 9^{th} and 11^{th} harmonic are effective and also 19^{th} and 21^{th} harmonics are effective ,too. IGBT is driven in 500 Hz. Clock cycle at this experiment. 9^{th} and 11^{th} harmonics are 450 Hz. and 550 Hz. So this harmonics is occurred by switching IGBT in 500 Hz.

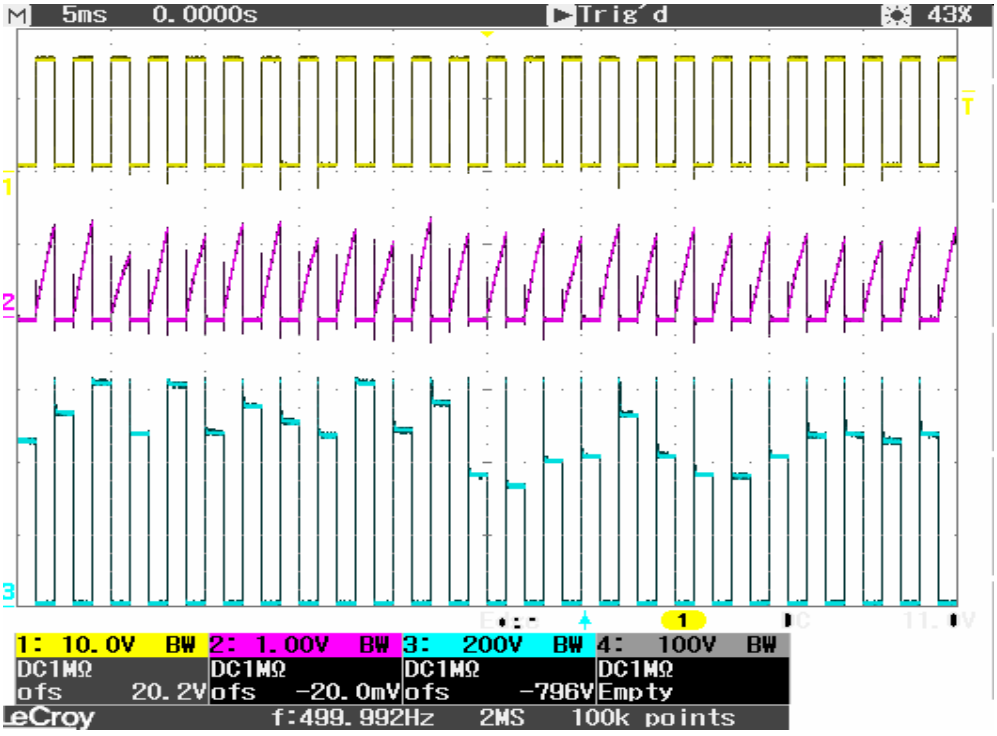

Figure 4.26 Duty cycle, IGBT current Ic , IGBT voltage Vce

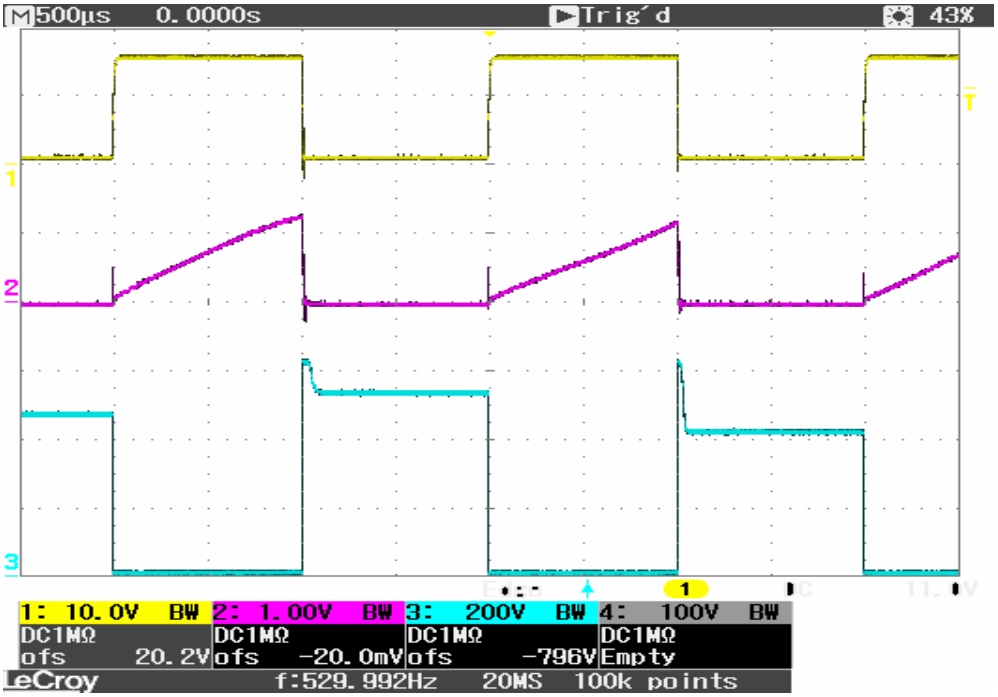

Figure 4.27 Duty cycle, IGBT current Ic , IGBT voltage Vce

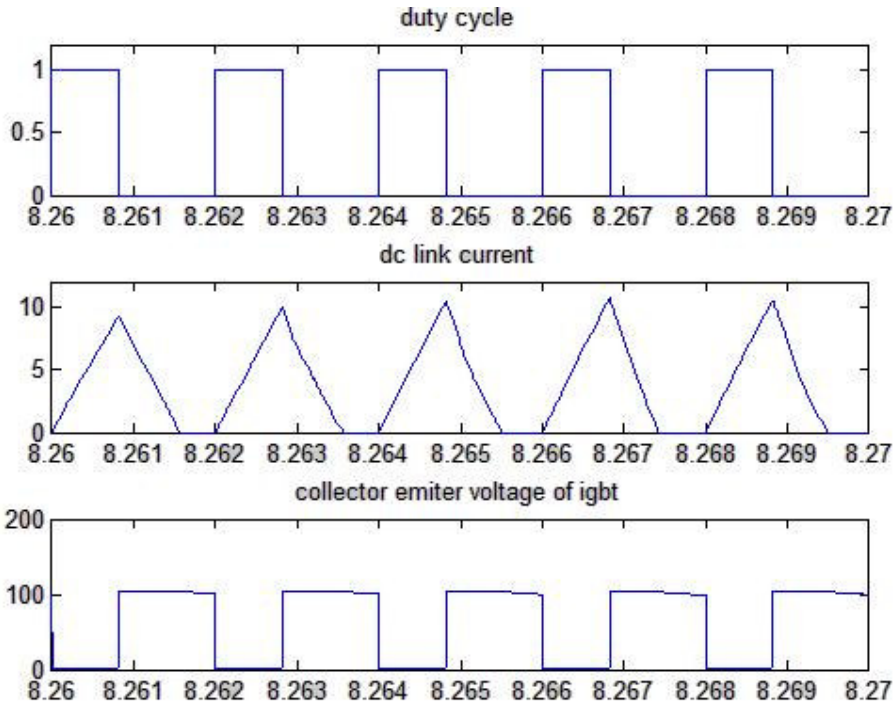

Figure 4.28 Duty cycle, IGBT current Ic , IGBT voltage Vce in simulation result

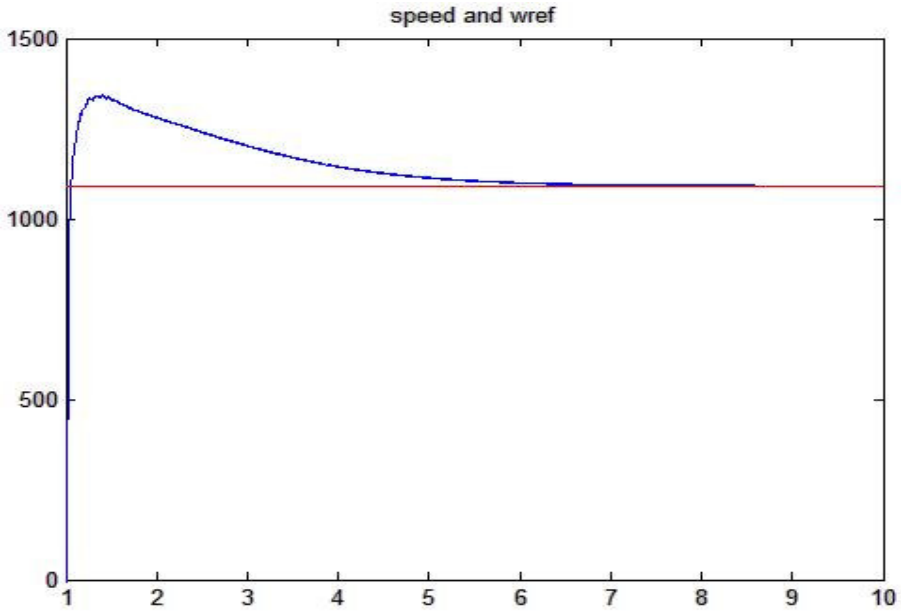

Figure 4.29 Reference speed and actual speed of induction motor in MATLAB/simulink simulation result

4.2 Three Chopped Resistor

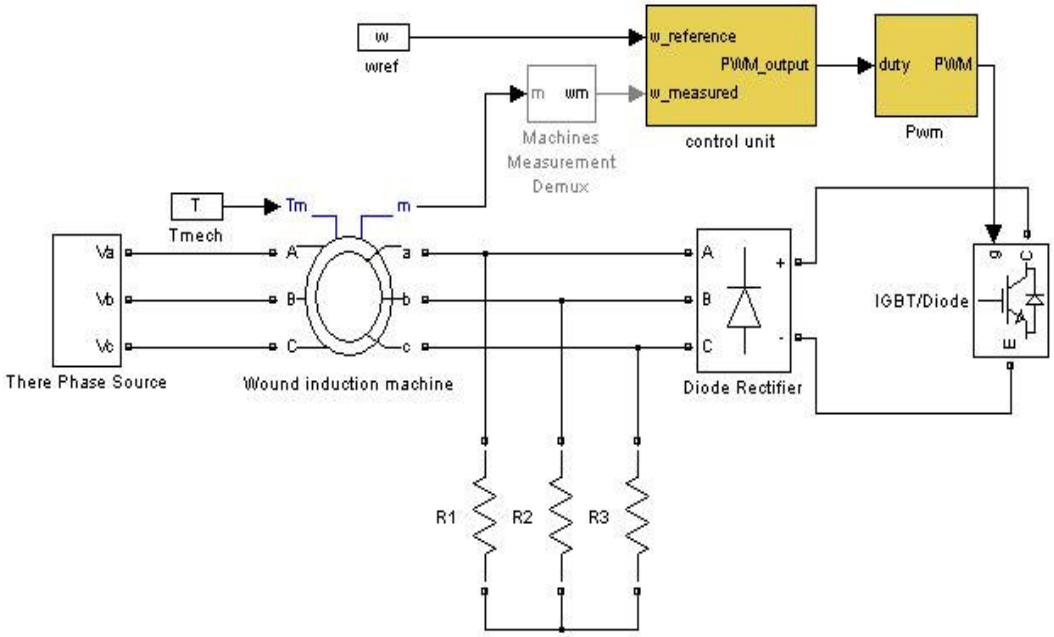

Figure 4.30 Schematic of the system

At simulation, induction machine parameters given in Appendix A are measured and used. load resistance is chosen 64 Ω. At the simulation, fuzzy logic controller is used, its all parameters and model same with experimental work.

In application, the shaft of the DC generator is coupled to wound rotor induction machine and 3.3 Nm load is applied. Torque is set to the wound rotor induction machine by the separately excited DC generator at speed 1100 rpm.

4.2.1 Experimental and simulation work for 2 Khz switching frequency

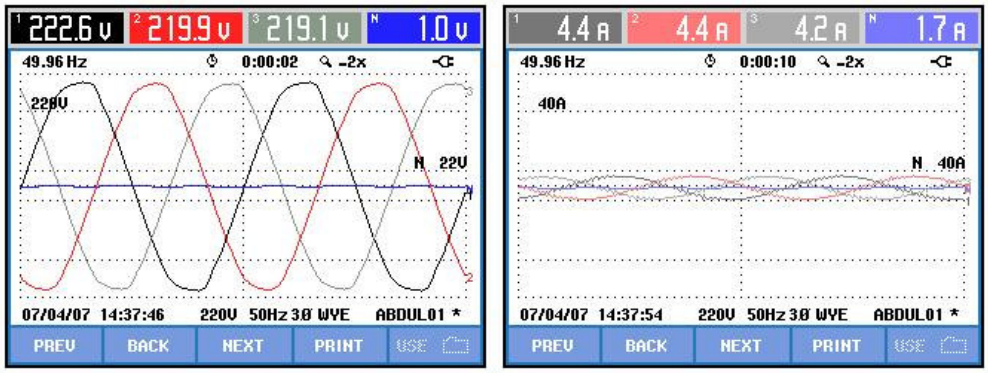

Figure 4.31 Input voltage and current signal for three phase

In figure 4.31 shows the variation of voltage and current in experiment and simulation.

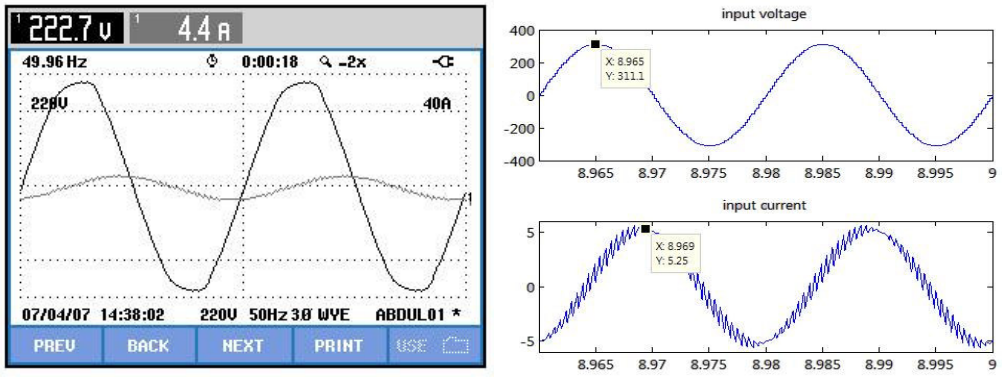

Figure 4.32 Input voltage and current signal for phase A in experimental work and simulation

In figure 4.32 shows the variation of voltage and current for phase A in experiment and simulation. Both graph shows amplitude and power factor is similar in experiment and simulation.

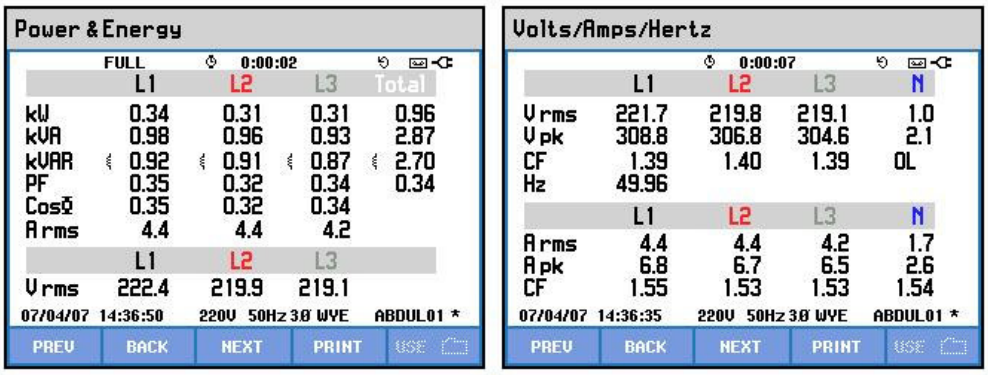

Figure 4.33 Active ,reactive power and input voltage , current value

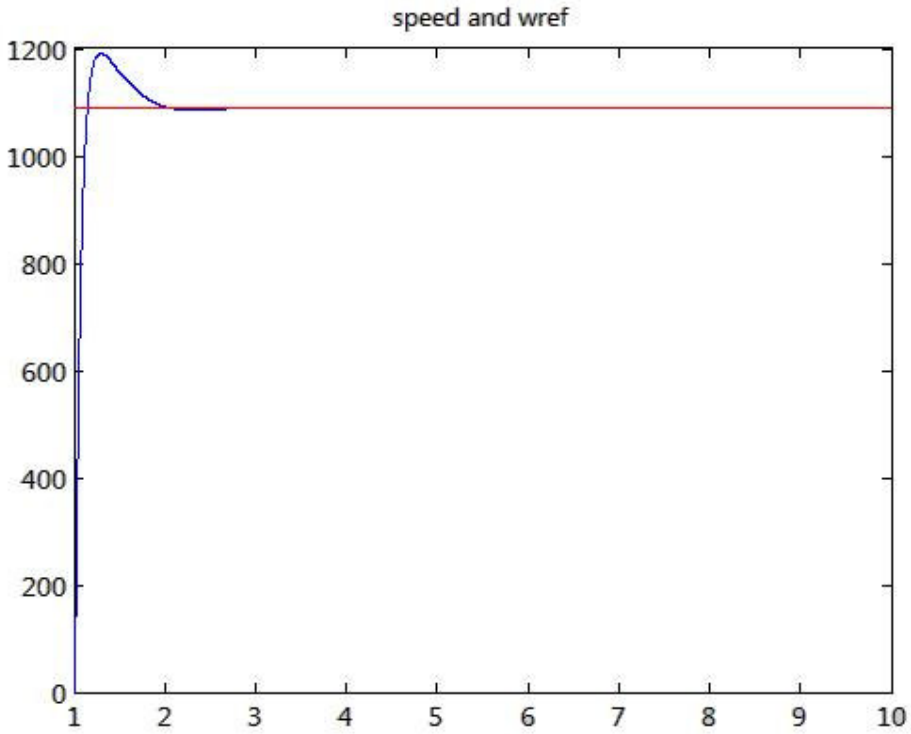

Figure 4.34 Reference speed and actual speed of induction motor in MATLAB/simulink simulation result

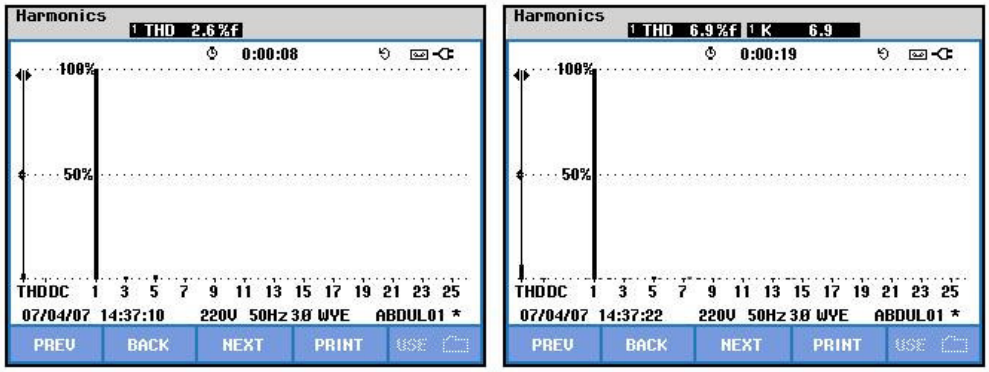

Figure 4.35 Voltage and current harmonics in source

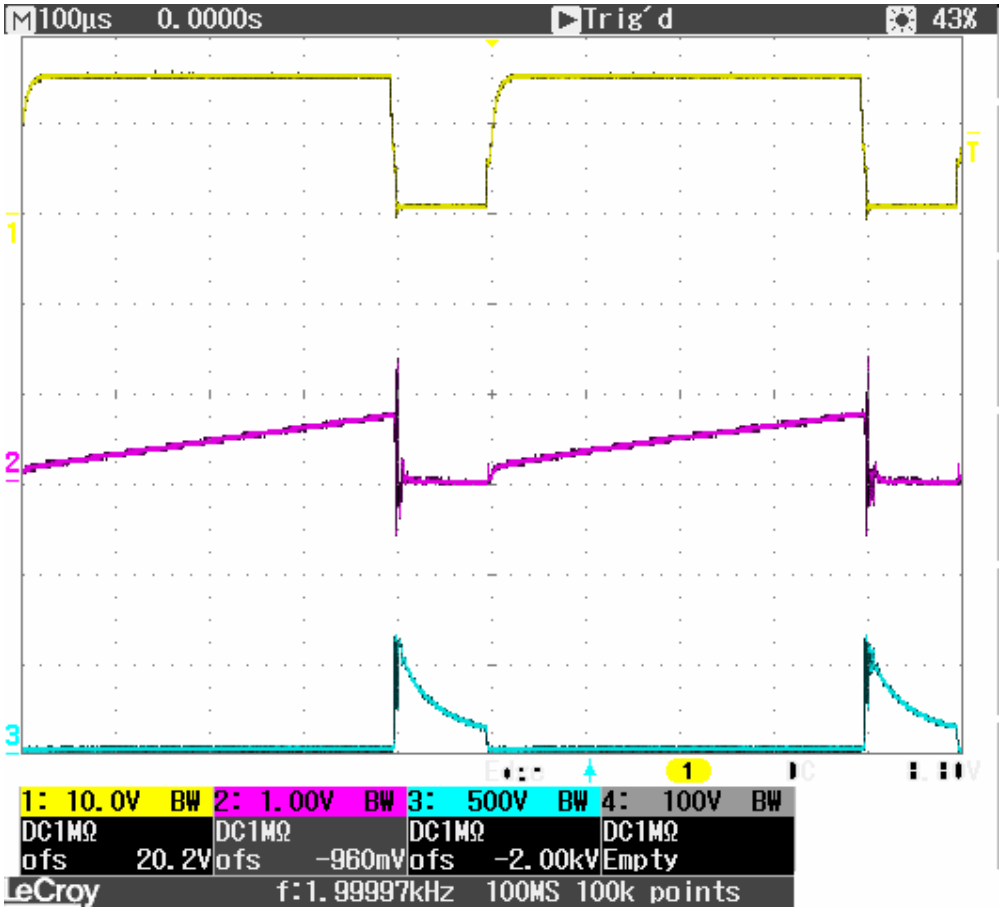

Figure 4.36 Duty cycle, IGBT current Ic , IGBT voltage Vce

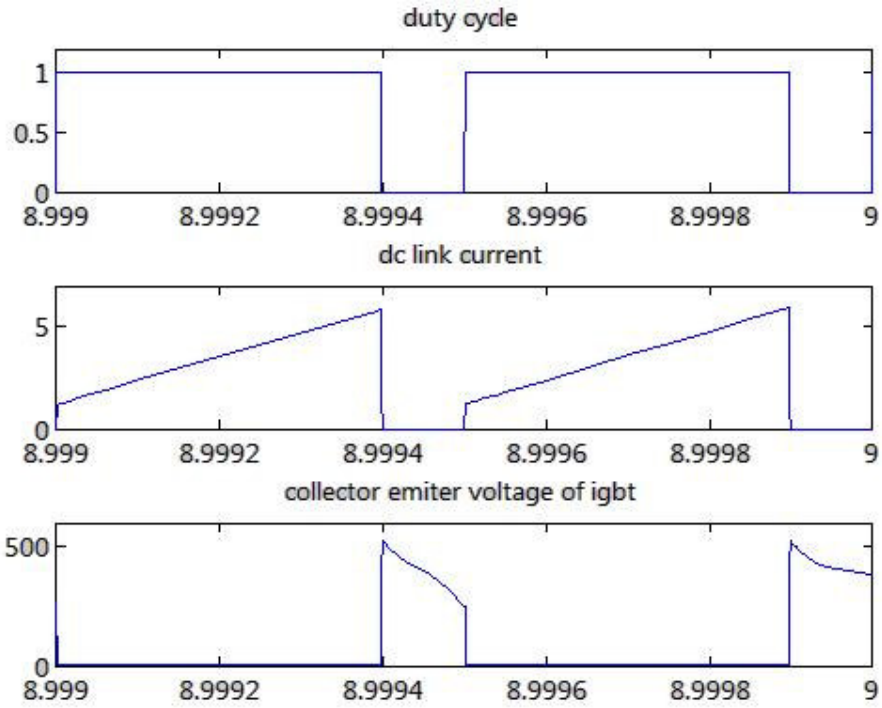

Figure 4.37 Duty cycle, IGBT current Ic , IGBT voltage Vce

Table 4.2 Simulation results

P (W)	Q (VAR)	S (VA)	Cos∅	Vinput(rms)	Iinput(rms)
700	2350	2452	0,285	220	3,75

If the figure 4.37 is compared with table 4.1, it can be seen that the results of Matlab model and experimental output are very near to each other. The duty cycle is %80 for 2Khz driving frequency.

Most important thing in three chopped resistor application is seen as 600 volt in pins of the IGBT's emitter – collector. This voltage is seen both experimental and simulation work . Figure 4.36 shows experimental work and blue graph shows emitter collector voltage of IGBT whose peak value goes to 600 volt and figure 4.37 shows simulation result of same experiment and peak value of the voltage is seen as 600 volt, too

Speed control of three chopped resistor system is more difficult than boost chopper and single resistor system. In spite of the same controller and induction motor drive same speed with same torque value, speed of the three chopped resistor system reach reference value lower than boost chopper and single resistor system.

Snubber circuit of IGBT is not so important in boost chopper with single resistor circuit, but in three chopped resistor circuit snubber circuit is so important. In turn on and turn off voltage of the emitter – collector of IGBT rise to 600 volt and there is only IGBT at system after full wave rectifier. So snubber has important role to protect IGBT in three chopped resistor circuit. At the boost chopper circuit this voltage reach maximum 400 volt and also there is a 1175 uf capacitor after full wave rectifier circuit importance of snubber circuit decrease.

4.2.2 Experimental and simulation work for 5 Khz switching frequency

3.3 Nm. Torque is applied to the induction machine in simulation and also experimental part. This torque is applied by separately excited dc machine.

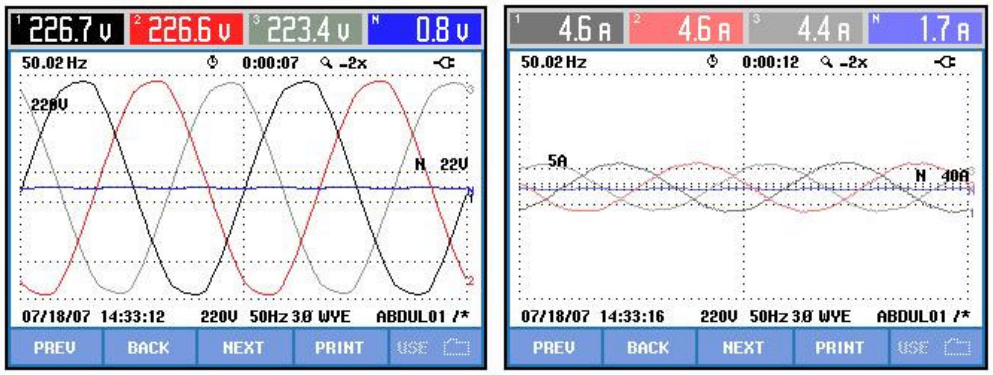

Figure 4.38 Input voltage and current signal for three phase

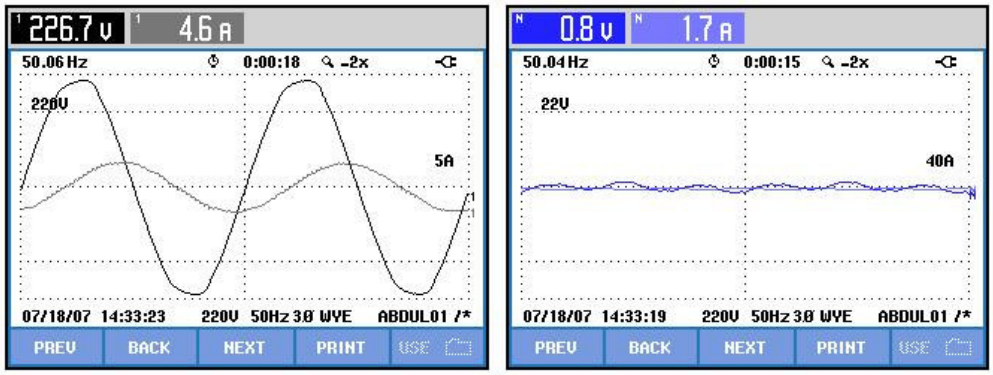

Figure 4.39 Input voltage ,current signal and neutral voltage , current signal

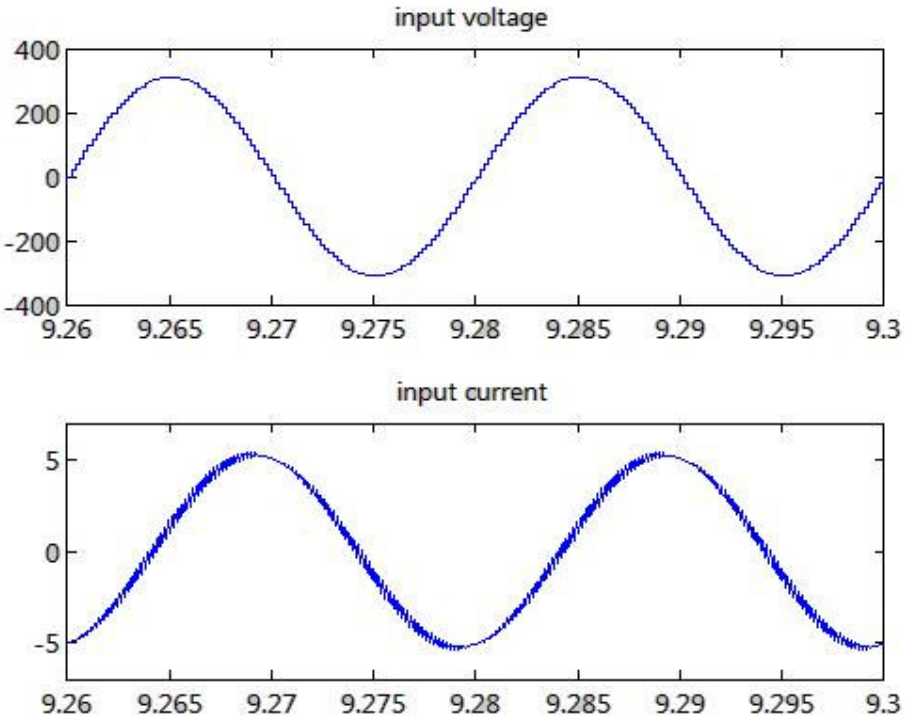

Figure 4.40 Input voltage and current signal in matlab simulation result

MATLAB/Simulink simulation result is seen in figure 4.39. It can be seen in these results voltage and current waveform is exactly same. Harmonics of input current is not so effective in both simulation and experimental result.

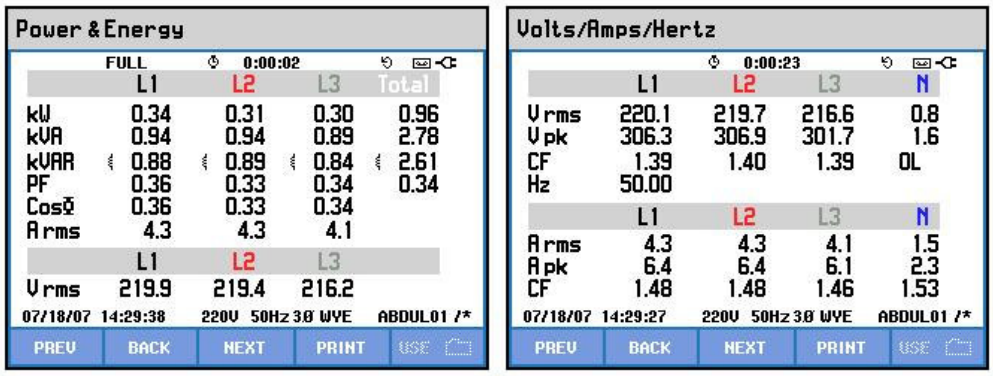

Figure 4.41 Active ,reactive power and input voltage , current value

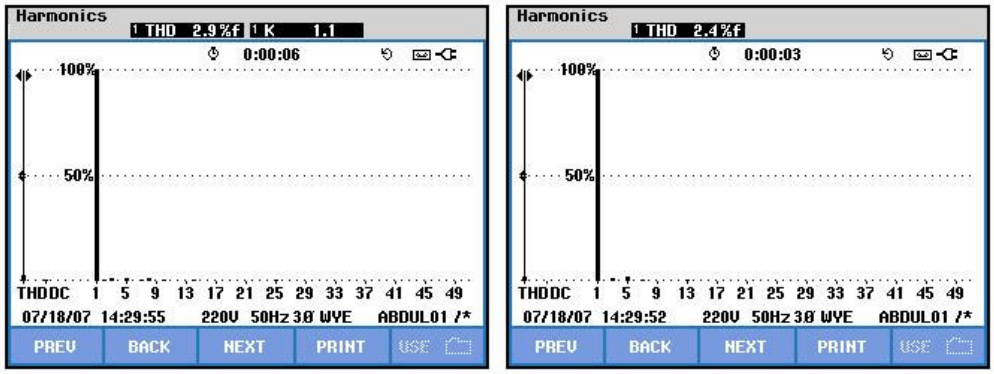

Figure 4.42 Input voltage and current harmonics

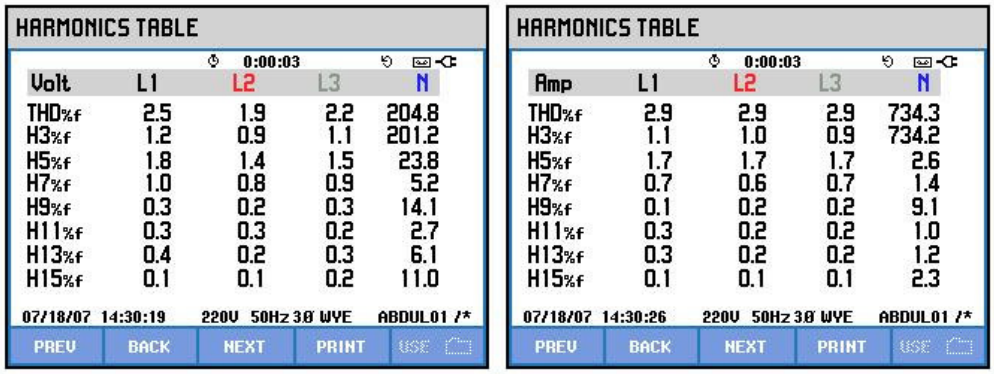

Figure 4.43 Voltage and current harmonics as table

In figure 4.41, voltage and current harmonic of the system is seen as graphically and in figure 4.42 this harmonic content is shown as numerically. In figure 4.41 voltage total harmonic distortion is seen as %2.4 it can be said voltage harmonic is not effective and also current total harmonic distortion is seen as %2.9, so current harmonics are not effective, too

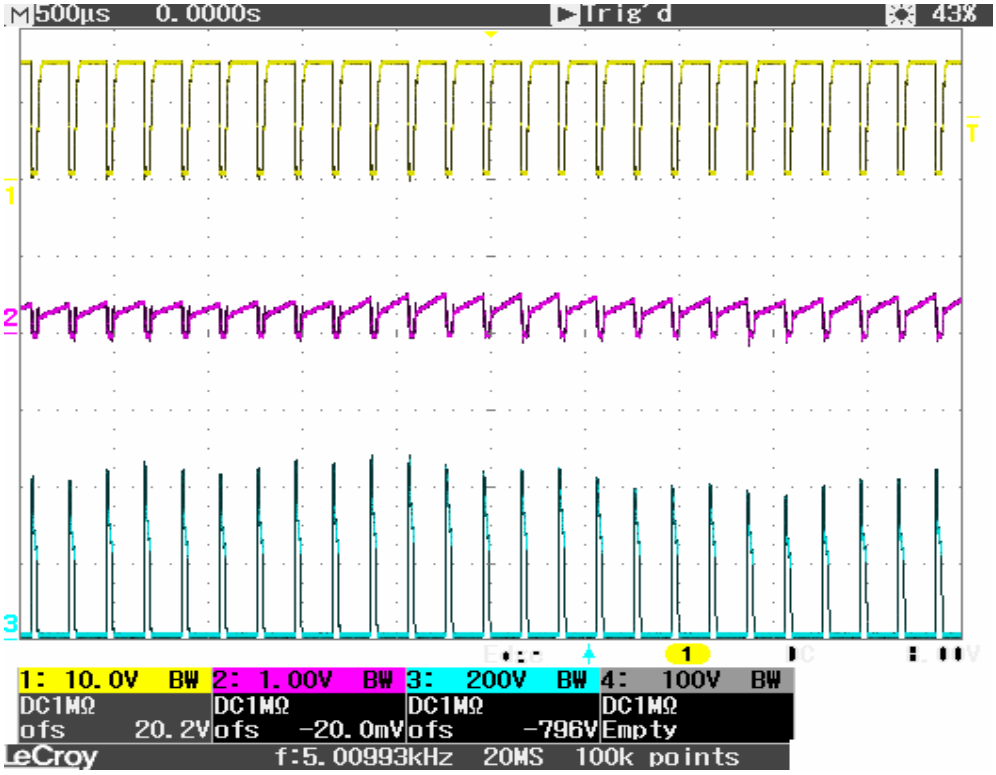

Figure 4.44 Duty cycle, IGBT current Ic , IGBT voltage Vce

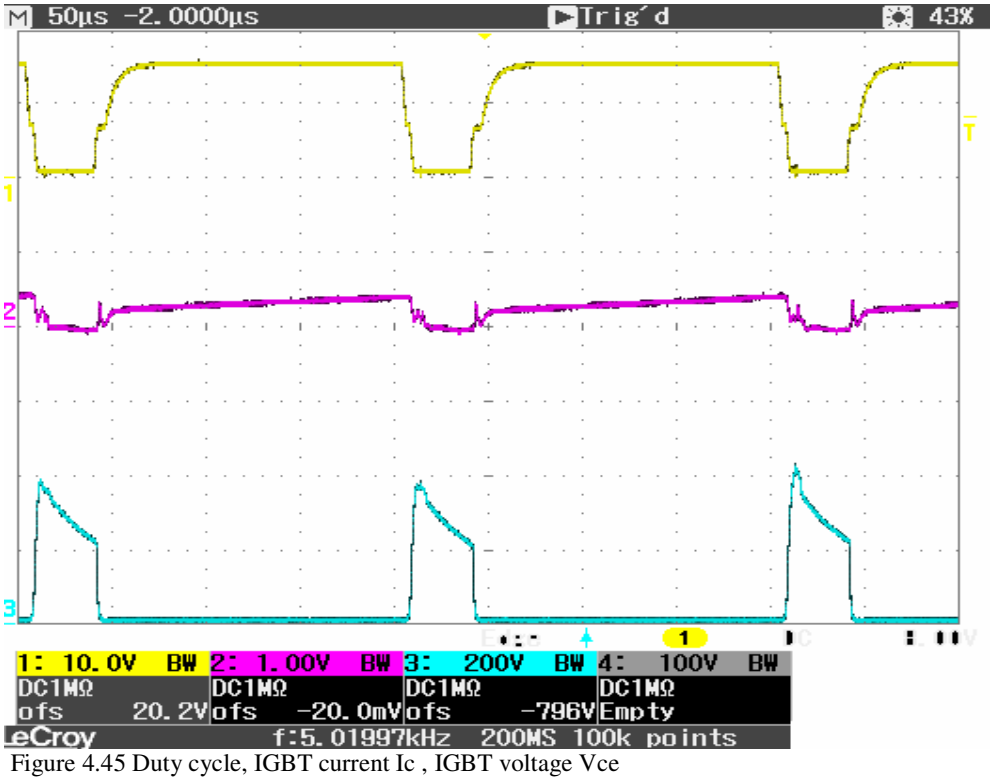

Figure 4.45 Duty cycle, IGBT current Ic , IGBT voltage Vce

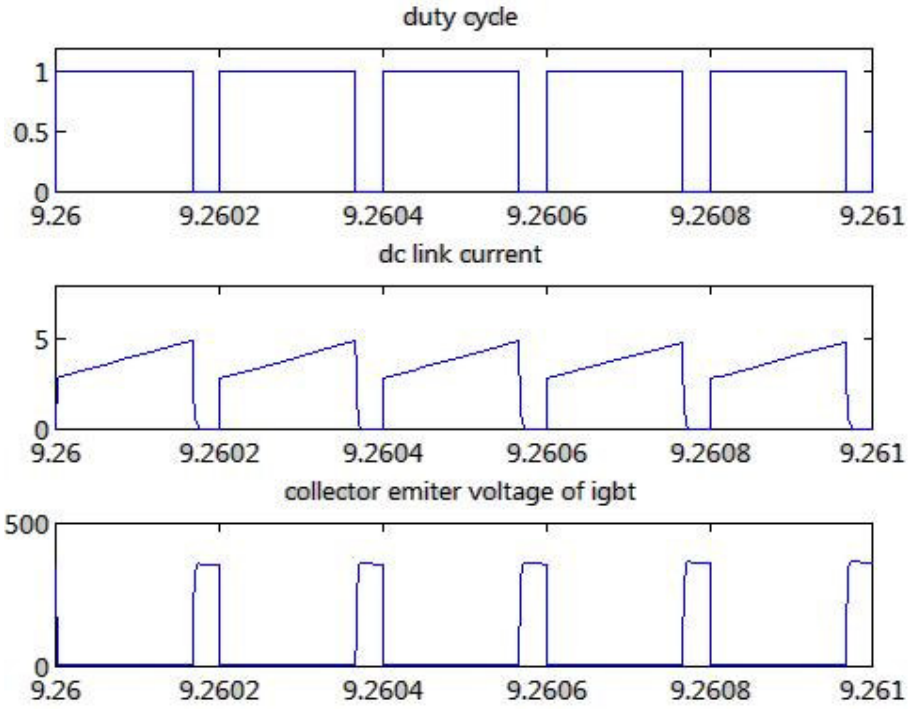

Figure 4.46 Duty cycle, IGBT current Ic , IGBT voltage Vce in simulation result

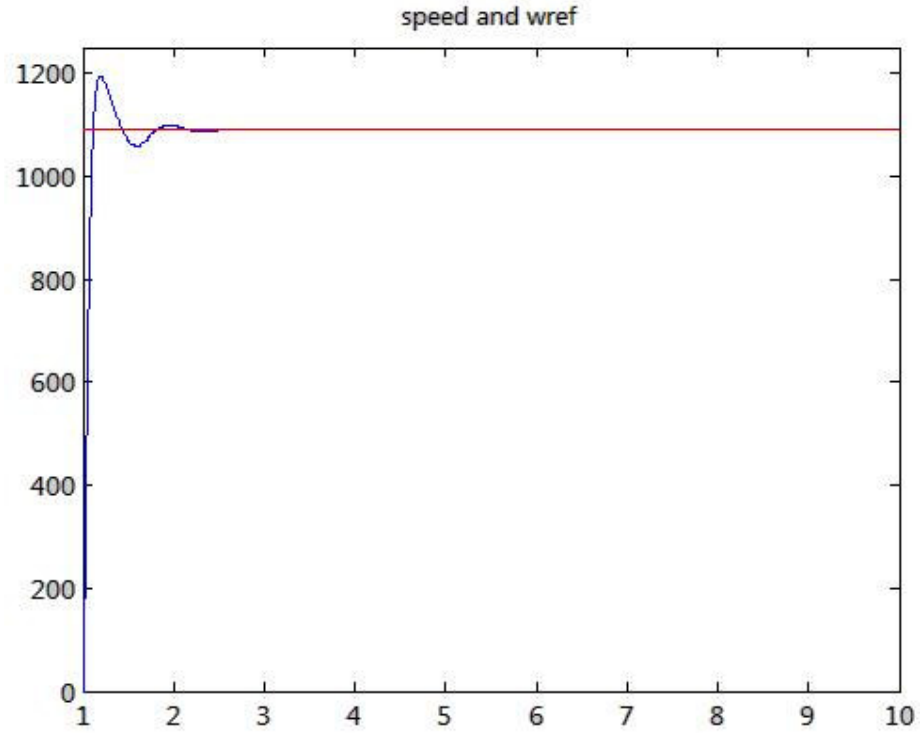

Figure 4.47 Reference speed and actual speed of induction motor in MATLAB/simulink simulation result

4.2.3 Experimental and simulation work for 0.5 Khz switching frequency

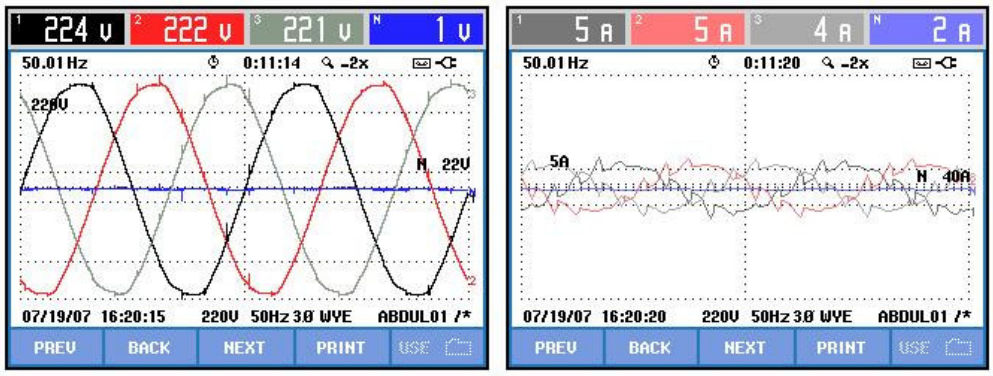

Figure 4.48 Input voltage and current signal for three phase

In figure 4.31 input voltage and input current waveform which, can be seen, is taken by power quality analyzer in experimental work. At the input current waveform , there is a neutral current about 1.7 A. it is happened instability of the source current.

In figure 4.48 shows the variation of voltage and current in experiment and simulation. In neutral current has 2 A. instability current in experiment..

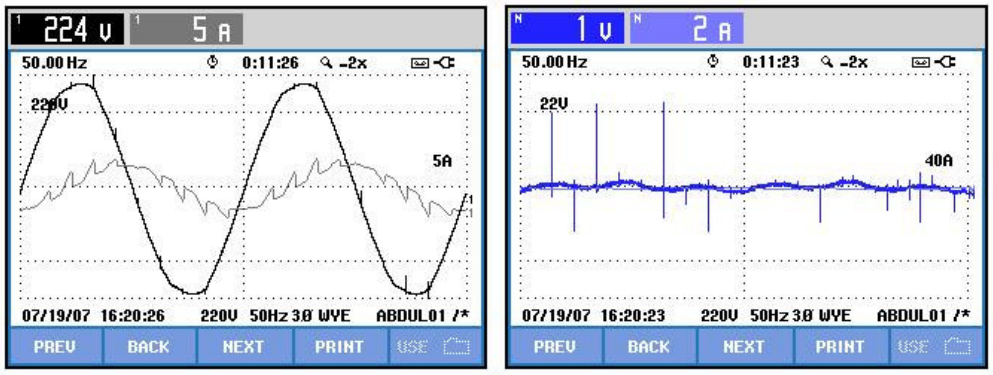

Figure 4.49 Input voltage ,current signal and neutral voltage , current signal

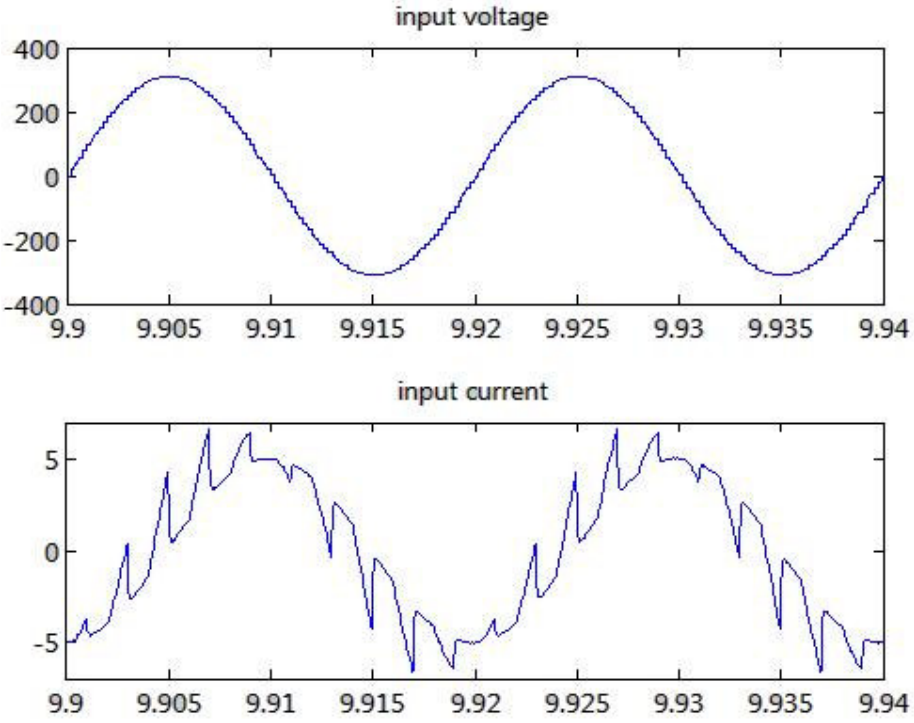

Figure 4.50 Input voltage and current signal in matlab simulation result

Experimental result of input voltage and input current waveform is seen in figure 4.49 and MATLAB/Simulink simulation result is seen in figure 4.50. It can be seen in these results that the voltage and current waveform are similar in both experimental and theoretical work. Harmonics of input current is effective in both simulation and experimental result. In figure 4.49 there is some disturbance in input voltage because of IGBT switching frequency is low which is 500 Hz.

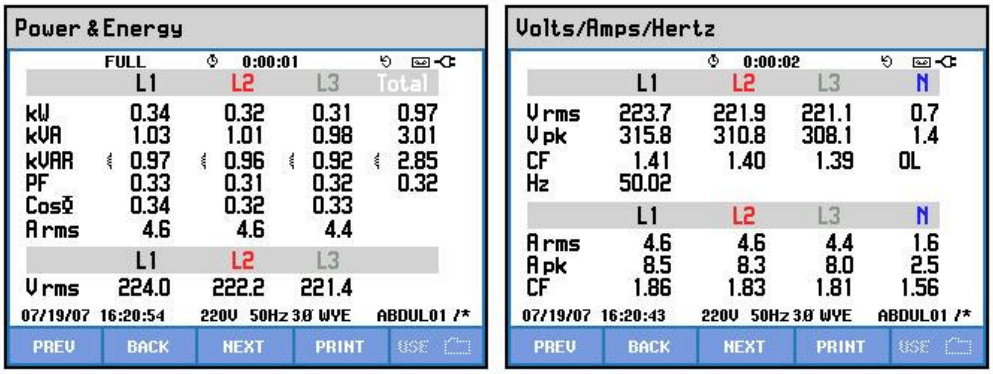

Figure 4.51 Active ,reactive power and input voltage , current value

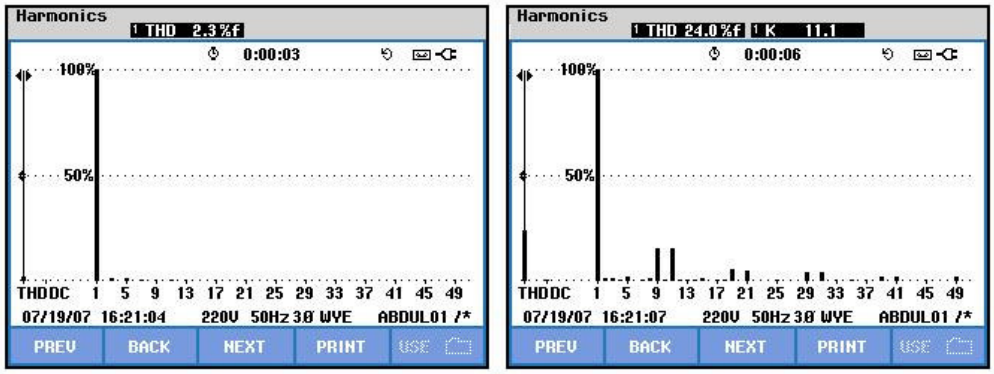

Figure 4.52 Input voltage and current harmonics

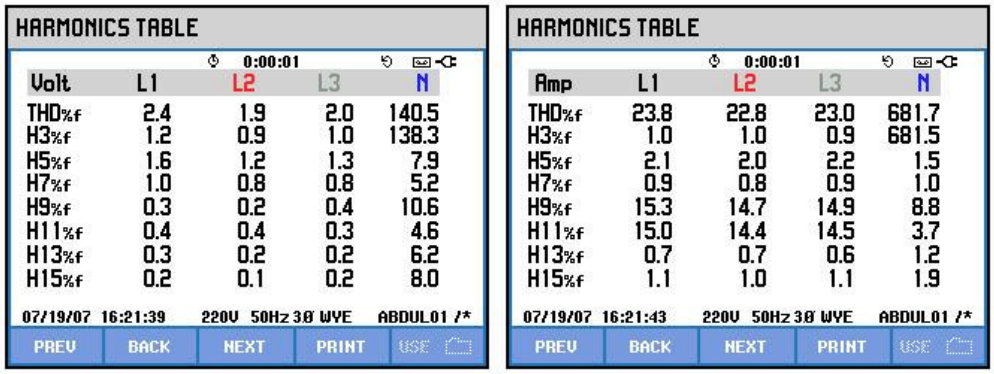

Figure 4.53 Voltage and current harmonics as table

In figure 4.52, voltage and current harmonic of the system is seen as graphically and in figure 4.53 this harmonic content is shown as numerically. In figure 4.52 voltage total harmonic distortion is seen as %2.3 it can be said voltage harmonic is not effective. But current total harmonic distortion is %24, that means harmonic content is effective and current signal is really distorted. In current harmonics graph 9^{th} and 11^{th} harmonic are effective and also 19^{th} and 21^{st} harmonics are effective ,too. IGBT is driven in 500 Hz. Clock cycle at this experiment. 9^{th} and 11^{th} harmonics are 450 Hz. and 550 Hz. So this harmonics is occurred by switching IGBT in 500 Hz.

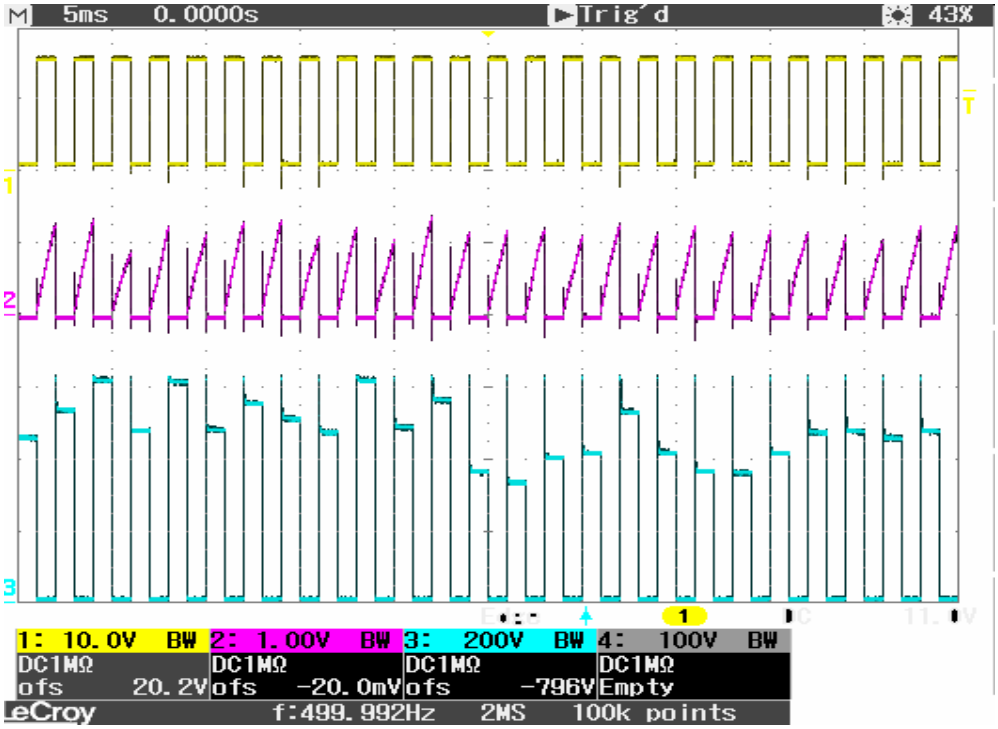

Figure 4.54 Duty cycle, IGBT current Ic , IGBT voltage Vce

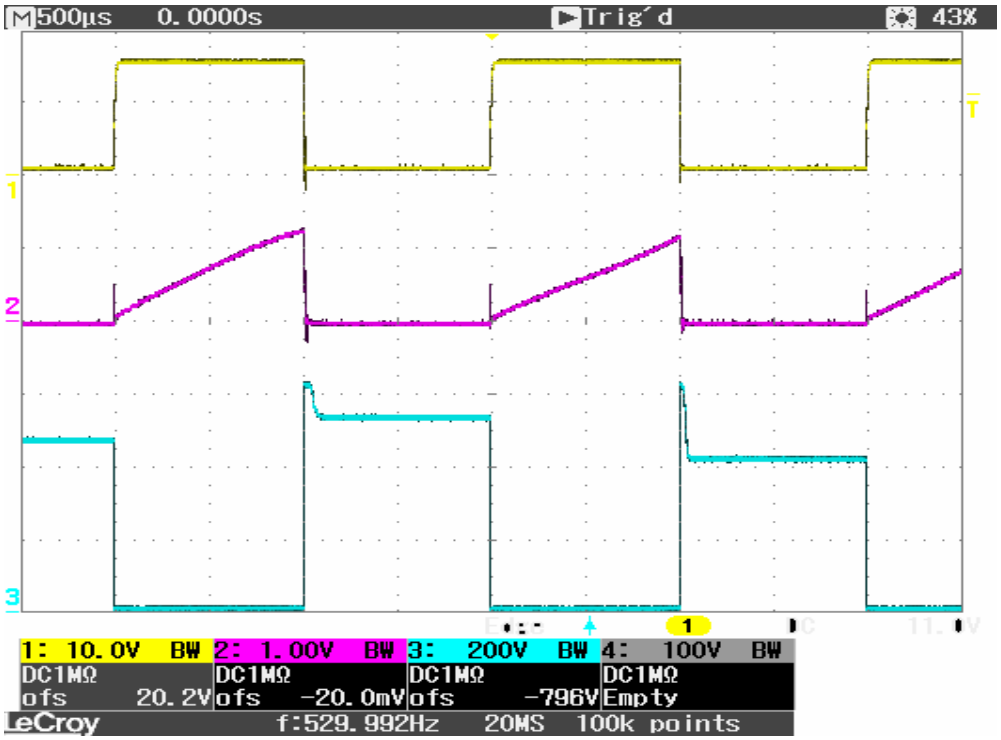

Figure 4.55 Duty cycle, IGBT current Ic , IGBT voltage Vce

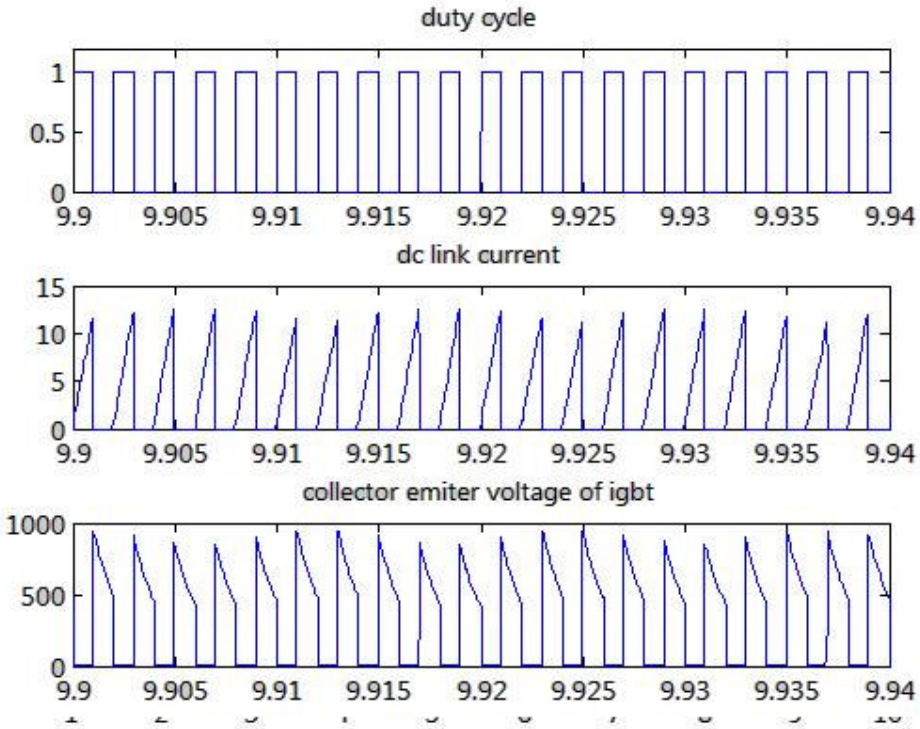

Figure 4.56 Duty cycle, IGBT current Ic , IGBT voltage Vce in simulation result

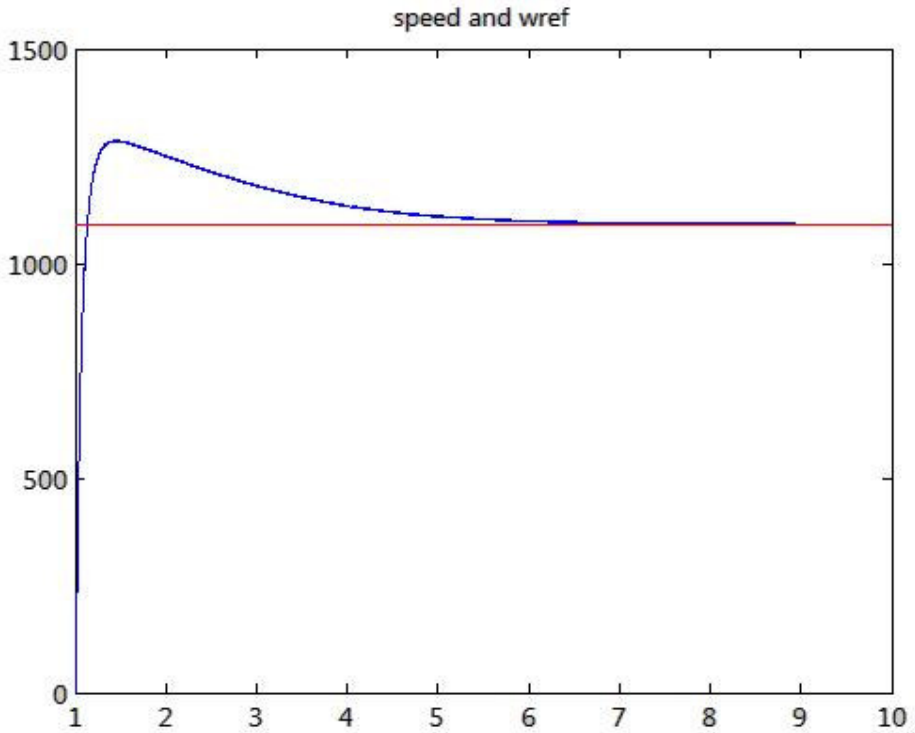

Figure 4.57 Reference speed and actual speed of induction motor in MATLAB/simulink simulation result

CHAPTER FIVE

HARMONIC ANALYSIS OF TWO SYSTEM

5.1 Harmonic Analysis in experimental work

These two systems are examined for power quality parameters such as harmonic currents. The simulation and experimental works are performed and their results are compared for both systems. In experimental work, fluke 430 series power quality analyzer is used and result is taken to computer and it is compared by MATLAB/simulink simulation results.

5.1.1 Three Chopped Resistor

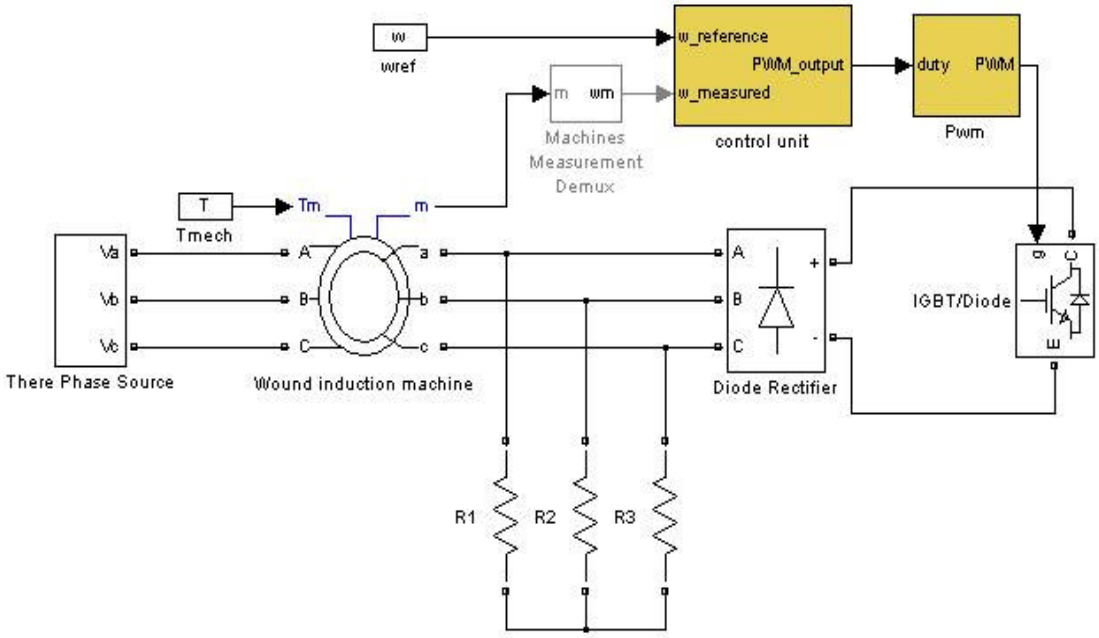

Figure 5.1 Schematics of the system

IGBT is driven with duty cycle and controlled fuzzy logic controller at three different frequencies 5, 2 and 0.5 KHz. In experimental part, graphically and tabulated results are taken by power quality analyzer. In graphical part, the first 50 harmonics are displayed and also total harmonic distortion is displayed for voltage and current waveforms. The first 15 harmonics of all three phases are displayed independently and also total harmonic distortion is displayed independently for

voltage and current, too. All the results are recorded under 3.2 Nm. constant torque and 1100 rpm.

5.1.1.1 Laboratory work for 5 KHz :

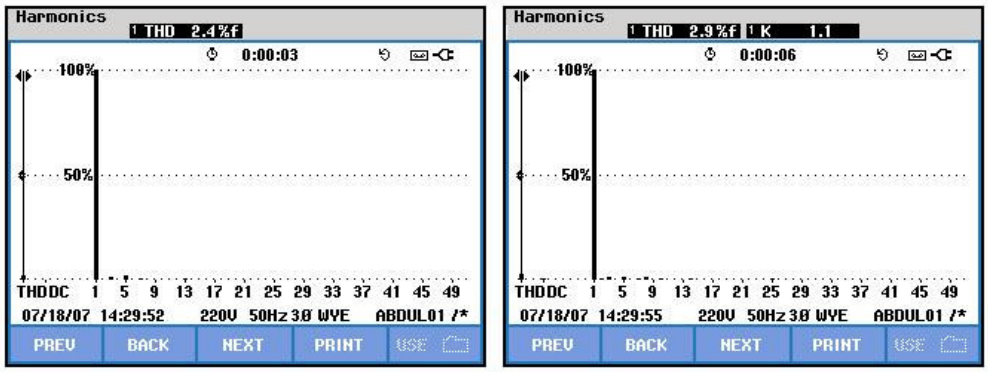

Figure 5.2 Voltage and current harmonic at the source side

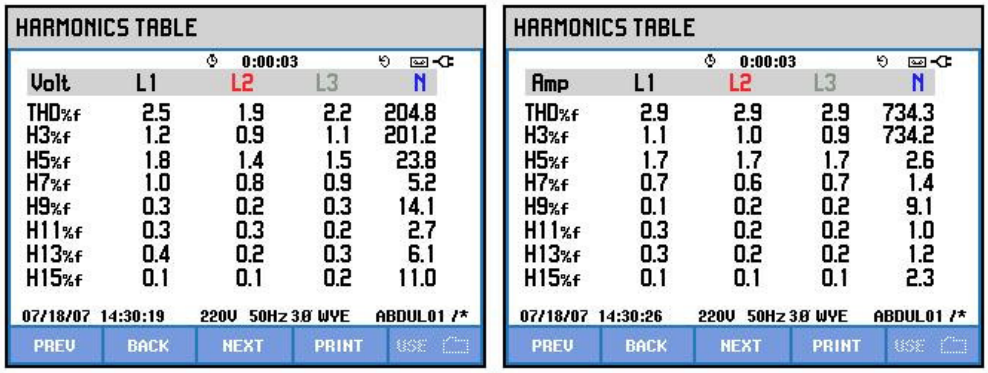

Figure 5.3 Voltage and current harmonic as tabulated at the source side

At 5 KHz frequency, the voltage and current harmonics are not effective and also total harmonic distortion is %2.4 for voltage harmonics and %2.9 for current harmonics. So at this frequency for driving IGBT for three chopped resistor is suitable.

5.1.1.2 Laboratory work for 2 KHz :

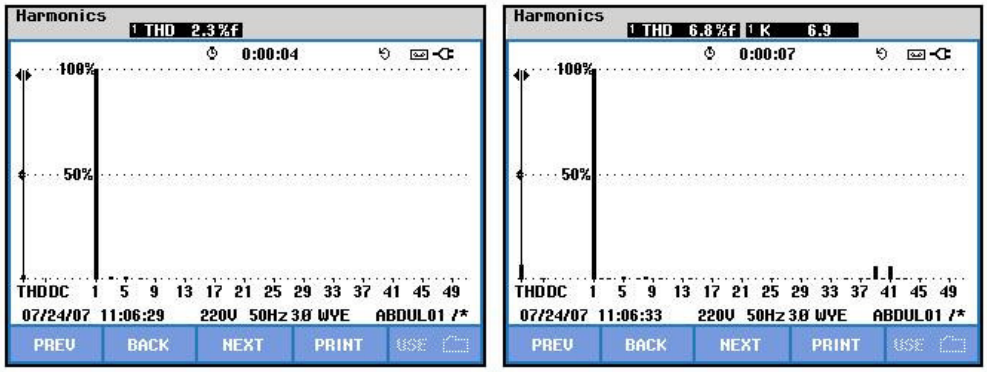

Figure 5.4 Voltage and current harmonic at the source side

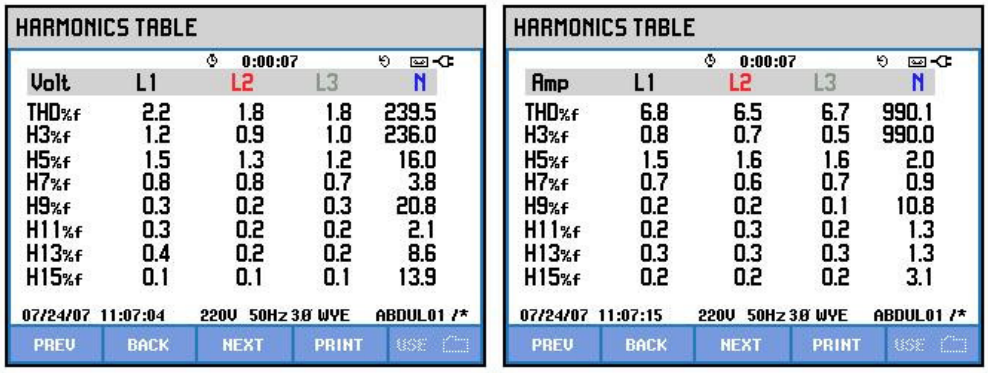

Figure 5.5 Voltage and current harmonic as tabulated at the source side

At 2 KHz frequency, the voltage and current harmonic is not so effective but in current harmonics 39th and 41st harmonics are effective. Total harmonic distortion is %2.3 for voltage harmonics and %6.8 for current harmonics. Because of the effect of 39th and 41st harmonics total harmonic distortion for current is increase importantly.

5.1.1.3 Laboratory work for 0.5 KHz

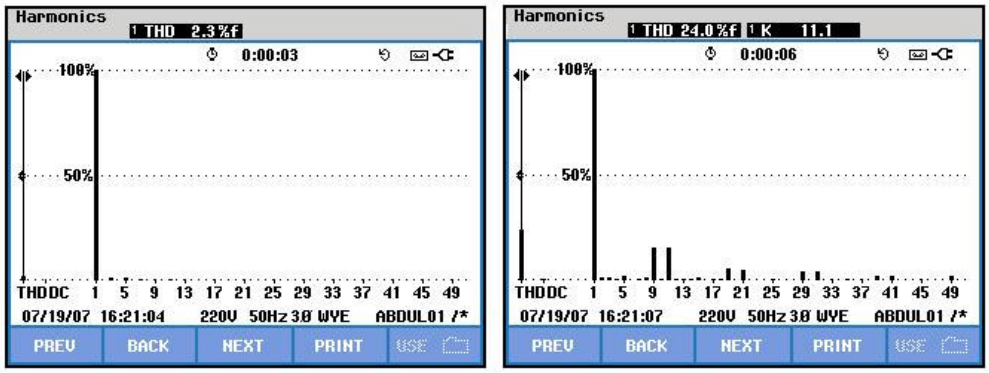

:

Figure 5.6 Voltage and current harmonic at the source side

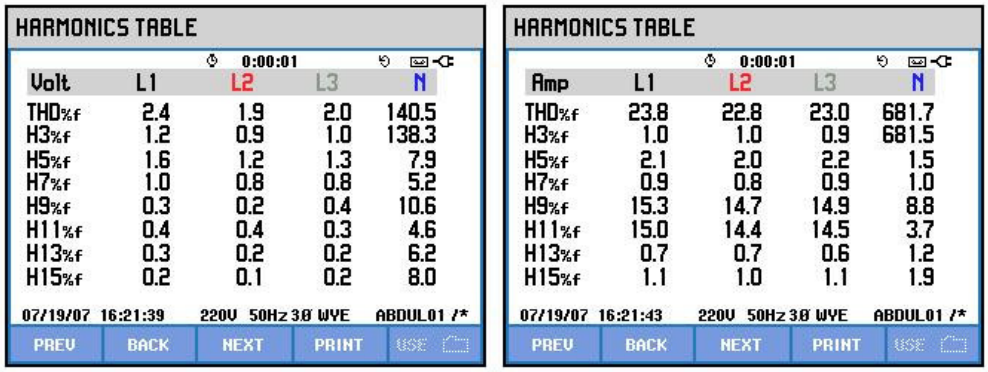

Figure 5.7 Voltage and current harmonic as tabulated at the source side

At 0.5 KHz frequency, the voltage harmonic is not so effective but at this time current harmonics are effective in system. current harmonics 9^{th} and 11^{th} harmonics are most effective harmonics , then 19^{th} and 21^{st} harmonics are effective and 29^{th} , 31^{st} , 39^{th} and 41^{st} harmonics effective, too. Total harmonic distortion is %2.3 for voltage harmonics and %24 for current harmonics. At the figure 5.6 shows voltage and current harmonics, in current harmonics graph show that harmonics are effective in 500, 1000 , 1500 ,2000 Hz.

5.1.2 Boost Chopper with Resistor

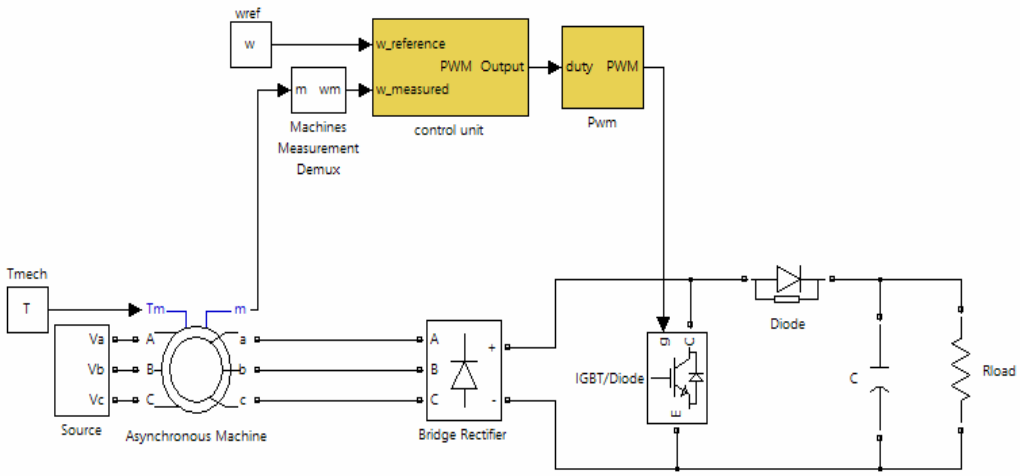

Figure 5.8 Schematics of the system

5.1.2.1 Laboratory work for 5 KHz :

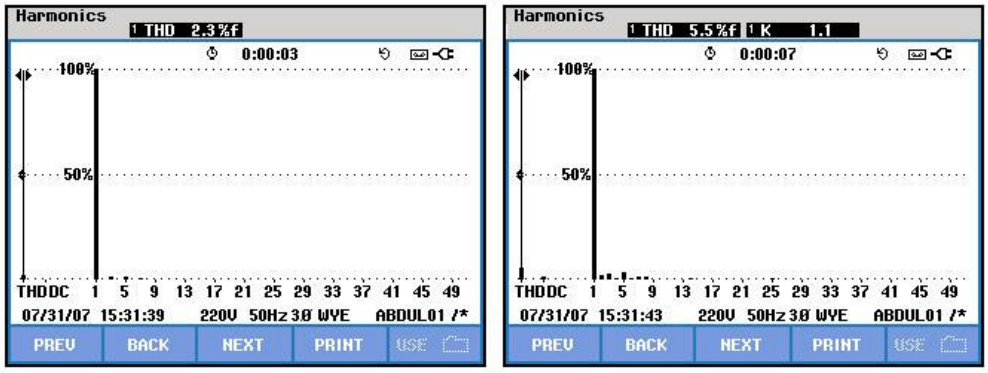

Figure 5.9 Voltage and current harmonic at the source side

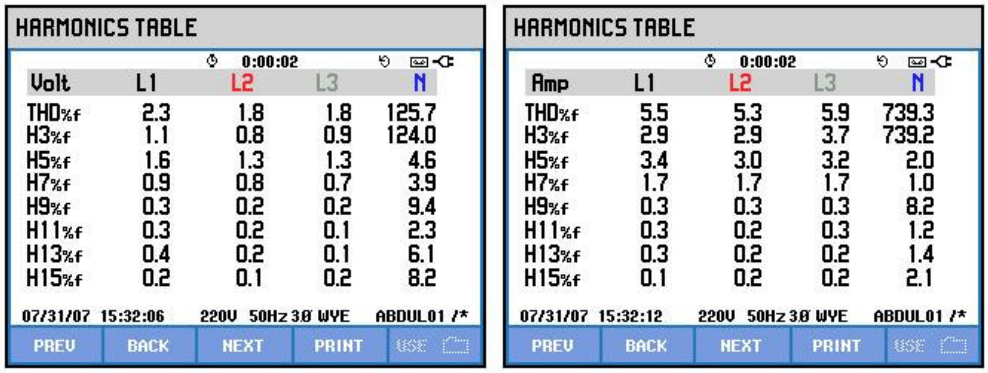

Figure 5.10 Voltage and current harmonic as tabulated at the source side

In 5 KHz frequency, the voltage is not so effective but current harmonics are effective in system 2nd, 3rd and 5th are most effective harmonics. There is an even harmonic which is 2nd harmonic that means in the current signal is not balanced in any time of the signal. Total harmonic distortion is %2.3 for voltage harmonics and %5.5 for current harmonics. Boost chopper with a single resistor system produce more source current harmonics in 5 KHz switching than three chopped resistor system used.

5.1.2.2 Laboratory work for 2 KHz:

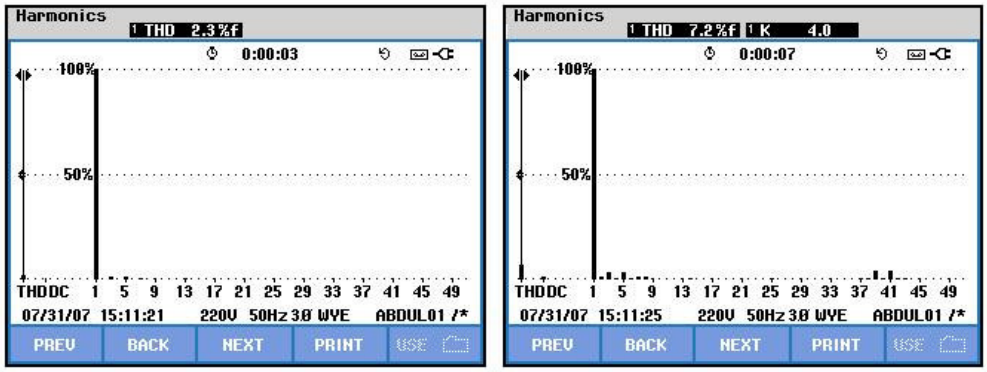

Figure 5.11 Voltage and current harmonic at the source side

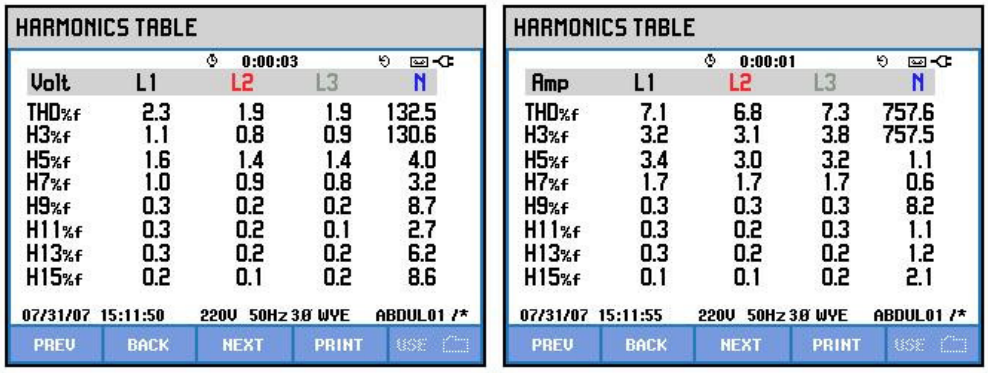

Figure 5.12 Voltage and current harmonic as tabulated at the source side

In 2 KHz frequency, the voltage is not so effective but in current harmonics 2^{nd}, 3^{rd}, 5^{th}, 39^{th} and 41^{st} harmonics are effective. Total harmonic distortion is %2.3 for voltage harmonics and %7.2 for current harmonics. If this results are compared with three chopped resistor system 39^{th} and 41^{st} harmonics are decreased but 3^{rd} and 5^{th} harmonics are effective and there is also even harmonic which is 2^{nd} harmonic, again.

5.1.2.3 Laboratory work for 0.5 KHz :

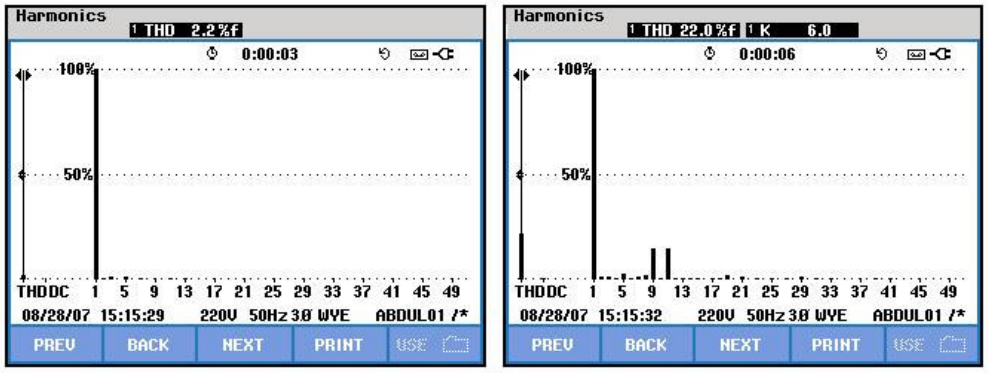

Figure 5.13 Voltage and current harmonic at the source side

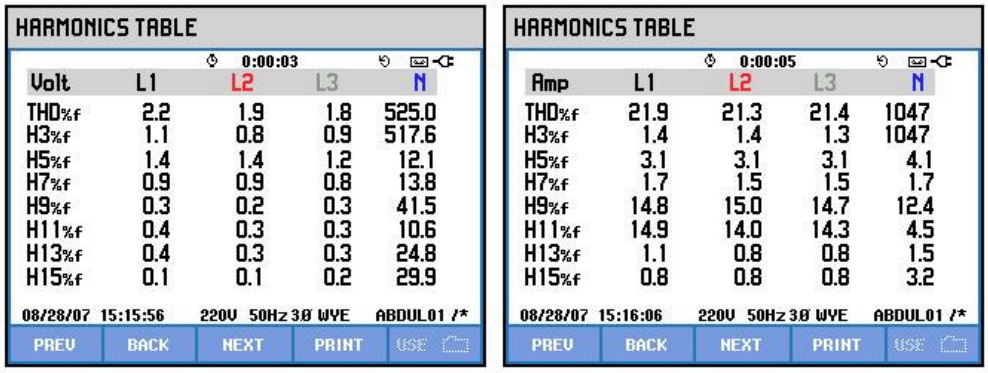

Figure 5.14 Voltage and current harmonic as tabulated at the source side

In 0.5 KHz frequency, the voltage harmonic is not so effective but at this time current harmonics are so effective in system. Current harmonics 9^{th} and 11^{th} harmonics are most effective harmonics , then 2^{nd}, 3^{rd} , 5^{th} , 7^{th} , 8^{th} harmonics are importantly effective harmonics and also 19^{th} , 21^{st} , 29^{th} , 31^{st} harmonics effective, too. Total harmonic distortion is %2.2 for voltage harmonics and %22 for current harmonics. All boost converter circuits have 2^{nd}, 5^{th} harmonics. If this result compared with three chopped resistor circuit high order harmonics are decreased in boost chopper with resistor circuit and low order harmonics are decreased in three chopped resistor circuit.

5.2 Comparing experimental work and simulation result for harmonic contents of system.

This both systems are compared with simulation and experimental results for three different switching frequencies 5, 2 and 0.5 KHz and also for three different speed 1300, 1100 and 900 rpm.

In simulation part, the MATLAB/simulink is used fast Fourier transform (fft) analysis is carried out during 10 cycle to preserve instantaneous changing on current signal.

5.2.1 Three Chopped Resistor

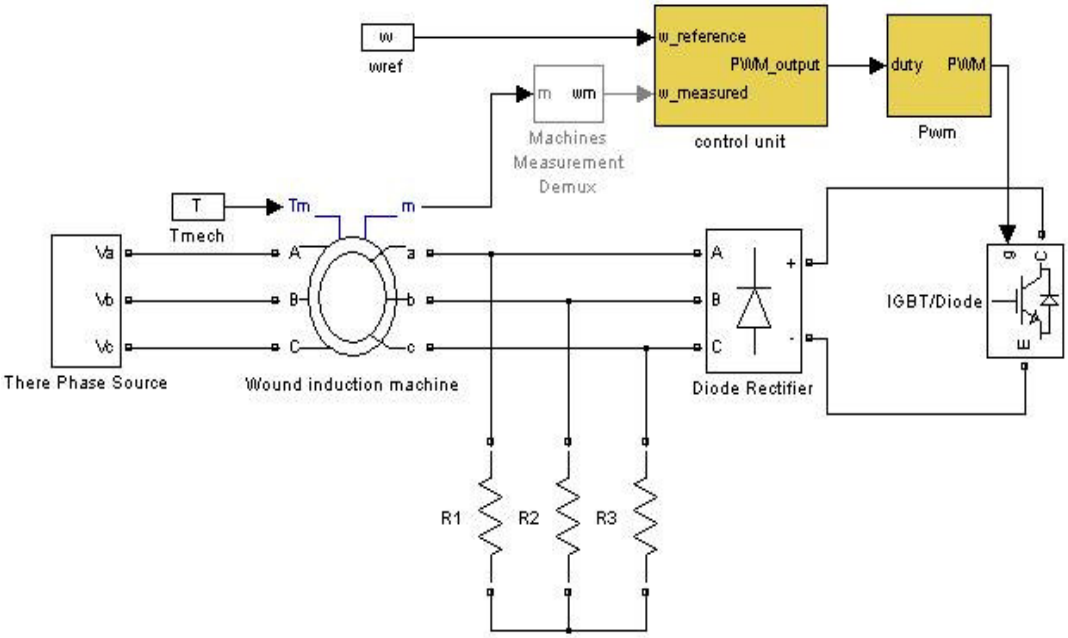

Figure 5.15 Schematics of the system

5.2.1.1 Laboratory work and simulation results for 5 KHz

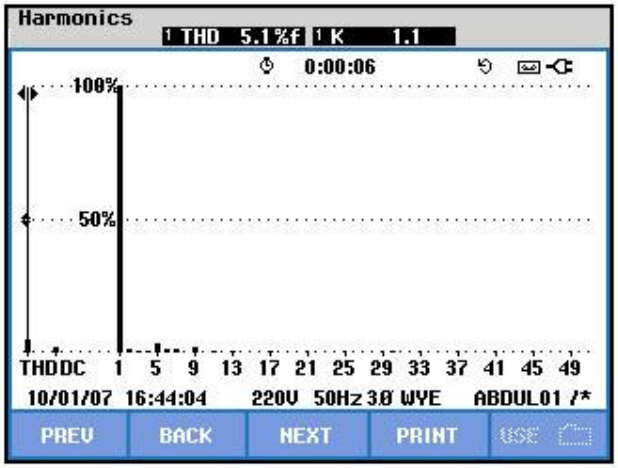

Figure 5.16 Current harmonics in the source at revolution=1300 rpm.

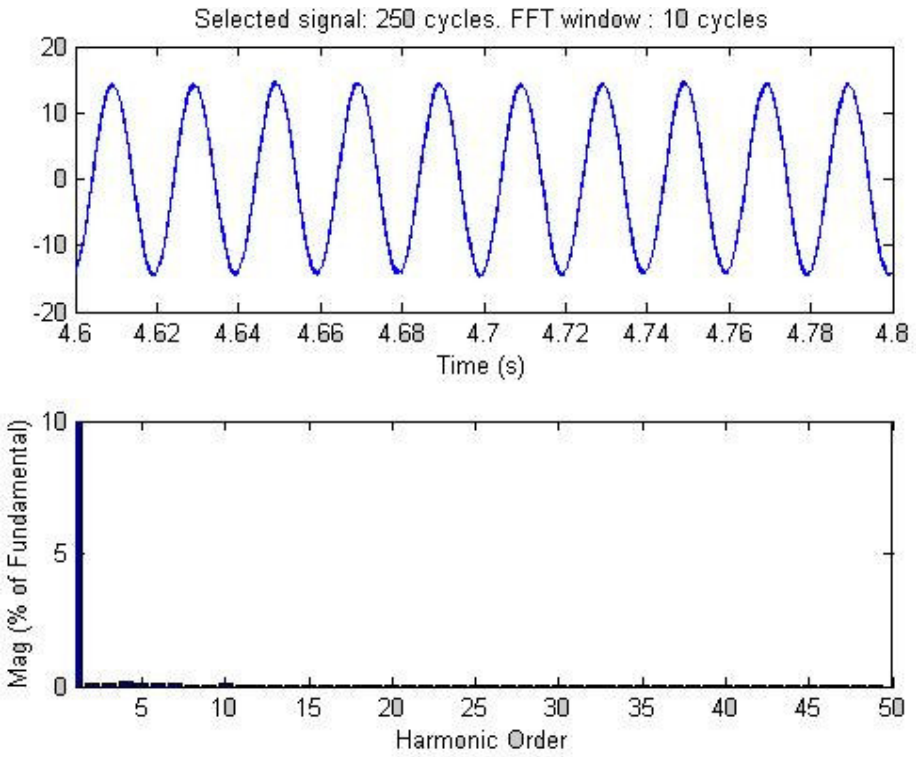

Figure 5.17 Current harmonics in the source at revolution=1300 rpm.

For 1300 rpm and 5 KHz, actually any harmonic is not effective on current signal in figure 5.16 low order harmonics are slowly effect the current signal and in figure 5.17 effect of low order harmonics can be seen.

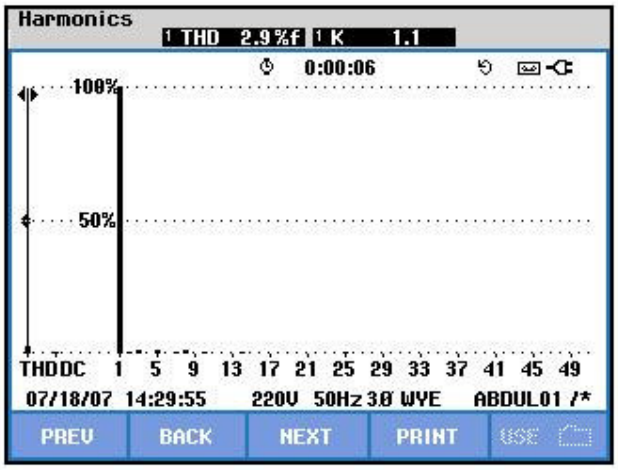

Figure 5.18 Current harmonics in the source at revolution=1100 rpm.

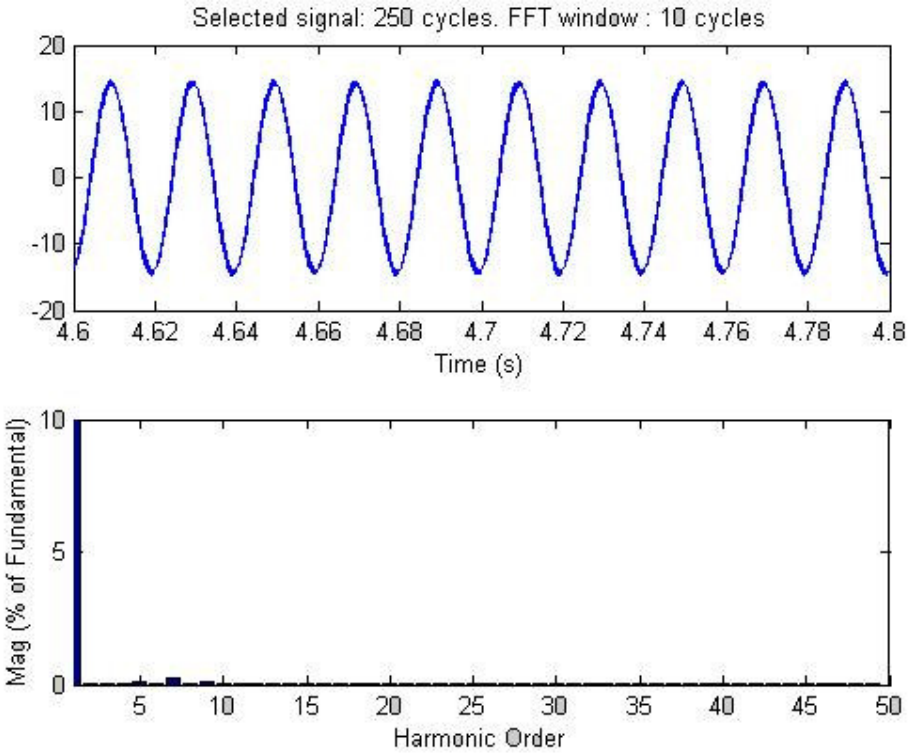

Figure 5.19 Current harmonics in the source at revolution=1100 rpm.

For 1100 rpm and 5 KHz, effect of low orders harmonics is decreased actually only 5th harmonics is seen on current signal and effect of 5th harmonics really low. In figure 5.18 can be seen experiment result of harmonic order and also figure 5.19 shows simulation result for same system and in figure 5.19 similar harmonic result can be seen with figure 5.18.

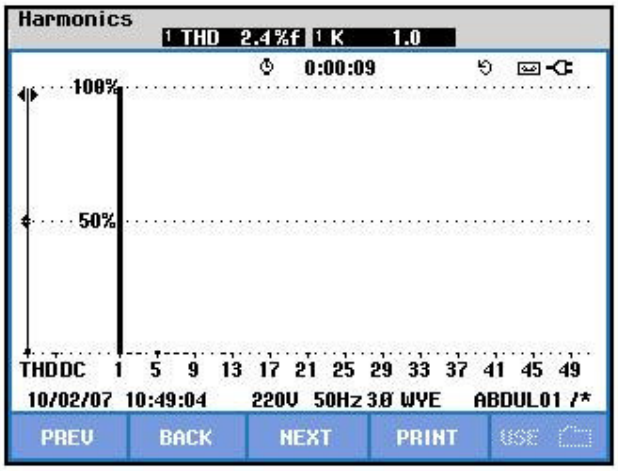

Figure 5.20 Current harmonics in the source at revolution=900 rpm.

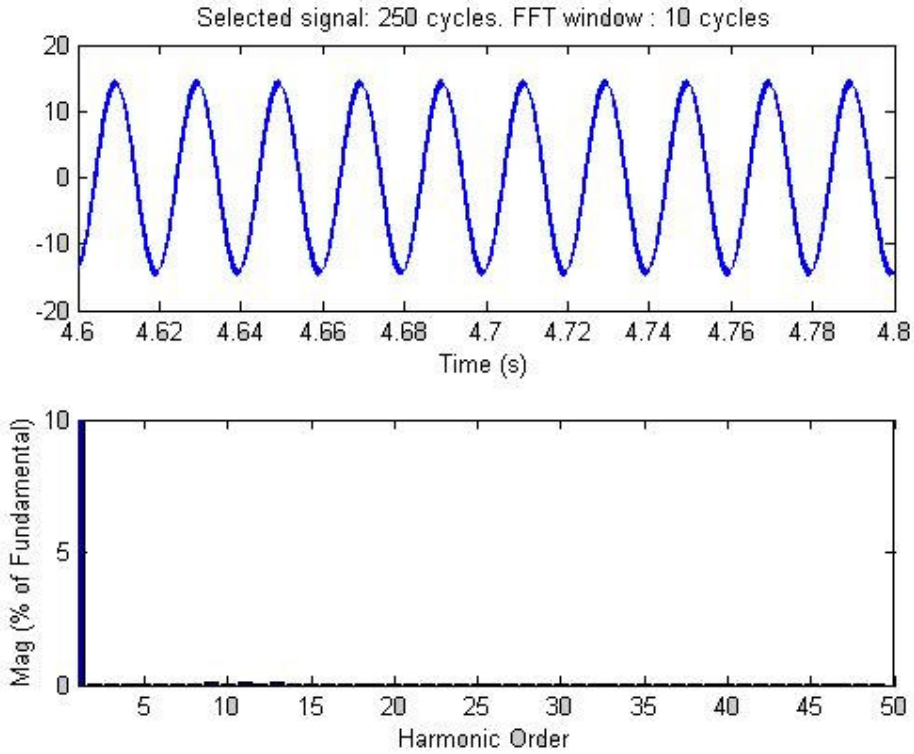

Figure 5.21 Current harmonics in the source at revolution=900 rpm.

For 900 rpm and 5 KHz duty cycle, effect of low orders harmonics is decreased actually only 5th harmonics is seen on current signal and effect of 5th harmonics really low. In figure 5.18 can be seen experiment result of harmonic order and also figure 5.19 shows simulation result for same system and in figure 5.19 similar harmonic results can be seen with figure 5.18.

5.2.1.2 Laboratory work and simulation results for 2 KHz

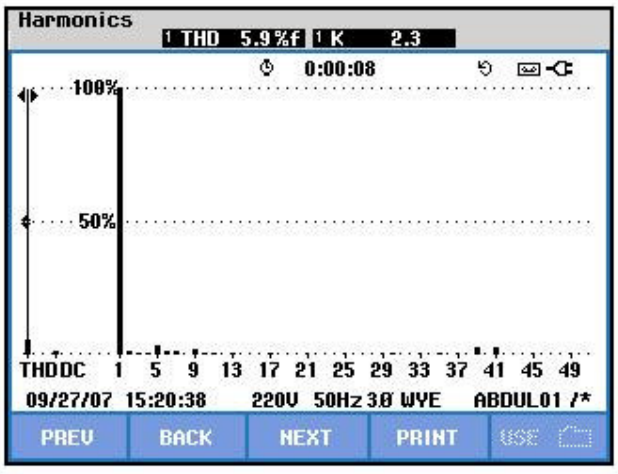

Figure 5.22 Current harmonics in the source at revolution=1300 rpm.

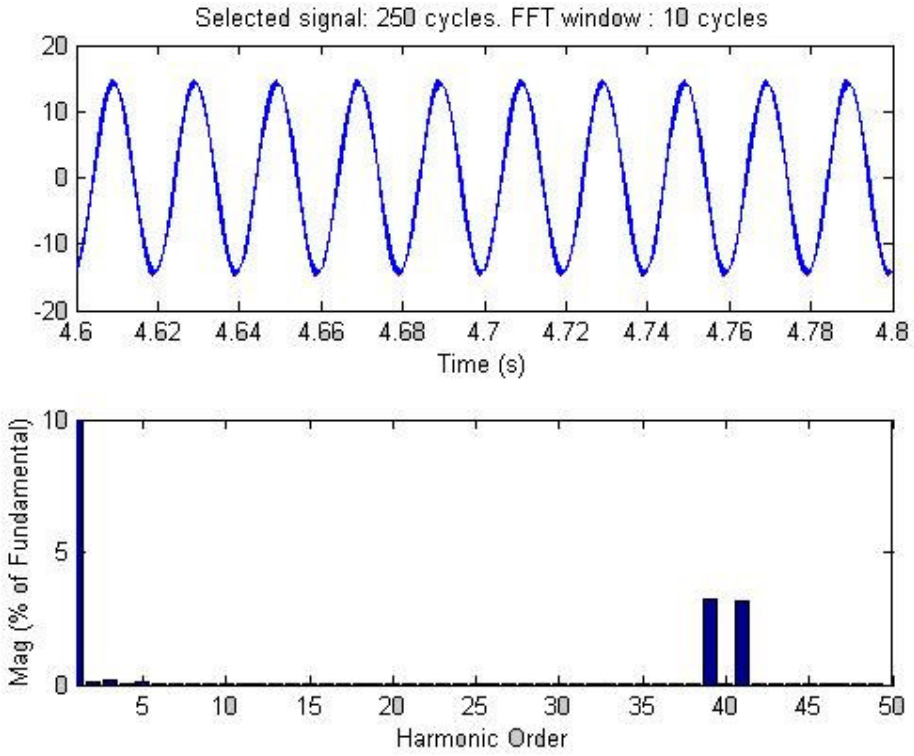

Figure 5.23 Current harmonics in the source at revolution=1300 rpm.

For 1300 rpm and 2 KHz duty cycle, figure 5.22 shows 5th,9th,39th, 41st harmonics are effectively seen on input current waveform. In figure 5.23 shows simulation results for same system and in this figure 39th and 41st harmonics are similar to experimental result only difference amplitude of 5th harmonic is lower than experimental results.

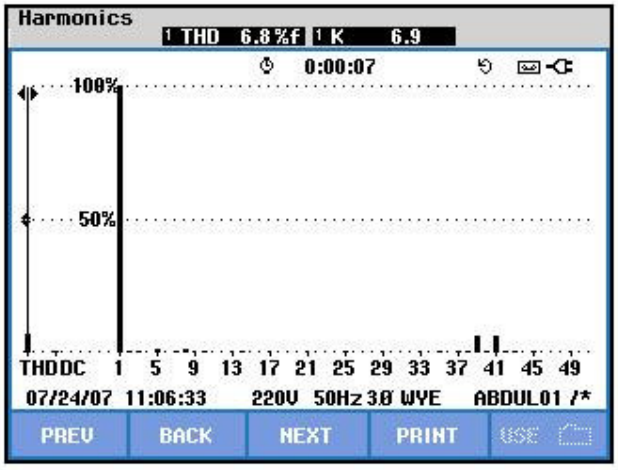

Figure 5.24 Current harmonics in the source at revolution=1100 rpm.

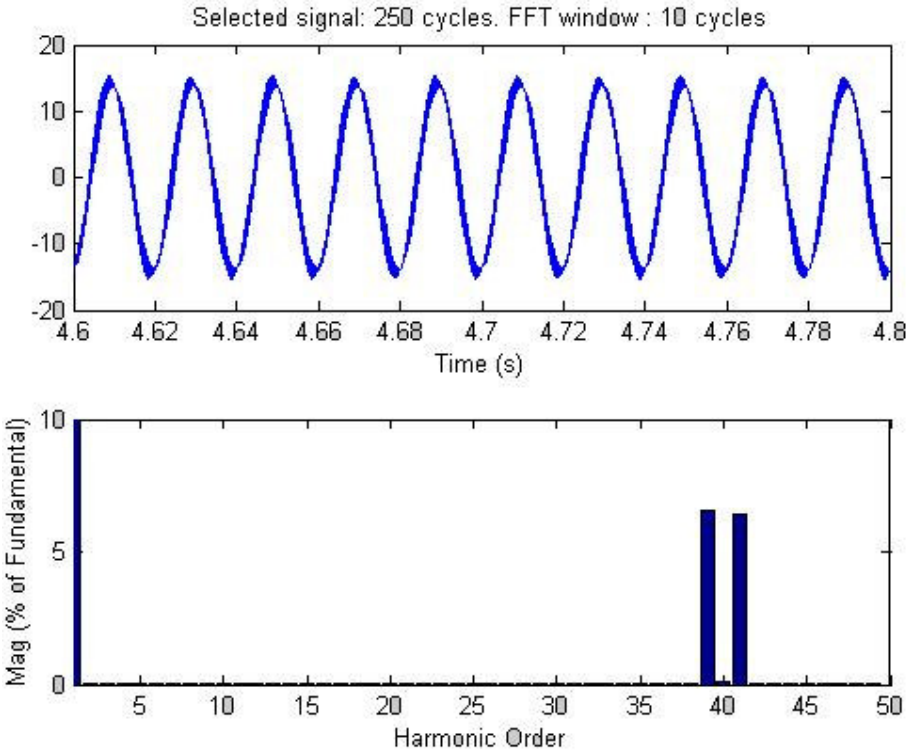

Figure 5.25 Current harmonics in the source at revolution=1100 rpm.

For 1100 rpm and 2 KHz, the effect of low orders harmonics is decreased actually only 5th harmonics is seen on current signal and effect of 5th harmonics really low. In figure 5.24 only high order harmonics effect can be seen, which are 39th and 41st harmonics and simulation results on figure 5.25 supports this results. If the results of 1300 rpm and 1100 rpm are compared, low order harmonics are decreased and high order harmonics increased.

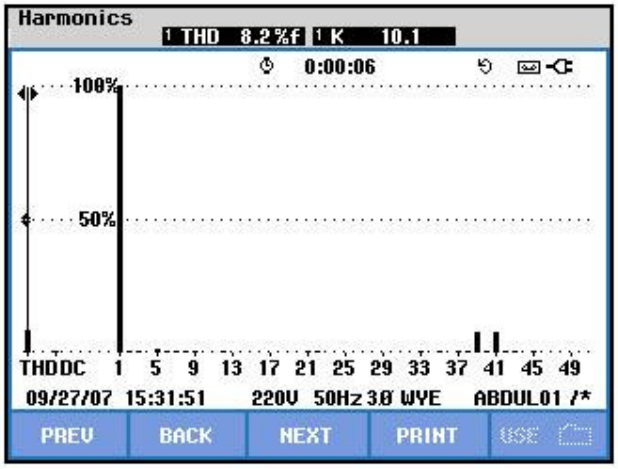

Figure 5.26 Current harmonics in the source at revolution=900 rpm.

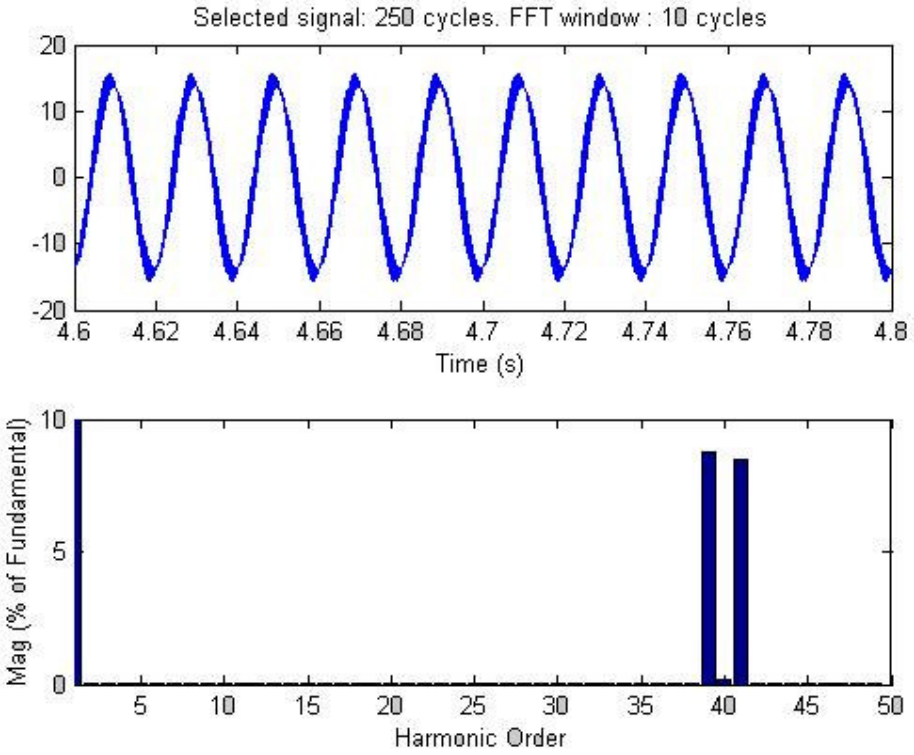

Figure 5.27 Current harmonics in the source at revolution=900 rpm.

For 900 rpm and 2 KHz, the effect of low orders harmonics is decreased and nearly ineffective on current signal but higher order harmonics are increased when the rotor speed is decreased. In figure 5.26 can be seen experiment result of harmonic order and also figure 5.27 shows simulation result for same system and result on both figure nearly same, effect of lower order harmonics are neglected and only 39^{th} and 41^{st} harmonics can be seen on input current signal , so experimental and simulation result are consistent to each other.

5.2.1.3 Laboratory work and simulation results for 0.5 KHz

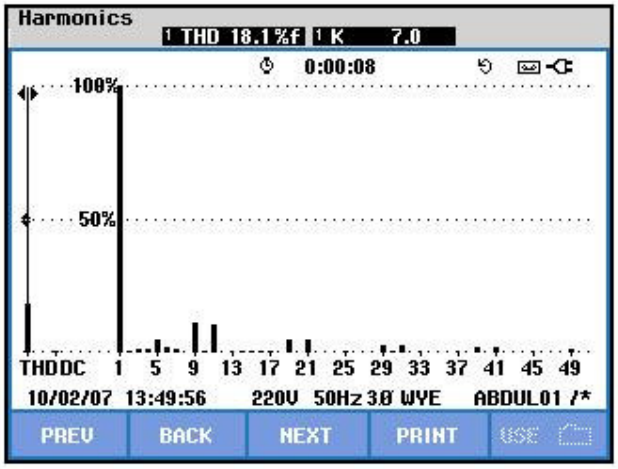

Figure 5.28 Current harmonics in the source at revolution=1300 rpm.

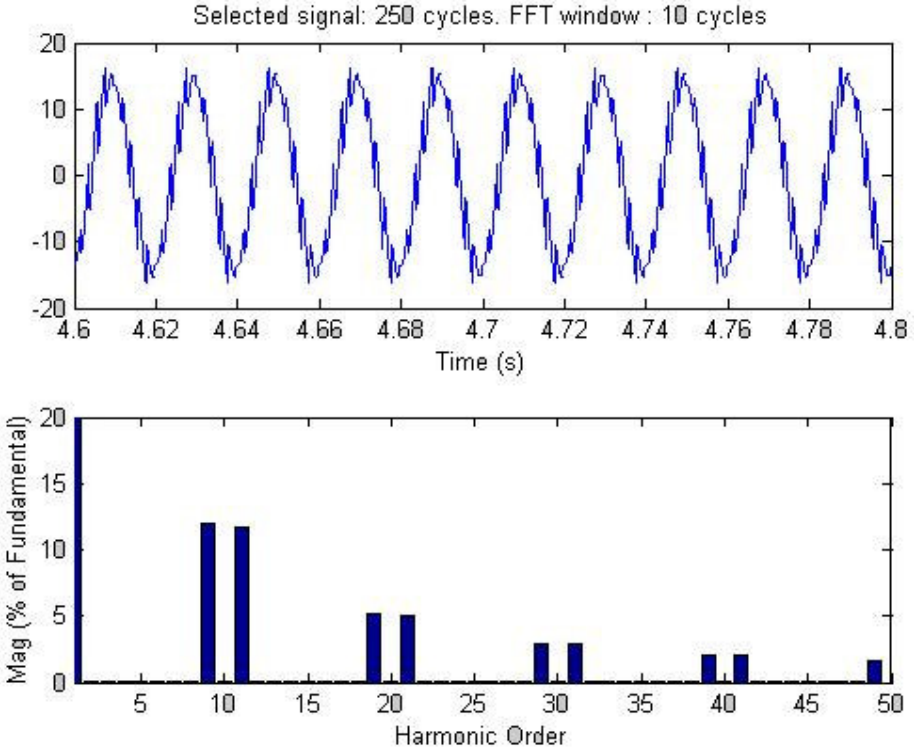

Figure 5.29 Current harmonics in the source at revolution=1300 rpm.

For 1300 rpm and 0.5 KHz, figure 5.28 shows harmonic results of input current in experimental work, and also figure 5.29 shows current harmonics in simulation, result of both figures can be seen as similar and most effective harmonics are 9^{th} , 11^{th} then 19^{th}, 21^{st}, 29^{th}, 31^{st}, 39^{th}, 41^{st}, 49^{th} amplitude of harmonics decreases with increasing harmonic order. Only differences between experimental and

simulation results is 5th harmonic, which is effective experimental work unlike simulation.

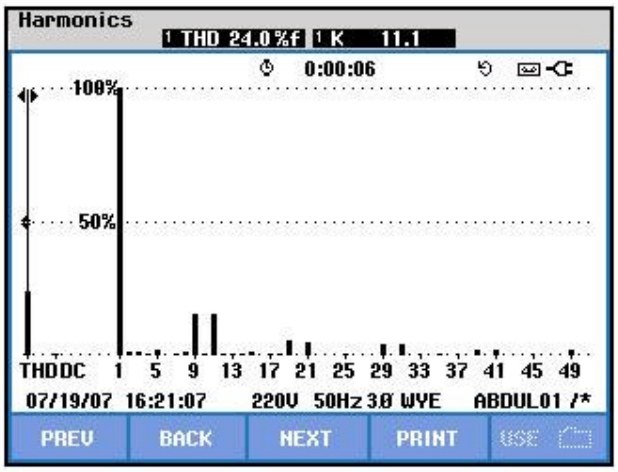

Figure 5.30 Current harmonics in the source at revolution=1100 rpm.

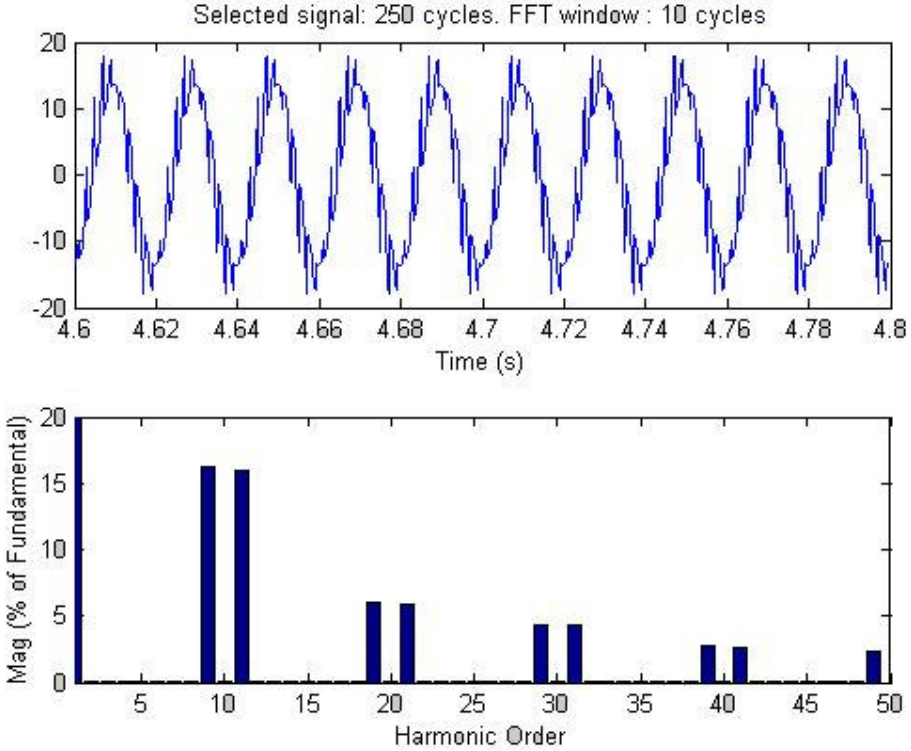

Figure 5.31 Current harmonics in the source at revolution=1100 rpm.

For 1100 rpm and 0.5 KHz, figure 5.30 shows harmonic results of input current in experimental work, and also figure 5.31 shows current harmonics in simulation, result of both figure can be seen as similar most effective harmonics are 9th , 11th then 19th, 21st it is continue as 29th , 31st , 39th, 41st 49th . The amplitude of

harmonics decreases with increasing harmonic order. 5th harmonics are effective on experimental work unlike simulation result but it is not effective like in 1300 rpm revolution.

In comparing figure 5.31 and figure 5.29 , it can be seen in figure 5.31 amplitude of harmonics increase despite of figure 5.29 , that means when speed decrease harmonic effect on input current increase for 1100 rpm.

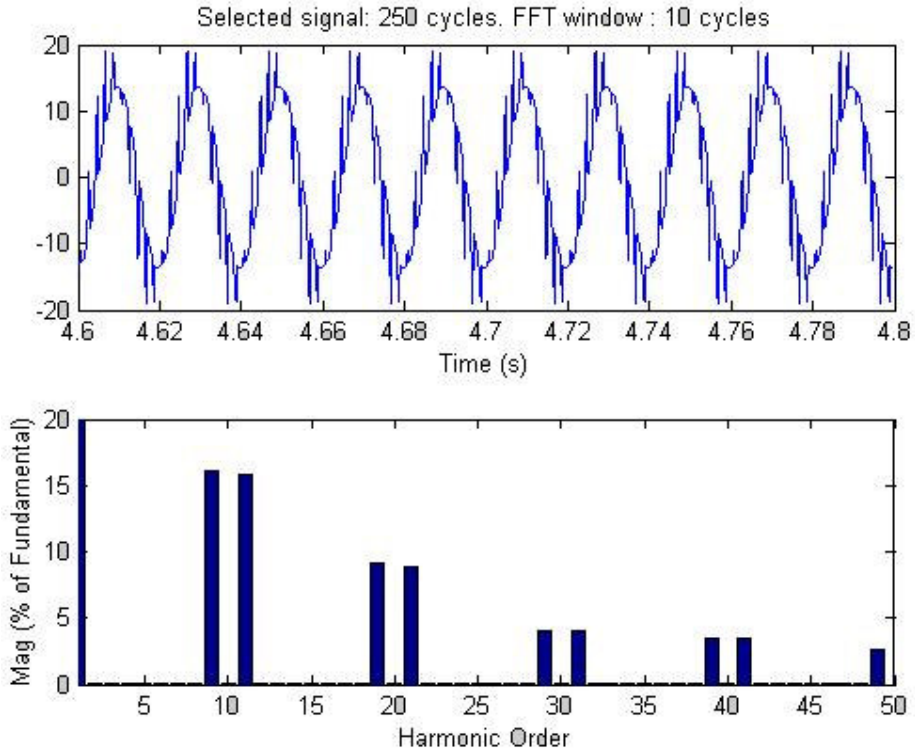

Figure 5.32 Current harmonics in the source at revolution=900 rpm.

For 900 rpm and 0.5 KHz duty cycle, figure 5.32 there is only simulation result for system. most effective harmonics are 9th , 11th then 19th, 21st it is continue as 29th , 31st , 39th, 41st 49th . in figure 5.32 can be seen amplitude of harmonics are decrease with increasing harmonic order.

Comparing figure 5.32, figure 5.31 and figure 5.29 , the harmonic effect increase a little in figure 5.32 according to figure 5.31 and also increases much according to figure 5.29 , that means when speed decreases harmonic effect on input current increases for 900 rpm, too.

5.2.1 Boost Chopper with Resistor

5.2.2

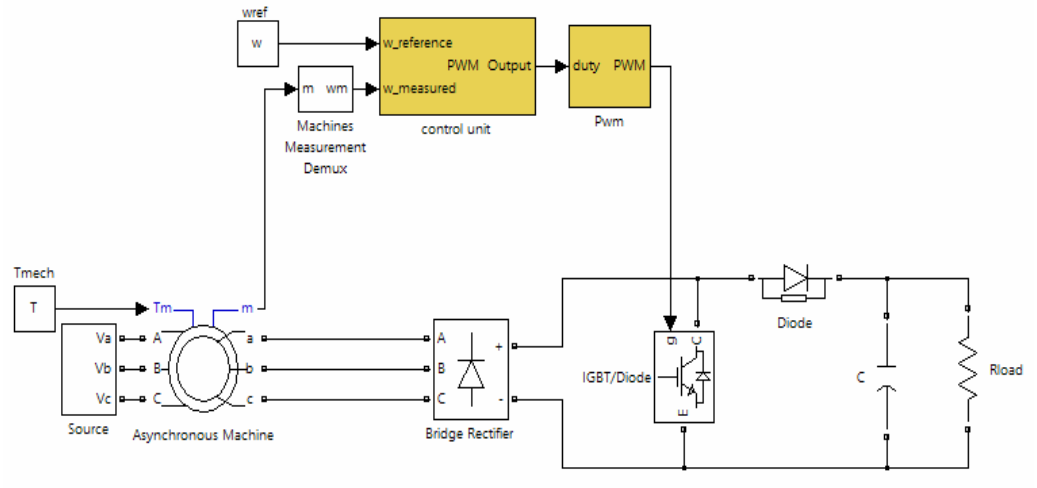

Figure 5.33 Schematics of the system

5.2.2.1 laboratory work and simulation results for 5 KHz

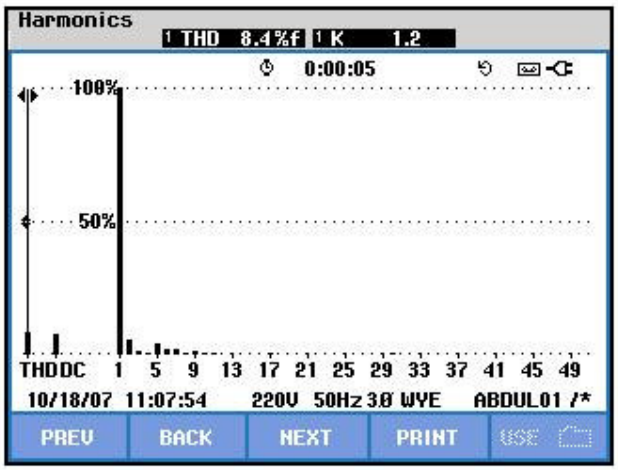

Figure 5.34 Current harmonics in the source at revolution=1300 rpm.

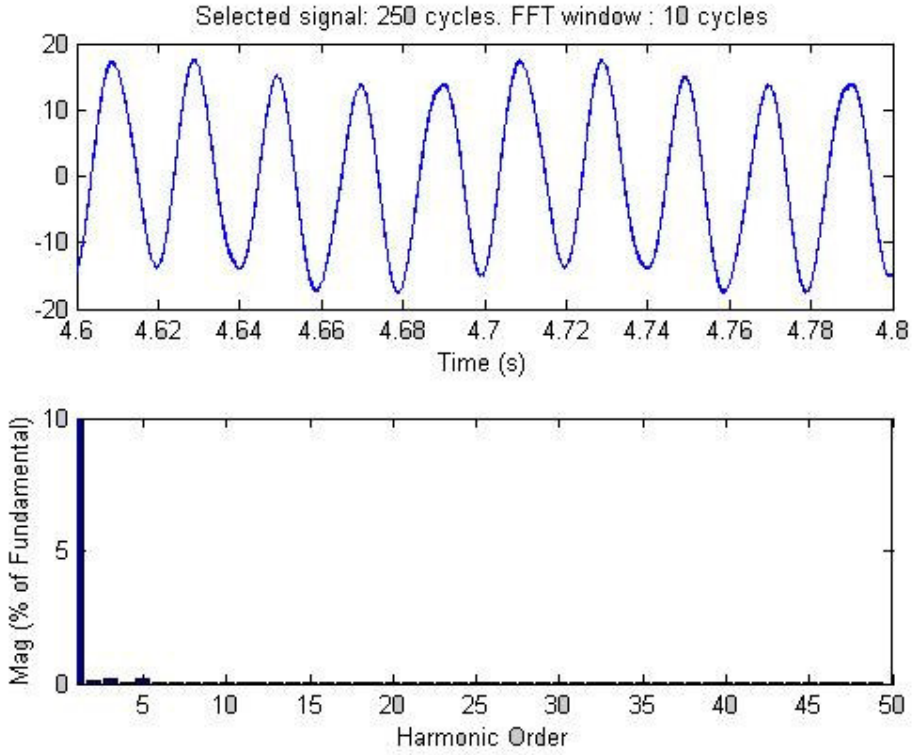

Figure 5.35 Current harmonics in the source at revolution=1300 rpm.

For 1300 rpm and 5 KHz, the actually any harmonic is not effective on current signal in figure 5.34 low order harmonics are slowly effect the current signal and in figure 5.35 effect of low order harmonics can be seen. Both graph show that 5^{th} harmonic effect system a little but in experimental work 2^{nd} harmonic is really

effective harmonic for the system on the contrary simulation result. All boost chopper with resistor circuit has second harmonic.

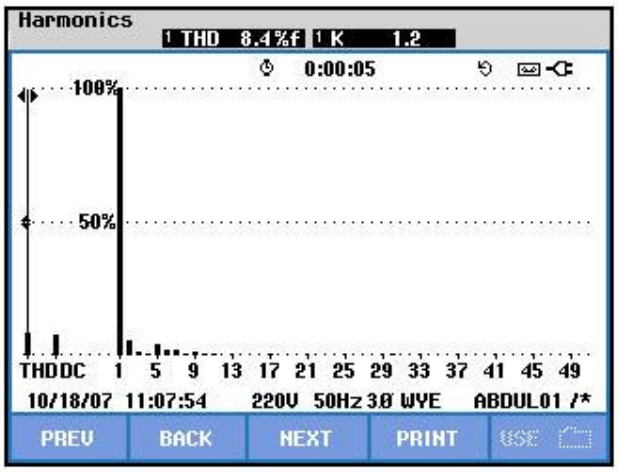

Figure 5.36 Current harmonics in the source at revolution=1100 rpm.

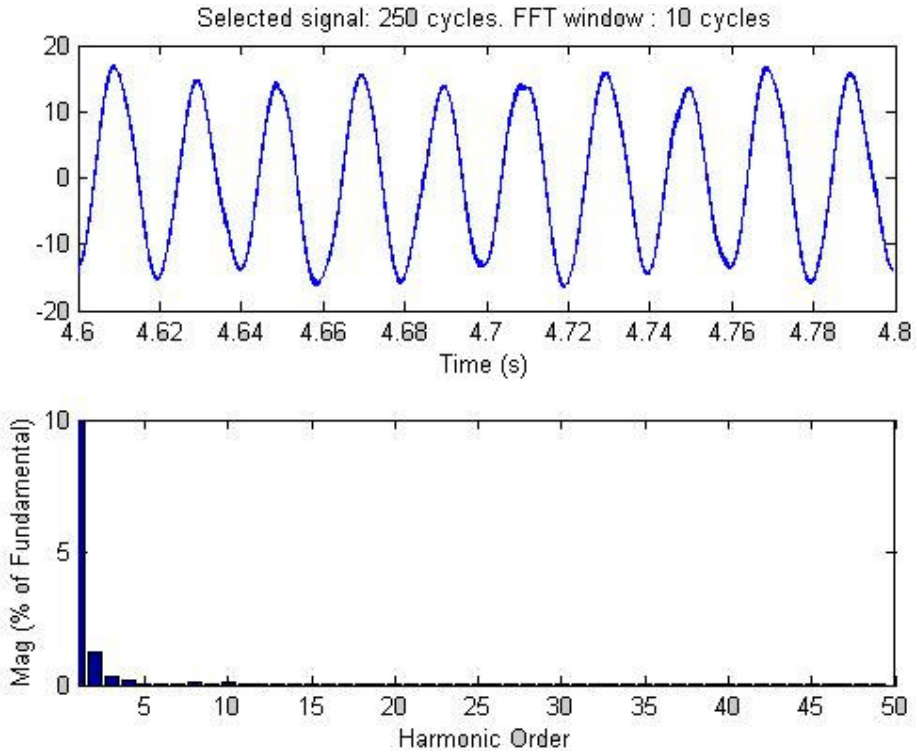

Figure 5.37 Current harmonics in the source at revolution=1100 rpm.

For 1100 rpm and 5 KHz, the low order harmonics are not so effective on current signal. 2nd harmonic is effective for experimental and simulation results. But in experimental part, the 5th harmonic is effective which can be seen in figure 5.36, in figure 5.37 5th harmonic is not seen.

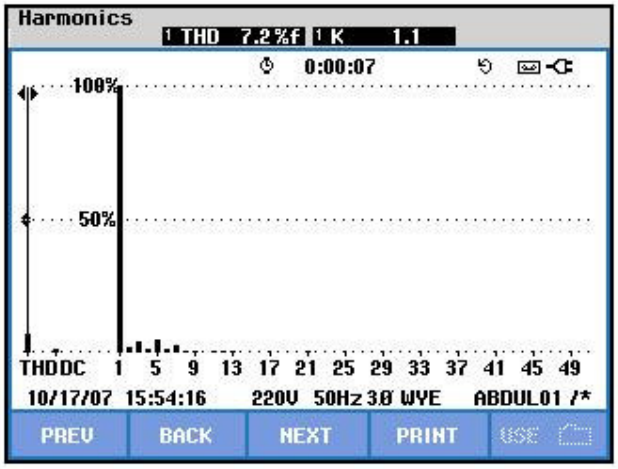

Figure 5.38 Current harmonics in the source at revolution=900 rpm.

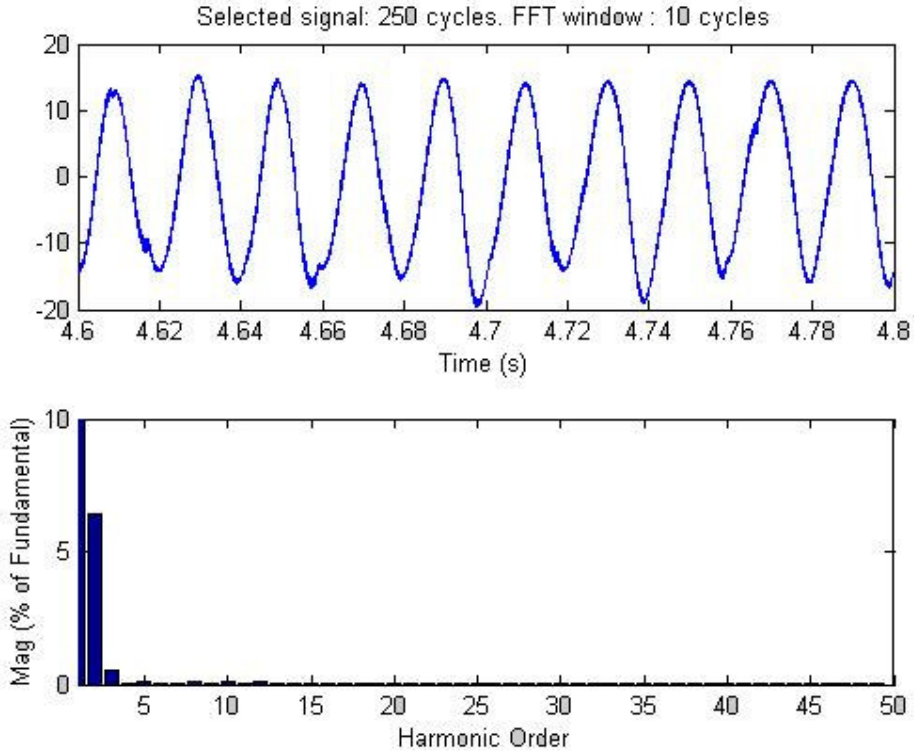

Figure 5.39 Current harmonics in the source at revolution=900 rpm.

For 900 rpm and 5 KHz, the actually any harmonic is not effective on current signal in figure 5.39 low order harmonics are slowly effect the current signal and in figure 5.39 effect of low order harmonics can be seen. Both graphs show that 5th harmonic effect system a little but in experimental work 2nd harmonic is really effective harmonic for the system on the contrary simulation result. All boost chopper with resistor circuit has second harmonic.

5.2.2.2 Laboratory work and simulation results for 2 KHz

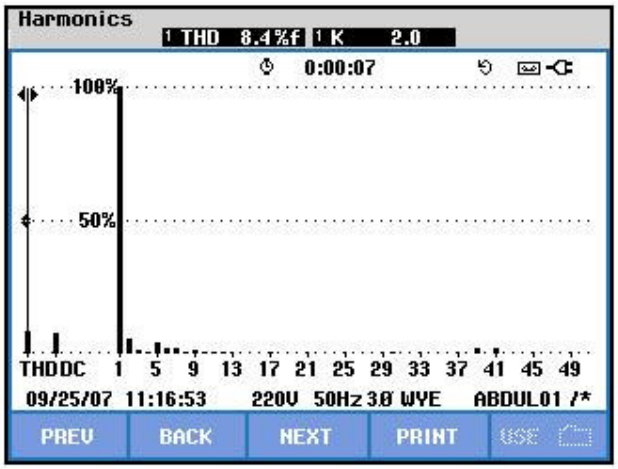

Figure 5.40 Current harmonics in the source at revolution=1300 rpm.

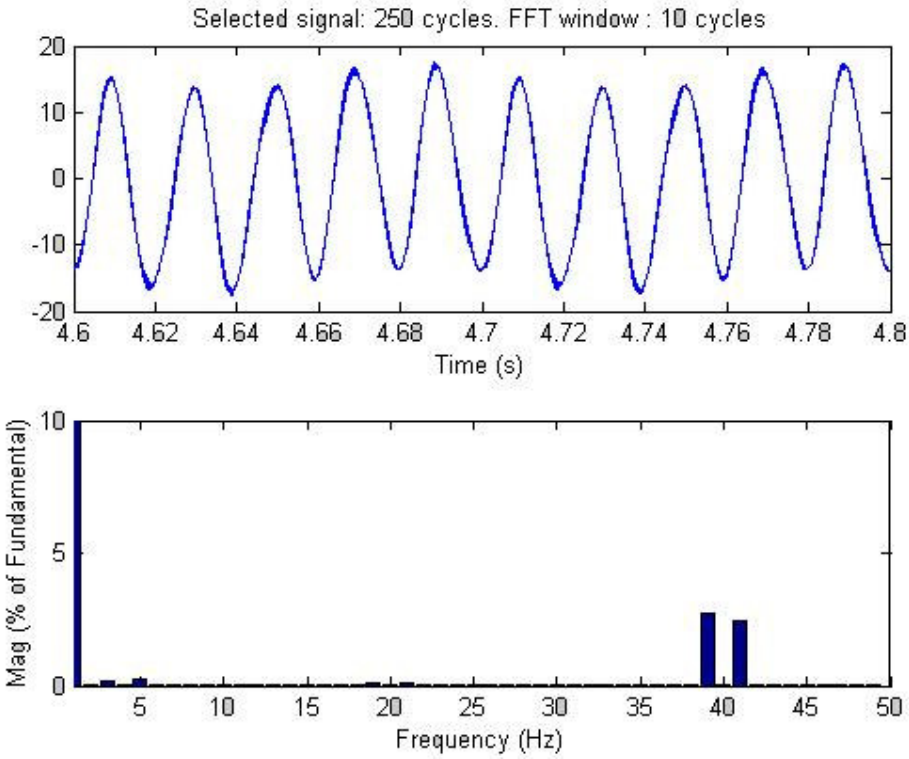

Figure 5.41 Current harmonics in the source at revolution=1300 rpm.

For 1300 rpm and 2 KHz, actually any harmonic is not effective on current signal in figure 5.40 shows experimental work result and figure 5.41 simulation result, both graphs seem similar. In figure 5.40, the 5th harmonic most effective harmonic and in figure 5.41 similar, too. In figure 5.40, the 39th and 41st harmonics are effective and in figure 5.41 simulation result similar.

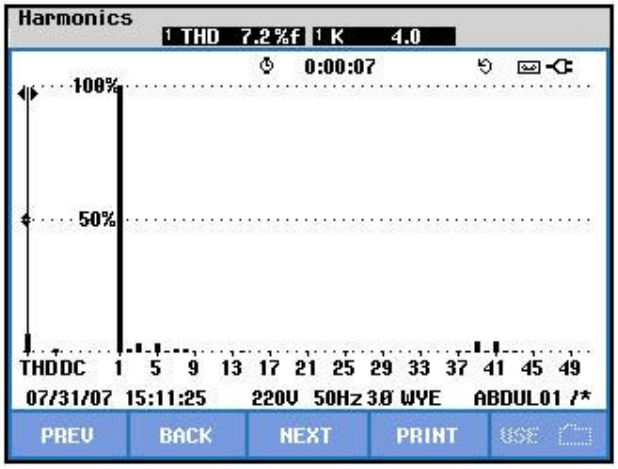

Figure 5.42 Current harmonics in the source at revolution=1100 rpm.

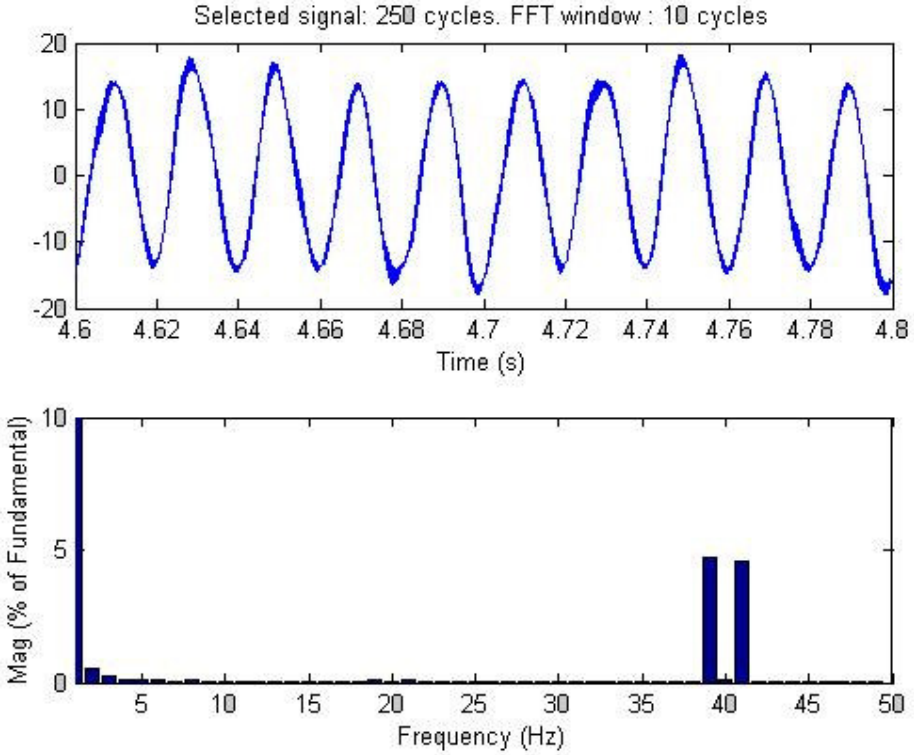

Figure 5.43 Current harmonics in the source at revolution=1100 rpm.

For 1100 rpm and 2 KHz, the actually any harmonic is not effective on current signal, the same harmonic content can be seen with figure 5.41 which is 1300 rpm and 2 KHz. If the rotor speed decreases, the 39th and 41st harmonics affect increase. Low order harmonic content is not affected by speed.

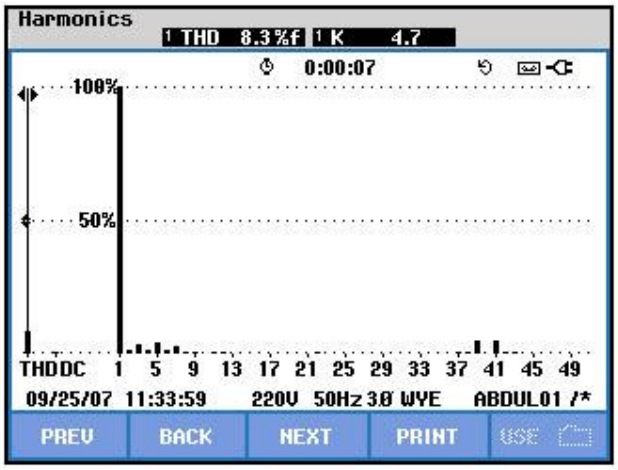

Figure 5.44 Current harmonics in the source at revolution=900 rpm.

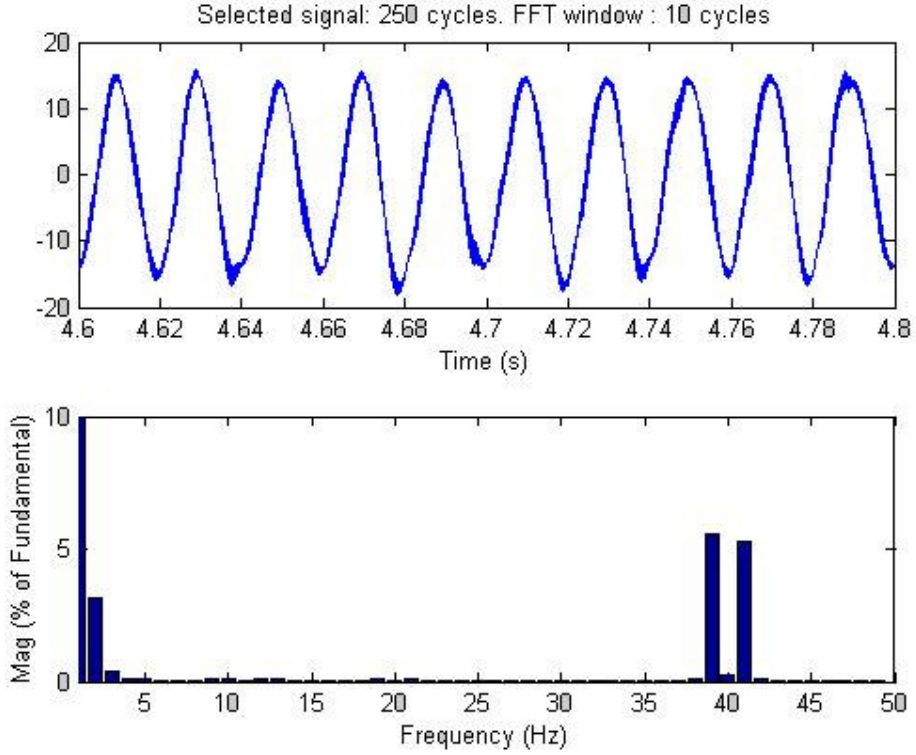

Figure 5.45 Current harmonics in the source at revolution=900 rpm.

For 900 rpm and 2 KHz, it is effected by a little by low order harmonics. In figure 5.44 shows 39th and 41st harmonics are effective on experimental work and also figure 5.45 consistent with it. In simulation work effect of 2nd harmonics is much, but experimental work this effect is not seen like simulation. In comparing with figure 5.33 and figure 5.31, 39th and 41st harmonics increase by decreasing speed.

5.2.2.3 Laboratory work and simulation results for 0.5 KHz

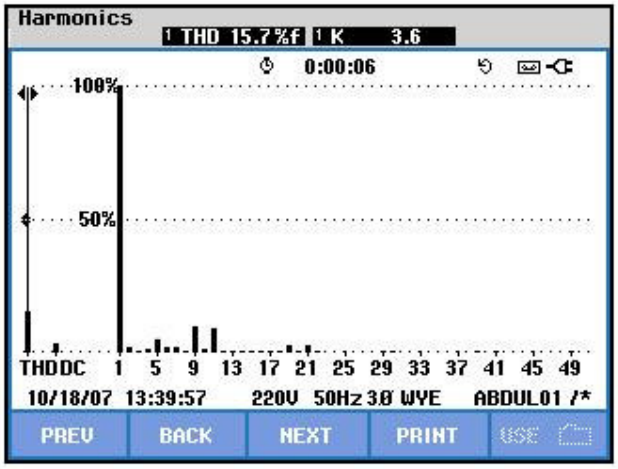

Figure 5.46 Current harmonics in the source at revolution=1300 rpm.

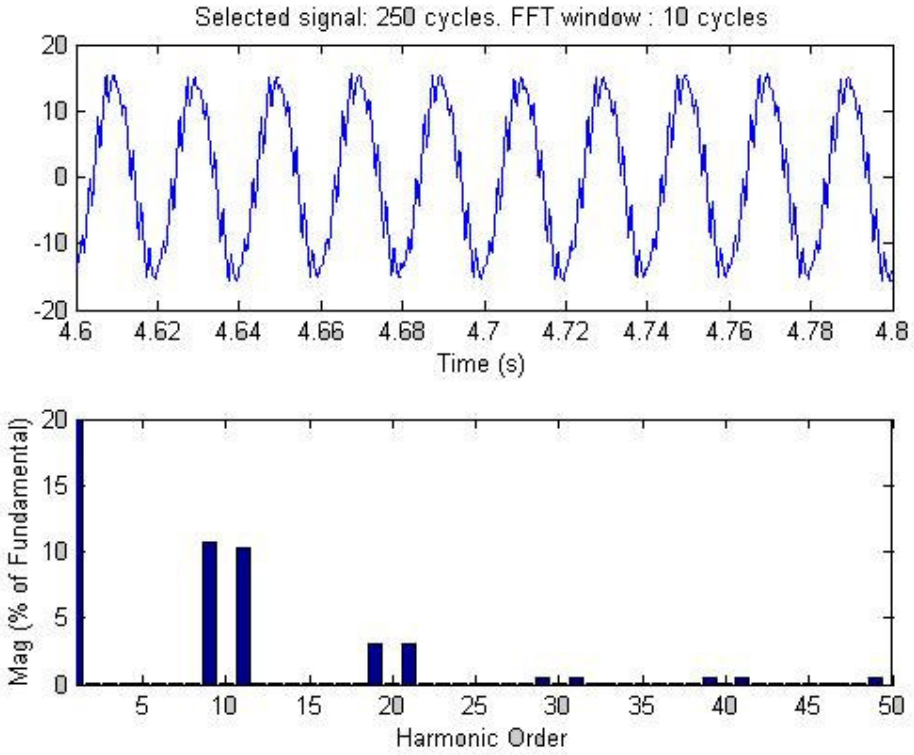

Figure 5.47 Current harmonics in the source at revolution=1300 rpm.

For 1300 rpm and 0.5 KHz, the 9^{th} , 11^{th} , 19^{th} and 21^{st} harmonic most effective harmonic content in figure 5.46 and figure 5.47. The experimental and simulation results are similar to each other, the amplitude of harmonics decreases with harmonic order increase for both graph. In figure 5.46, the 5^{th} harmonic is effective a little but simulation is not seems.

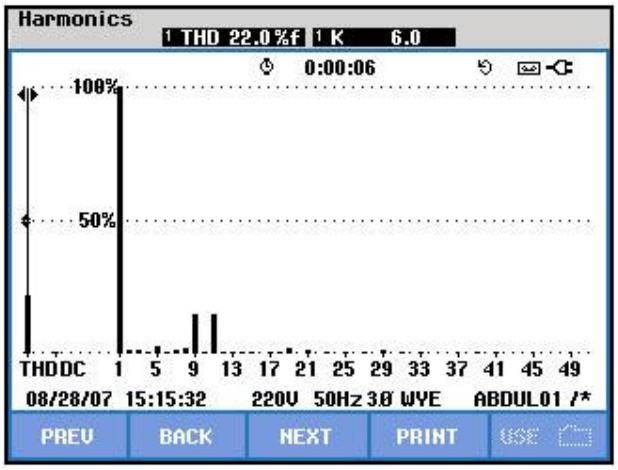

Figure 5.48 Current harmonics in the source at revolution=1100 rpm.

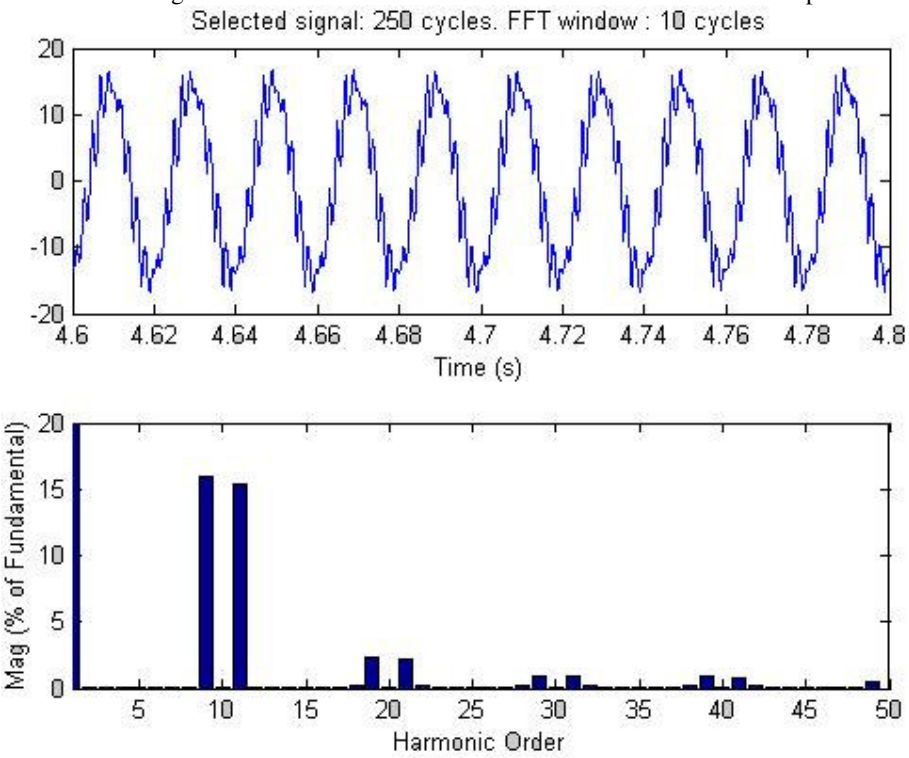

Figure 5.49 Current harmonics in the source at revolution=1100 rpm.

For 1100 rpm and 0.5 KHz, the 9th, 11th, 19th and 21st harmonics are most effective harmonic content in figure 5.46 and figure 5.47. The experimental and simulation result are similar to each other, the amplitude of harmonics decreases with harmonic order increases for both graph. Comparing figure 5.47 with figure 5.49, the 9th and 11th harmonics increase with decreasing rotor speed. And also 5th harmonics effect is not effective on experimental or simulation result.

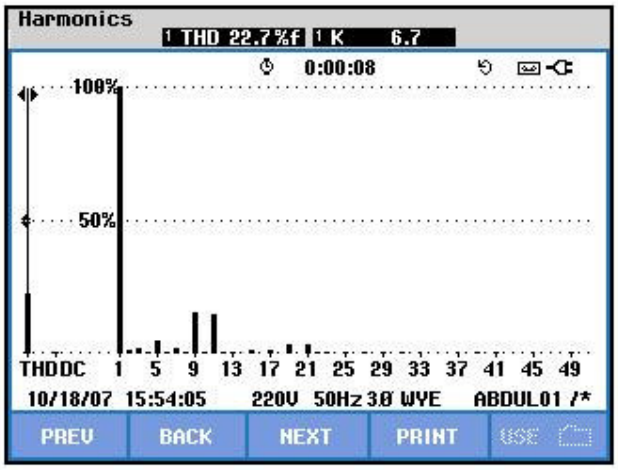

Figure 5.50 Current harmonics in the source at revolution=900 rpm.

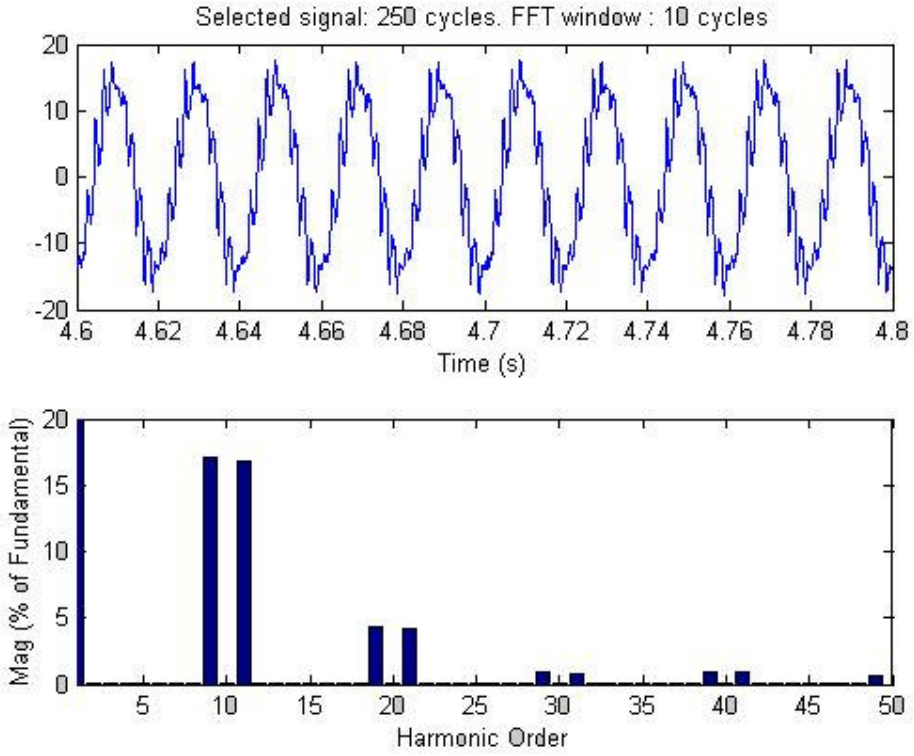

Figure 5.51 Current harmonics in the source at revolution=900 rpm.

For 900 rpm and 0.5 KHz, the 9^{th}, 11^{th}, 19^{th} and 21^{st} harmonics are most effective harmonic content in figure 5.50 and figure 5.51. The experimental and simulation results are near to each other, the amplitude of harmonics decreases while the harmonic order increases for both graphs. The 9^{th} and 11^{th} harmonics increase with decreasing speed.

CHAPTER SIX

CONCLUSION

In this thesis, two different type slip energy system are compared at three different control frequency and different rotor speeds. The systems are analyzed in MATLAB/simulink. They are built in the laboratory and results are compared in thesis.

Controller which is fuzzy logic, is written in C language and loaded to DSP2812. The systems are controlled by close loop fuzzy logic PI controller. In fuzzy logic controller PI gain parameters are adjusted by trial and error method in simulation work and they are used in experimental work too. The controller produces duty cycle for driving IGBT in both systems.

Results of experimental work and simulation are consistent and verified. Both system produce harmonic when frequency of control PWM signal is decreased. Harmonic content is most effective in 500 Hz. The power quality measures may cause filtering applications of line currents at the low operating frequency. In high switching frequency, Total harmonic distortion increase when the rotor speed increases. But in low switching frequency, total harmonic distortion decrease when the rotor speed increase.

In three chopped resistor system, collector emitter voltage of IGBT must be higher than boost chopper with a single resistor system. It is observed that in experiment and simulation this voltage reach about 600 volt in experiments and simulation.

REFERENCES

Akpınar E. and Pillay P.,(1990) (*IEEE Transaction on Energy Conversion Vol.5 No:1, march*). "Modeling and performance of slip energy recovery induction motor drives"

Akpınar E. and Pillay P.,Ersak A. (1992) "Starting Transient in slip energy recovery Induction motor_Drives- Part1:formulation and modeling" *IEEE Transactions on Energy Conversion Vol.7 No:1, March 1992*

Azizi H., Vahedi A., Masoum M.A.S. Study of Slip Energy Recovery of Induction Motor Drive Using Matlab/Simulink

El-Hawary_M.E.(*Power Engineering Letters*)-IEEE Power Engineering Review, april2001

Jarocha Robert W. (2005) Comparison of the modified subsynchronous cascade drive

Mattavelli P. , Rossetto L ,Spiazzi G. , Tenti P. General Purpose Fuzzy Controller for DC-DC Converters

Natarajan K. , Qui J. (2006) Sampled-data modeling of PWM Boost Converter in Continuous and Discontinuous Inductor Current Modes

Pravadalioglu S. , Akpınar E. Implementation of Fuzzy Controller for DC-Servo Drive Using a Low Cost Microcontroller

Ross, T.J. (1995). Fuzzy *Logic with Engineering Applications*. New York: McGraw-Hill.

Sürgevil T. (2004) P.H.D. thesis . Modeling And Simulation of Wind Energy Conversion System Using pwm Converter

Tunyasrirut S., Ngamwiwit J., Tadayoshi Furuya and Yamamoto Y. Self-tuning Fuzzy Logic Controller for Direct Torque Control of Slip Energy Recovery System

Ohyama K. , Arinaga S. and Yamashita Y. Modeling and Simulation of Variable Speed Wind Generator System Using Boost Converter of Permanent Magnet Synchronous Generator

Xin X. , Hui L. (2005) "Research on multiple Boost Converter Based on MW-level Wind Energy Conversion System" *ICEMS 2005 pp 1046-1049*

Fuzzy Logic Toolbox_For Use with Matlab (User's Guide ver.2)

Paolo Dadone PHD thesis. Design optimization of Fuzzy Logic System

APPENDIX A

Wound Rotor Induction Machine Parameters

The following parameters are obtained from the manufacturer of motor.

S3 ED %	Nominal Power kW	Nominal Speed 1/rev	Nominal Current A Stator	 Rotor	Rotor Voltage V	Rotor Constant K	Moment M_D/M_N	Inertial Moment J kgm^2	Weight kg
100	3,5	1420	8,8	17	140	4,8	3,4	0,033	77

The no-load and locked rotor tests are performed on the machine to calculate the equivalent circuit parameters. The results of these tests are given below:

Table 3.2 induction no-load and block rotor test results

At Block Rotor Test			At No Load Test		
Power (W.)	Voltage (V.)	Current (A.)	Power (W.)	Voltage (V.)	Current (A.)
432	79	7,8	580	380	4,02

The friction power and windage power is measured as 180 watts. Based on these measurements, the parameters are obtained and given below:

Table 3.3 induction motor calculated parameters

Rstator (ohm)	Rrotor' (ohm)	Lstator (H.)	Lrotor' (H.)	Lmutual' (H.)
1,183	1,183	0,008508	0,0085008	0,1757

These motor parameters are used in motor model in simulink to simulate the system. Calculated inductance and resistances are divided by two in order to obtain rotor and stator side resistance and inductance.

APPENDIX B

Source code of inductance resistance effect on boost converter

```
%Abdül Balıkçı
%This code is written for seeing effect of inductance resistance.
clear all
clc
for y=1:1:1000
    x=y/1000;
    i(y)=x;
    f(y)=1/(1-x);                    % normalized voltage for an
ideal converter
    g(y) = 1/(1/(10*(1-x))+(1-x));  % for a highly resistive
inductor
    h(y) = 1/(1/(100*(1-x))+(1-x)); % for a slightly resistive
inductor
end
plot(i,f)
hold on
plot(i,g,'r')
hold on
plot(i,h,'g')
axis([0,1,0,8])
legend('RL=0','R/RL=10','R/RL=100')
xlabel('duty cycle')
ylabel('normalized voltage gain')
```